UNIVERSITÀ DEGLI STUDI DI PADOVA

Dipartimento di Ingegneria Industriale

Corso di Laurea Magistrale in Ingegneria Chimica e Dei Processi Industriali

Tesi di Laurea

TECHNO-ECONOMIC ANALYSIS OF CATALYTIC TRANSFER HYDROGENATION AND DIRECT HYDROGENATION PROCESSES FOR THE PRODUCTION OF JET FUELS FROM WASTE COOKING OIL

Relatore:
Prof. A.BERTUCCO

Autore:
RUSTEM NAURZALIYEV
N.m.:1132728

Correlatori:
PhD. E.BARBERA
Prof. S.KUMAR
Old Dominion University (ODU)

13 APRIL 2018

Abstract

The aim of the thesis consist on the process simulation and techno-economic analysis of two processes to produce Jet fuel from a renewable waste cooking oil feedstock: Hydroprocessed Renewable (HRJ) from the UOP/ENI Ecofining^{TM} technology, which have been recently commercialized, and Catalytic Transfer Hydrogenation(CTH), in stage of research. In particular, Catalytic Transfer Hydrogenation process will be built from experimental data of the reaction system generated at Dr. Sandeep Kumar's ODU laboratory. Two processes have to be compared in terms of the results of process simulation and by economic analysis. The rigorous profitability analysis based on the economic model will be performed in order to evaluate the economic attractiveness of HRJ process and compare it with the one of CTH.

Contents

List of Figures

List of Tables

Introduction

Today in the United States, 92% of the transportation fuels are petroleum derived products and about 5% are based upon a renewable feedstock. At this day, no single alternative fuel technology or production pathway is able to satisfy the demand for technical and economic reasons. Nevertheless, the use of alternative fuel is strongly motivated by environmental issues and oscillating trends in petroleum prices. Specifically, among transportation fuels great interest is focused towards the Jet fuels. The U.S. Energy Administration Information (EIA) predicts considerable increment (approximately 40%) in the Jet fuel consumption between 2015 and 2040.

Different technologies exist in literature that can convert biomass into Jet fuels, whether in the research and development, demonstration or commercial stages. Among these only Hydroprocessed Renewable Jet fuel (HRJ) is well developed and mature process which have been commercialized in recent past.

Recently, an alternative reaction process has been proposed via Catalytic Transfer Hydrogenation (CTH) with the aid of organic molecules as hydrogen donors in the presence of catalyst. Therefore, it is interesting to develop a process based on this idea and to assess the related production costs.

Accordingly, the background and the scope of the work are the topics of the first Chapter of the thesis. The process simulation was carried out in Aspen Plus. The detailed development of the process flow diagrams of both the processes investigated is presented in Chapter 2. HRJ process was modeled referring to the UOP-ENI Ecofiningâ block diagram and published literature. Instead, the CTH process diagram was synthesized from the experimental data of the reaction system, kindly provided from prof. Kumarâs Biomass Research Laboratory at Old Dominion University (ODU). At the end of the chapter, the performances of the two processes are compared, quantifying the raw material consumption, the product yields and the consumption of utilities.

In order to carry out the analysis of the capital investment, the selection of the technology and the information regarding the sizing of process units are required. With this aim, Chapter 3 is concerned about the sizing of technologies such as trickle bed and fixed bed reactors, gas-liquid separators and heat exchangers, with particular attention to some critical performance variables, such as multiphase interaction, the size of the catalyst particles and their effect on the operating pressure drops.

Chapter 4 describes the process economics for evaluating the cost of production, calculated from well-established petroleum and chemical engineering methods and cost estimation techniques based on the results of the simulations. The economic model and the assumptions for the evaluation of profitability criteria of HRJ and CTH are described here, and the results are presented at the end of the chapter.
Last, the Conclusions summarizes the thesis work, major findings and suggestion for future work.

The author would like to express sincerest gratitude to prof. Sandeep Kumar (Old Dominion University) for his collaboration with University of Padova and sharing all information in preparing this work. Many thanks to Elena Barbera for her time, effort and support through the entire thesis work.

Chapter 1

BackGround & Alternative Renewable Jet Fuels

1.1 Background

1.1.1 Petroleum transportation fuels

Most of the energy consumed in the United States and worldwide is non-renewable, as it comes from fossil sources. Coal, petroleum, natural gas, and uranium are examples of non-renewable energy sources, and the U.S. energy consumption in 2016 was based on these for 89.3% of the total consumption, as shown in Figure 1.1 as reported by U.S. Energy Information Administration (EIA)[1]. These energy sources are called non-renewable because their supplies are limited.

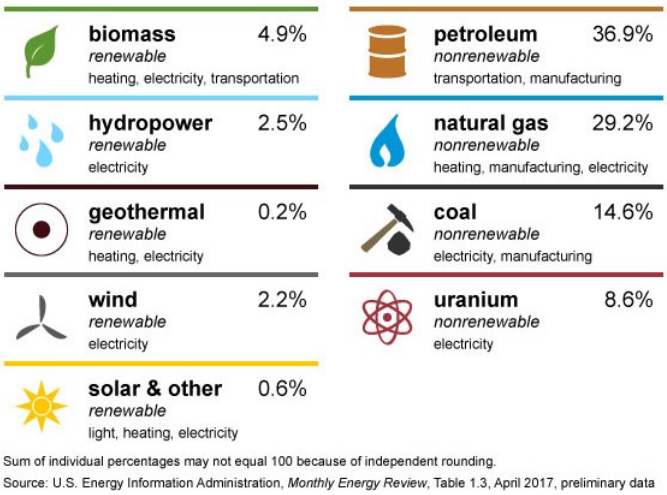

Figure 1.1: U.S energy consumption by source, 2016 (Energy Information Administration-EIA)

Petroleum is the main source of energy for transportation. In 2016, petroleum products provided about 92% of the total energy the U.S. transportation sector used, as pictured

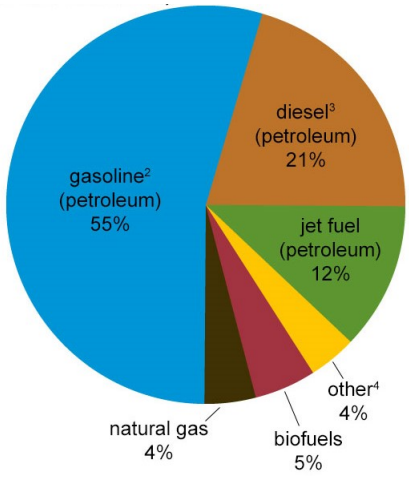

Figure 1.2: Transportation Energy Sources for 2016 (source EIA).

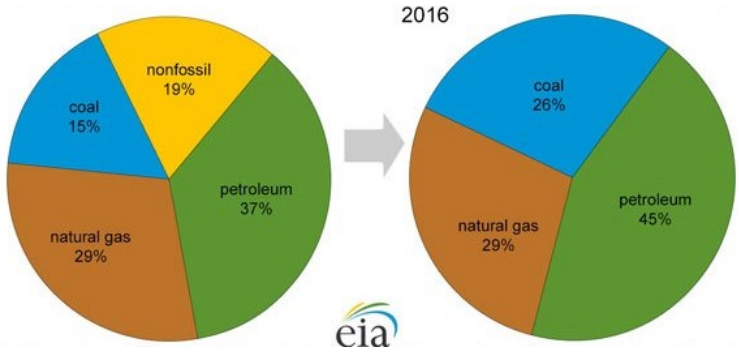

Figure 1.3: U.S Energy consumption and carbon dioxide emission by major fuel type in 2016 (source EIA).

in Figure 1.2. Biofuels, such as ethanol and biodiesel, contributed about to 5% only of the total energy the transportation sector used, while natural gas contributed to about 4%. Electricity provided less than 1% of the total energy used.
About half of U.S. energy-related CO_2 emissions are products from petroleum : specifically, in 2016, about 45% of them came from burning petroleum fuels, 29% from natural gas, and 28% from coal, as shown in Figure 1.3 [1]. Although the industrial sector is the largest consumer of energy (including direct fuel use and electricity purchased from the electric power sector), the transportation sector emits more CO_2 because of its near complete dependence on petroleum fuels.

1.1.2 Alternative and Renewable Jet fuels

For the reasons described above, in the latest years strong efforts have been directed towards the development of alternative and renewable fuels. At this day, no single alternative fuel technology or production pathway is able to satisfy the demand, both for technical and economic reasons. Nevertheless, the use of alternative fuels is strongly motivated by environmental issues and oscillating trends in petroleum prices. One of

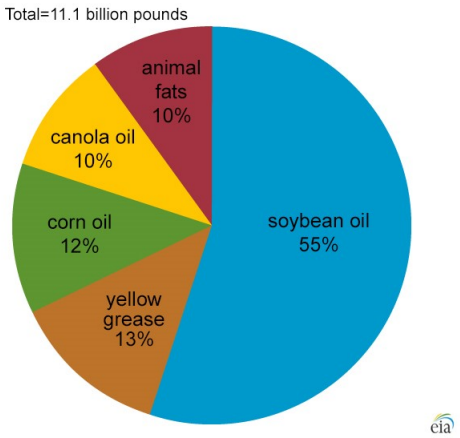

Figure 1.4: Raw materials for biodiesel production in the U.S.in 2016 (source EIA).

the main renewable fuel sources is biomass, especially for the production of liquid fuels. In particular, the development of bio-jet fuels is of tremendous interes in the aviation sector, which cannot rely on different types of fuel.
The U.S. government considers biofuels to be carbon-neutral because the plants that are the sources of the feedstocks for making biofuel, such as soybeans and palm oil trees, absorb carbon dioxide (CO_2) as they grow. The absorption of CO_2 by these plants offsets the CO_2 that is formed while making and burning the fuel.
Like biodiesel, also bio-Jet fuels are made from grain oils and animal fats. Generally speaking, oil-derived jet fuels compete with biodiesel and hydroprocessed renewable diesel for feedstock availability.
In 2016, soybean oil was the source of about 55% of the total feedstock (raw material) used to produce biodiesel in the United States. Canola oil and corn oil together account for about 22% of the bio-diesel feedstock, recycled grease about 13%, and animal fats about 10% of the total, as reported in Figure 1.4 by EIA [1].
Biofuels are nontoxic and biodegradable. Compared to petroleum fuels, which are refined from crude oil, biofuels combustion is claimed to produce fewer air pollutants such as particulates, sulfur dioxide, hydrocarbons, and air toxics [2].

1.1.3 Future Demand of Jet Fuel

An economic motivation for the production of bio-Jet fuels is the future demand of the products. According to U.S. Energy Information Administration (EIA), a significant increase is expected of the consumption of the Jet fuels in Organisation for Economic Co-operation and Development regions (OECD) with respect to that of gasoline or biodiesel by 2040, as shown in Figure 1.5 (EIA). Therefore, the conversion of biomass into Jet fuel rather than other biofuels could be more attractive for future investments. EIA predicts approximately 40% increase (7 to 11.5 quadrillion Btu) in jet fuel con-

sumption between 2015 and 2040 [1]. Furthermore, in its 2016 report, Air Transport Action Group (ATAG) [3] claimed that 278 billion liters of jet fuel was consumed by commercial operators leading to 781 million ton of CO_2 emission.

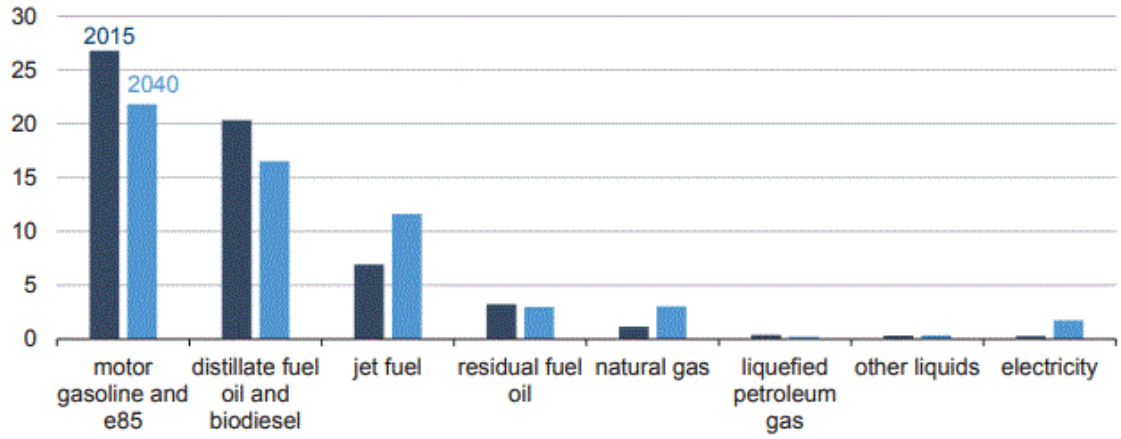

Figure 1.5: Future fuel consumption (quadrillion Btu) in OECD regions. In particular, the future demand of Jet fuels (EIA).

1.1.4 Recycling of Waste Cooking Oil (WCO)

Waste cooking oil mainly refers to frying oils used at high temperatures, edible fat mixed in kitchen waste and oily waste water directly discharged into the sewer. In the U.S. more than 2.5 billion gallons of used cooking oil is produced every year [4]. This has been found to be a major issue especially when it comes to disposal. Used cooking oil has always been considered as a waste and an environmental burden.
Moreover, the consumption of edible oil is expected to increase from 145 to 660 millions tons by 2050, and its disposal will pose enormous challenges [5]. Therefore, recycling waste cooking oil will allow to reduce the costs of waste-water treatment as well.
Some researchers have raised concerns for the potential interference of nutritional consumption of virgin fatty acids that are employed in the jet/diesel fuel production [6]. In view of this, there is a continuous research for non-edible oil as a feedstock for jet/diesel fuel. Few of the proved non-edible oils are jatropha, fatty acid distillates and microalgal lipids. Waste fats and oils are a good alternative source since they are largely cheaper than virgin oil, and a non-edible feedstock, which is therefore not in competition with food chain and do not create an additional demand for agricultural land.
Converting waste cooking oil into biofuel could represent a solution, dealing simultaneously with food and environmental security, in terms of damages of water, soil pollution, and Green House Gas (GHG) emissions.

1.2 Transportation fuels

1.2.1 LPG, Gasoline, Jet Fuel and Diesel

Transportation fuels are most liquid mixtures to facilitate handling. Motor gasoline, jet, and diesel fuels are hydrocarbon mixtures characterized by different physical properties. The molecular size of hydrocarbons affect the range at which they boil. In general, the longer the length of the carbon chain, the higher is the bolling point. The boiling point ranges of gasoline, jet fuel and diesel are summarized in Table 1.1 [7]. It can be seen that motor gasoline is the lightest liquid transportation fuel, followed by kerosene, and then diesel. Gasoline is made of hydrocarbons in approximately in the range of C4 - C12. Jet fuel is a bit heavier, with carbon atoms ranging from C9 to C15. Diesel fuel range is typically the one constituted by longer hydrocarbons from C9 to C24. It is worth noting that Diesel fuel includes a wider range of boiling points, including also those of Jet Fuel. Jet fuels have to respect stricter quality requirements compared to fuels used in road transport because Jet fuel is a type of aviation fuel designed specifically to power gas-turbine engines. It means that in operational conditions diesel engines can burn jet fuel without modification, but not the other way around.

Table 1.1: Boiling Point Ranges of Typical Oil Fraction [7].

Fraction	Boiling Point Ranges °C
Light and heavy naphtha - Gasoline	30-170
Kerosene - Jet Fuel	170-270
Light gas oil (LGO) - Diesel	270-320
Atmospheric gas oil (AGO)	320-426
Vacuum gas oil (VGO)	426-565
Vacuum reduced crude (VRC)	565+

1.2.2 Specifications of Kerosene based Jet Fuel

Figure 1.6 reports the jet fuel specifications of two typical jet fuels, for commercial (Jet A) and military aircrafts (JP-8). Commercial jet fuel Jet A is a civilian grade nearly identical to JP-8. In particular, one of the security specifications is the high flash point for the fire-hazard consideration. The standards for certifying aviation fuels are:

- ASTM D1655;
- International Air Transport Association Guidance Material (Kerosene Type);
- United Kingdom Ministry of Defence, Defence Standard (Def Stan) 91-91 (ONGC and Quality Control Laboratory 2008; Agusdinata, Zhao, et al. 2011;

- ASTM Specification D7566 (Standard Specification for Aviation Turbine Fuel Containing Synthesized Hydrocarbons);

In particular, the standard for alternative jet fuel is ASTMD7566 which lists the fuel properties and criteria required to control the production and quality of a renewable fuel for aviation safety (American Society for Testing and Materials 2013) [8].

	Jet A-1				JP-8
	ASTM D1655-04a	IATA	Def Stan 91-91	ASTM D7566	MIL-DTL-83133E specification
Acidity, Total (mg KOH/g)	0.1, max	0.015, max	0.012, max	0.1, max	0.015, max
Aromatics (vol%)	25, max	25, max	25, max	25, max (8, min)	25, max
Sulphur, Total (wt%)	0.3, max	0.3, max	0.3, max	0.3, max	0.3, max
Distillation Temperature:					
10% Recovery (°C)	205, max	205, max	205, max	205, max	205, max
20% Recovery (°C)	—	—	—	—	—
50% Recovery (°C)	—	—	—	— (15, min)	—
90% Recovery (°C)	—	—	—	— (40, min)	—
Final BP (°C)	300, max	300, max	300, max	300, max	300, max
Flash Point (°C)	38, min	38, min	38, min	38, min	38, min
Freezing Point (°C), max	-47	-47	-47	–40 Jet A ; –47 Jet A-1	-47
Viscosity @ -20°C (cSt)	8, max	8, max	8, max	8, max	8, max
Net Heat of Comb. (MJ/kg)	42.8, min	42.8, min	42.8, min	42.8, min	42.8, min
Density @ 15°C (kg/m3)	775-840	775-840	775-840	775-840	775-840

Figure 1.6: Jet Fuel Specifications [8].

The jet fuel cannot be blended with diesel; it is kerosene-based with specified carbon chain length, and has a relatively higher flash point due to fire-hazard consideration and relatively lower freeze point to ensure good cold flow properties at high altitude.

1.3 Conventional bio-Jet Fuel production process

1.3.1 Hydroprocessed Renewable Jet Fuel (HRJ)

Different technologies exist in literature that can convert biomass into Jet fuels, whether at the research and development, demonstration or commercial stages: they include alcohol-to-Jet (ATJ), oil-to-Jet (OTJ), gas-to-jet (GTJ) and sugar-to-Jet (STJ) processes. Most of the literature has been focused on approved technologies, such as Fischer-Tropsch (FT) synthesis and Hydroprocessed Renewable Jet (HRJ) processes. The ATJ or STJ processes are still at the development stage, therefore only a few references are available in the literature. On the other hand, the HRJ conversion technology is at a relatively high maturity level and is already commercially available. More details on other conversion technologies can be found in the works of Wang et al. and Berzegianni et al. [8, 9]. Therefore, in this study as a matter of simplifying we will refer to the HRJ as a Conventional jet fuel process.

In the HRJ production process, the oil-based feedstocks are converted into bio-jet fuels through hydroprocessing technologies, including hydrotreating, deoxygenation, isomerization and hydrocracking.
These bio-jet fuels are chemically equivalent to petroleum fuels and their production, storage, distribution are compatible with existing refinery infrastructure. Moreover, additional benefits include potentially lower greenhouse gas emissions (GHG) if a renewable feedstock such as Waste Cooking Oil (WCO) is used.

1.3.2 Triglycerides

Triglycerides make up the structure of all vegetable oils and fats found in nature. They are primarily composed of long chains of fatty acid esters. The side chains of triglycerides are either saturated, monounsaturated or polyunsaturated. They can be classified by the length and saturation degree of their side chains, for example C18:1 has 18 atoms of carbon and 1 unsaturated bond. The acid portion of the ester linkage (fatty acids) usually contains an even number of carbon atoms in a linear chain of 12 to 24 carbon atoms with up to three unsaturated bonds. Usually the position of unsaturated bonds are 9, 12 such as in linoleic oil C18:2 [10].
The vegetable oil composition is commonly described by its content of fatty acids as summarized in Table 1.2 for palm, canola, jatropha, soybean, sunflower and waste cooking oils.
When processing vegetable oils, the fatty acid profile is important. Long-chain oils can be broken down to small molecules to produce jet fuels, but the overall yield will be reduced while increasing the production of co-products such as diesel. If starting from small molecules, the target jet product yield will be high with fewer co-products. There is a trade-off between main product (jet fuel) and value-added co-product ratios.
More hydrogen supply is required when a higher amount of unsaturated fatty acids is present in the oil. Vegetable oils, waste cooking oil, and algal oil are in the diesel fuel range C16-C22. Moreover, oleic acid (C18:1) is predominant in vegetable oils, whereas algal oil contains significant amount of C22.
The hydrogen requirement was estimated by Pei Lin Chu et al. [11] for different oils (including main as soybean, used cooking oil, palm, rapeseed, jatropha) for the same operating conditions. These authors found that the overall performance of the process based on different oil composition, such as thermal energy consumption, was significantly lower for the process with used cooking oil rather than based on the virgin oil, owing to the additional energy demand required for oil extraction.

Table 1.2: Typical composition of vegetable oils, taken from [8]

	Palm	Rapeseed	Soybean	Jatropha	Camelina	Algal	Waste cooking
profile	%	%	%	%	%	%	%
C14:0	0.5-2	0-1	0	0.5-1	0	10	1
C16:1	0	0	0	0	0	21	5
C18:0	2-7	0.4-3	2-6	5-10	3	0	9
C18:1	38-52	22-60	22-34	37-63	17	5	53
C18:2	0	12-14	43-56	19-41	23	0	14
C18:3	5-11	5-7	5-11	0	31	0	1
C18:4	0	0	0	0	0	6	0
C20:0	0	3-5	0	0.3	0	0	0.1
C20:1	0	0-1	0	0	12	0	1
C20:5	0	1	2	3	4	23	0
C22:0	0	0-3	0	0	0	0	0.03
C22:1	0	0-5	0	0	3	0	0.07
C22:6	0	0	0	0	0	8	0
C24:0	0	0-3	0	0	0	0	0.04

1.3.3 Process description

HRJ fuel is produced in two stages. The first one uses hydrogen gas and hydrotreating catalyst to saturate double bonds of the unsaturated oil, cleave the propane backbone from the triglycerides and therefore, remove oxygen from the feed. The second stage, known as isomerization and cracking, isomerizes the paraffinic molecules and reduces the molecular chain lengths to improve liquid properties, such as cold weather flow and the flash point.

The chemical route of HRJ process is shown in Figure 1.7. The first stage of the process includes a set of chemical reactions. In a first step the double bonds of the triglyceride are saturated with hydrogen over the hydrotreating catalyst. Next, the propane backbone is cleaved from the molecule, leaving three long fatty acid chains. Finally, the oxygen is removed from the fatty acid molecules on the metal sites of the catalyst [12].

The oxygen removal occurs via two pathways. One reaction forms H_2O and is called hydrodeoxygenation. The other pathways to remove oxygen in the form of CO_2 or CO are generally known as decarboxylation. Some authors prefer to define the CO removal as decarbonilation instead of using the more general definition. In particular, the hydrodeoxygenation reaction requires higher amount of moles of hydrogen gas than decarboxylation, because of the formation of water molecules. The hydrotreating stage leads to the production of C15-C18 hydrocarbons, i.e. a liquid mixture within the boiling point range of diesel, which is commonly called âgreen dieselâ or renewable diesel.

The second step takes the straight carbon chains (paraffins) and rearranges them into

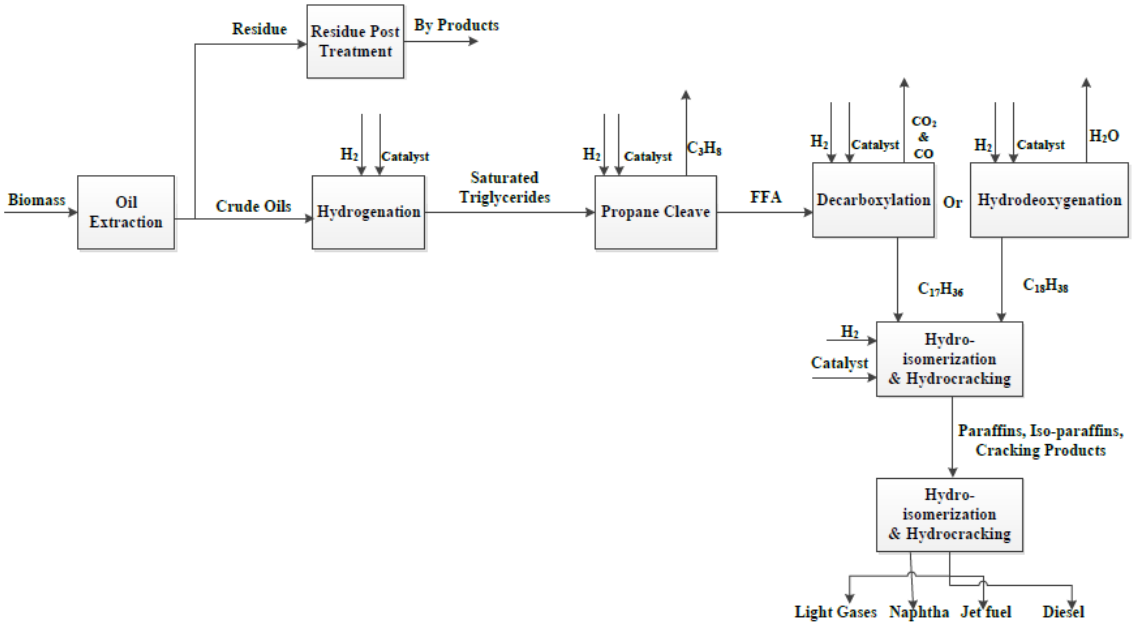

Figure 1.7: Chemical Route in the HRJ process: from triglyceride to paraffinic and Iso-paraffinic hydrocarbons [8].

branched structures, i.e. iso-paraffines.Therefore, the renewable oil is converted from an unsaturated triglyceride to the final product of saturated hydrocarbons. The resulting product of the second stage is a mixture of different boiling point ranges products, including naphta, kerosene and diesel. In particular, the naphta and kerosene ranges are derived from hydrocracking reactions occuring in the second stage.
As an example, a triolein molecule (characterized by 3C18:1 fatty acids) hydroconversion into hydrocarbons, $C_{17}H_{36}$ and $C_{18}H_{38}$, by decarboxylation, decarbonilation and hydrodeoxygenation paths is illustrated in Figure 1.8. It can be noted how the three reaction pathways require different amounts of hydrogen for each mole of fatty acid, i.e. zero for decarboxylation, one for decarbonilation and three for hydrodeoxygenation.

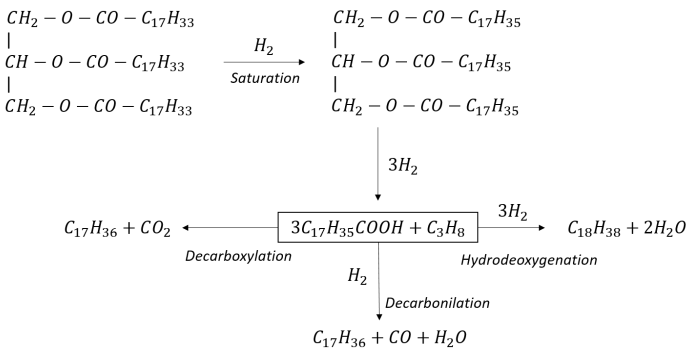

Figure 1.8: Triolein hydroconversion reactions: decarbonilation, decarboxylation and hydrodeoxygenation paths.

1.3.4 Hydrotreating Catalyst

As it was seen in the previous section, the selectivity of the catalyst used in the process may determine hydrogen consumption, favoring one reaction pathway over another. A number of different catalysts have been studied over the last decades. The most commonly used aree sulfiding bimetallic catalyst such as $NiMo/\gamma Al_2O_3$ and $CoMo/\gamma Al_2O_3$. However, other catalysts based on Pt and Pd metals have been also investigated. The catalyst based on Nichel, Molybdenum and Cobalt metals are characterized by a selectivity towards the decarboxylation route, which reduces capital and operating expenses resulting from extra hydrogen production. Whereas, noble based catalysts, such as Palladium and Platinum, determine longer chain molecules ($C_{18}H_{38}$) and less CO and CO_2 emissions, by leading to hydrodeoxygenation reaction path.
In the literature there are many excellent works focused on the effect of different types of catalyst and process conditions on process performances and product yield [13, 14, 15, 16]. In particular, the reviews from Boyas et al. [17], Bezergianni et al. [9] and Kumar et al. [18] review the effects of operating conditions, the catalyst and the feedstock on the final product distribution of hydrotreating process.
In most cases, the extent of both pathways (hydrodeoxygenation and decarboxylation) is elucidated from the liquid hydrocarbon distributions, so that knowing the value of the C17/C18 ratio is a common way to determine the dominant path of the reaction. The product distribution is also influenced by the reaction pressure since at a high hydrogen pressure the hydrodeoxygenation will be the preferred pathway. On the other hand, at a lower hydrogen pressure the decarboxylation reaction will be enhanced. Thus, the CO_2/CO ratio in the product distribution is also used to determine the selectivity towards decarboxylation/decarbonilation reactions.

1.3.5 UOP/ENI Ecofining Hydroprocessed Jet Fuel process

Uop Honeywell Co. with decades of experience in refining technology now is offering in collaboration with ENI an alternative process to produce renewable diesel and jet fuel based on biofeedstocks. The technology for converting fats and oils to fuels has evolved from petroleum refining, as the same units for the desulfurization (HDS) process are used. In addition, the operation of renewable feedstock in hydrotreating unit requires same operating conditions at high hydrogen pressure and temperature. The main difference consist on the amount of hydrogen required for the reaction, which is higher for biofeedstock, determined by the larger amount of oxygen than sulfur in the petroleum crude oil.
The process is based on the hydrotreating catalyst, which results in deoxygenation via hydrodeoxygenation and decarboxylation reactions in hydrotreating unit (R1) and a

hydrocracking/isomerization unit (R2) to obtain a synthethic paraffinic kerosene with carbon distribution of C9-C15, as illustrated in a block diagram in Figure 1.9 [12, 19]. The isomerization is necessary to obtain specifications of Jet fuel also, in particular the low freeze point.
The conversion of the feed in R1 is complete (100%) and full deoxygenation is performed [12]. The isomerization reaction is also selective and consequently, little amount of hydrogen is needed. Make up hydrogen is added for process losses and reaction consumption. The developed Ecofining process has started to be commercialized recently

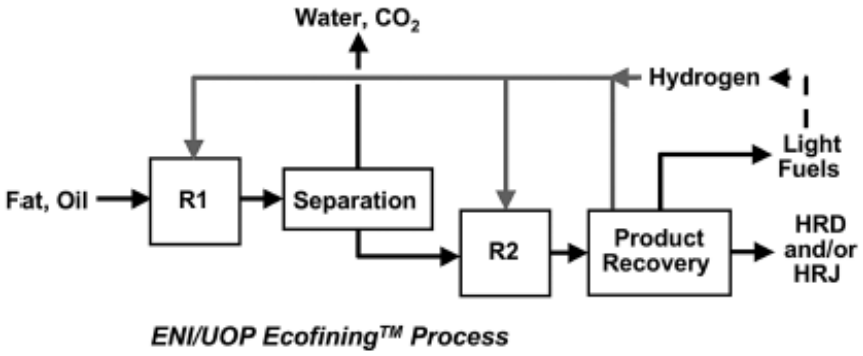

Figure 1.9: UOP/ENI Ecofining process for the production of HRD or HRJ.

[12], and in a life cycle analysis, UOP/ENI reported that the renewable diesel produced by the Ecofining process is economically competitive with biodiesel production [20].
In Chapter 2, the simulation of HRJ, so called Conventional process, will be based on this block diagram and information from literature. Therefore, more detailed information about this process will be addressed in Chapter 2.

1.4 Bio-Jet Fuels via Catalytic Transfer Hydrogenation

1.4.1 Catalytic Transfer Hydrogenation

Catalytic Transfer Hydrogenation is a process where the reduction of multiple bonds is achieved with the aid of organic molecules that serv as hydrogen donors e in the presence of a catalyst. The hydrogen transfer reactions can be realized in principle by means of thermal degradation, or by homogeneous or heterogeneous catalysis. The reaction of hydrogen transfer as Eq. (1.1) with the aid of catalyst and solvent can be generalized to an acceptor A:

$$DH_x + nA \rightarrow nAH_x + D \tag{1.1}$$

The donor DHx can be any organic compound, whose oxidation potential is sufficiently

low so that the hydrogen transfer can occur under mild conditions. At higher temperatures, especially in the presence of catalysts, almost any organic compound can donate hydrogen (catalytic cracking), but this has little potential for controlled synthesis [21]. Many organics and alcohols can be used as hydrogen donor solvents. The difficulty consist in understanding if the donation of different solvent is the effect of participation of the donor in the hydrogen step or whether the difference simply reflects the ease of dehydrogenation of the various solvents. The former is more likely being inferred from the fact that if the solvent is left for some hours in the same conditions, without an acceptor, the solvent is in many cases completely dehydrogenated [21].
The temperature is the critical variable of the catalytic transfer hydrogenation. At higher temperatures, in the range of 300-350°C, the hydrogenation donation becomes more critical, in general in such conditions aromatic molecules are formed since the dehydrogenation step is more favored rather than the hydrogenation one.
Many studies have been reported in the literature for different systems of acceptors, catalysts and solvents. An old but not obsolete review on this subject is the one by Brieger et al. [21] where all works from other authors are well summarized.

1.4.2 Hydrogen donor

The choice of donor is determined by the ease of reaction and other advantages such as availability and safety. Formic acid and propanol are amongst the most popular solvents to be employed in catalytic transfer hydrogenation.
Formic acid exhibits two parallel pathways depending on the catalyst used, i.e. decarboxylation (desired) Eq. (1.2) and dehydration Eq. (1.3):

$$HCOOH \rightarrow CO_2 + H_2 \tag{1.2}$$

$$HCOOH \rightarrow CO + H_2O \tag{1.3}$$

While formic acid and propanol are low hydrogen storage media (4.3 wt% and 13.3 wt%, respectively), still these are among the best liquids for hydrogen storage and transport. Moreover, formic acid and propanol can be obtained from renewable sources. In fact, formic acid can be produced by aqueous catalytic partial oxidation biomass and alcohols by fermentation. In catalytic transfer hydrogen process of this study a 2-propanol (iso-propanol) solvent will be considered since it contains more hydrogen (13.3 %w) and it is safer to handle than formic acid. In addition, 2-propanol solvent seemed to be promising since has better jet fuel yields as was found in the performance analysis of different solvents by S.Kumar laboratory [22].

1.4.3 Motivation

In the Hydroprocessed Renewable Jet (HRJ) fuel process, the use of hydrogen gas has different impacts on the safety and the environment. In the other alternative Jet fuel pathways, hydrogen remains a key input, needed for almost all of them, such as Fischer-Tropsch conversion to synthetic paraffinic kerosene (FT-SPK).
The principal motivation of developing CTH process respect to the HRJ process is the reduction of greenhouse gases (GHG). The Steam Methane Reforming (SMR) plant as a commercial technology for the production of hydrogen releases large high amount of CO_2 as a waste product of reforming reactions. Moreover, hydrogen is not readily soluble in liquid components, leading to a diffusion-limited process, so that the excess of hydrogen and stronger process conditions are required for the process. In particular, the operating pressures is typically increased up to an order of 10 MPa to enhance the reaction rates. This operating conditions increase the capital costs of equipment and the hazards related to the storage and transportation of hydrogen gas.
In addition, HRJ process use sulfided catalysts, which require toxic material (H_2S) for catalyst activation during the start-up.
All the aforementioned challenges can be avoided by Catalytic Transfer Hydrogen since it applies an alternative hydrogen source without the necessity of using it.

1.5 Aim of the thesis

The scope of the thesis consist on the process simulation and techno-economic analysis of two processes to produce Jet fuel from a renewable waste cooking oil feedstock: Hydroprocessed Renewable from the Ecofining technology, which have been recently commercialized, and Catalytic Transfer Hydrogenation, in stage of research. In particular, Catalytic Transfer Hydrogenation process will be built from experimental data generated at Dr. Sandeep Kumarâs ODU laboratory. Two processes have to be compared in terms of the results of process simulation and by profitability economic analysis.

Chapter 2

Process Simulation

The process modelling of Conventional Jet Fuel and Catalytic Transfer Hydrogenation is described in two independent parts in the following chapter. The feed considered is a Wasting Cooking Oil (WCO) with the composition provided by S.Kumar [22]. In order to determine the amount of products and the energy consumption, a base case process simulation was developed in Aspen Plus, which comprises reaction system, separation of products, recycle and heat integration. All decisions and assumptions for the modelling of all the units are described in detail. The performance of both of the two processes are compared in Results of Simulation. Final process flow diagrams (PFD), referenced throughout the text, are attached at the end of the chapter.

2.1 Conventional Jet fuel process

2.1.1 Block diagram

The synthesis of Green Jet fuel process is based on UOP-Eni Ecofining process block diagram, where the distillate products are obtained through two reaction systems and intermediate separation of by-products, presented in Figure 2.1 [23]. Many types of feedstock might be processed, including Vegetable Oils, Animal Fats and Greases. In the first reaction system, the feedstock is fed with hydrogen to the hydrodeoxygenation reactor in order to produce n-Alkanes based on fatty acid composition, type of catalyst and operating conditions. By-products from the parallel reactions (CO, CO_2, H_2O) are separated in the flash drum, operated at the reaction pressure. The gaseous stream is a mixture of non-reacted hydrogen, CO_2 and CO. The liquid is immiscible mixture of organic liquid and water

In the second stage, the liquid phase product is isomerized and cracked in the presence of hydrogen in a hydrocracking reactor. This step is necessary to obtain a kerosene boiling range and Jet Fuel requirements. Light fuels and, if present residual diesel, are the valuable by-products. The latter might be recycled to increase Jet Fuel production

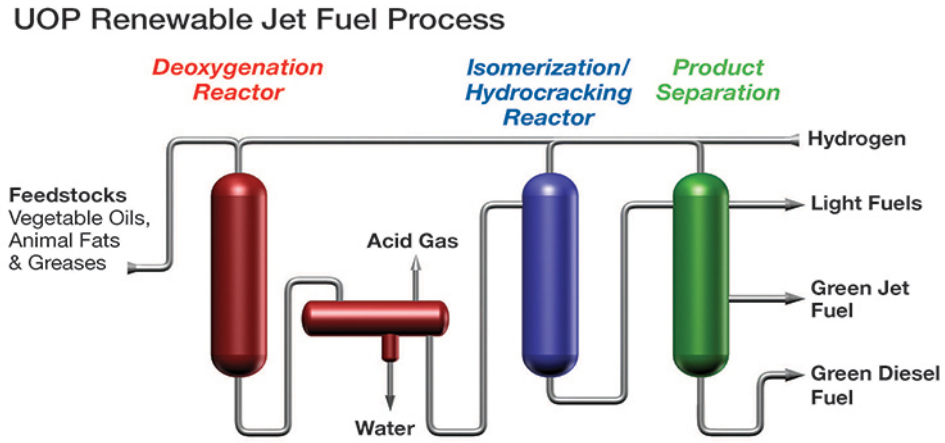

Figure 2.1: UOP Renewable Jet Fuel process scheme.

or directly sold if its market value is high.

2.1.2 Feed basis and composition of waste cooking oil (WCO)

The feed flowrate of waste cooking oil (WCO) for the process is 1000 ton/day. Hydrogen to feed ratio may vary between 2-4 %w depending on degree of unsaturated bonds. A ratio of 2.6 %w/w is assumed in our case, based on the data from Pei Lin Chu et al. for a similar feed [11].The composition of fatty acids in the WCO is shown in Table 2.1, where the number of unsaturated bonds is specified after the length of the carbon chain: for example, C18:1 indicates a fatty acid with 18 atoms of carbon and 1 unsaturated bond. The given composition is normalized to get the sum of 100% of fatty acids.

Table 2.1: WCO composition

	Data % w/w	Normalized % w/w
C18:1	0.176	0.186
C18:2	0.496	0.523
C15:0	0.17	0.179
C19:0	0.107	0.113
Others	0.052	
Total	1.000	1.000

2.1.3 Hydrodeoxygenation Reaction System (HDO)

The hydrodeoxygenation reactor is modelled as an RStoich model defining the conversion of decarboxylation (R.1, R.4, R.7, R.10), decarbonilation (R.2, R.5, R.8, R.11) and hydrodeoxygenation (R.3, R.6, R.9, R.12) reactions for given species in the feed (see Table 2.2). The overall consumption of hydrogen in the HDO reactor is determined by the:

(a) Hydrogenation of double bonds of unsaturated fatty acids;

(b) Scission of 1 propane from glycerol backbone triglyceride molecule: $3H_2$ for each triglyceride;

(c) Decarnobilation /decarboxylation (DCO) and hydrodeoxygenation (HDO) reactions with fatty acids;

(d) Water-Gas Shift (WGS), R.13 in Table 2.2, and Methanation (METH) reactions.

Table 2.2: HDO reactions stoichiometry

R.1	C18:1 + H_2 = C_{17} H_{36} + CO_2
R.2	C18:1 + 2 H_2 = C_{17} H_{36} + CO + H_2O
R.3	C18:1 + 4 H_2 = C_{18} H_{38} + $2H_2O$
R.4	C18:2 + 2 H_2 = C_{17} H_{36} + CO_2
R.5	C18:2 + 3 H_2 = C_{17} H_{36} + CO+ H_2O
R.6	C18:2 + 5 H_2 = C_{18} H_{38} + $2H_2O$
R.7	C15:0 = C_{14} H_{30} + CO_2
R.8	C15:0 + H_2 = C_{14} H_{30} + CO + H_2O
R.9	C15:0 + 3 H_2 = C_{15} H_{32} + $2H_2O$
R.10	C19:0 = C_{18} H_{38} + CO_2
R.11	C19:0 + H_2 = C_{18} H_{38} + CO + H_2O
R.12	C19:0 + 3 H_2 = C_{19} H_{40} + $2H_2O$
R.13	CO + H_2 O $\leftrightarrow$ CO_2 + H_2

The conversion of HDO is based on data from Veriansyah et al. [24] at 400 °C, 9.2 MPa and 2h of reaction time with Nickel-Molybdenum (NiMo) catalyst. In Table 2.3, all experimental information from Veriansyah et al. are managed. NiMo catalyst is the mostly used in commercial hydrotreating units due to comparable performance with other metals and the cost of production, which is significantly lower than the one based on platinum (Pt)/palladium (Pb), as it can be seen in Table 2.4.

Table 2.3: HDO reaction variables based on NiMo/γ-Al_2O_3 catalyst from Veriansyah et al. [24]

Reaction Variable	value	units
Pressure	9.2	MPa
Temperature	400	°C
Residence Time	2	hr
Loading NiO/MoO_3	2.4%/11.8%	wt%
HDO/DCO	0.29	-
CO_2/CO	22.7	-
Conversion	100	-

In total, 12 reactions are specified, that take into account the complete hydrogenation of unsaturated bonds. The conversion of HDO and DCO reactions is determined taking into account experimental C17/C18 and CO/CO_2 ratios since they indicate the

Table 2.4: Metal price in January 2018. [25]

Metal	price (Jan 2018)	
Nichel	13.3	$/kg
Molybdenum oxide	16	$/kg
Cobalt	81.5	$/kg
Palladium	33,330	$/kg
Platinum	32,240	$/kg

preferable reaction route (see section 1.3.4). Thus, the conversion of WCO is equal to 0.68 for decarboxylation, 0.03 for decarbonilation and 0.29 for hydrodeoxygenation, determining overall full fatty acid conversion.
In the modelling, also the consumption of hydrogen for scission of propane from triglyceride is considered, for the reason that WCO is characterized with model compounds of fatty acids. The overall hydrogen consumption and propane formation are based on stoichiometric relation of reaction b (see Chapter 1) and they are calculated in Table 2.5. Thus accordingly, in the outlet stream from the HDO reactor propane C_3H_8 SEP blocks (see H2TRYG Sep block, PFD).

Table 2.5: Trygliceride scission: hydrogen for reaction and formation of propane.

Trygliceride scission	**Mole (kmol/day)**	**Mass (ton/day)**
Fatty acids formed	3.64	1000
Propane formed	1.21	53.45
Hydrogen consumed	3.64	7.33

The products in the gas phase (CO, CO_2, H_2, H_2O) may give rise to WGS and METH reactions which may additionally consume hydrogen, as it was noted in reaction d. However, in Veriansyah et al. experimental analysis of gaseous products METH reaction over Ni-Mo catalyst was not observed. Hence, only WGS reaction is considered by an adding an REquil module which was used to estimate the equilibrium reaction in the gas phase (see WGS-HDO block, PFD). The reaction input is the WGS equilibrium (R.13) at the same process condition (400 °C and 9.2 MPa).
Table 2.6 summarizes all the process input and models used for the simulation of HDO reactor.

2.1.4 Separation of by-products of HDO reactor

The product stream of HDO reactor is a mixed phase at 400°C and 9.2 MPa. The product phase distribution can be seen in Appendix B (Stream Table). A high-pressure flash can be used to separate gaseous and liquid phase products (see By-P-Sep block, in the PFD). At lower temperatures, 100% of hydrocarbon recovery is achievable in the liquid phase. Moreover, the two liquid phases (water and hydrocarbons) become

Table 2.6: HDO reactor input in Aspen Plus

Process input - HDO reactor	
Pressure (MPa)	9.2
Temperature (°C)	400
Conversion X of decarboxylation	0.68
Conversion X of decarbonilation	0.03
Conversion X of hydrodeoxygenation	0.29
Aspen models used	RStoich (R.1-R.12) + REquil (R.13) + Sep (Trygliceride deg.)
Property method	Peng-Robinson

completely immiscible at 40°C and 9.2 MPa. Therefore, complete separation of water, organic liquid and gaseous products (CO_2, CO, H_2) is performed in a 3 phase equilibrium (Vapor-Liquid-Dirty water) flash as indicated in the stream table in Appendix B. Table 2.7 summarizes process inputs of 3 phase separation of by products.

Table 2.7: By products separation from HDO reactor: input parameters in Aspen Plus.

Process input By-P-SEP	
Pressure MPa	9.2
Duty Q (adiabatic operation) kW	0
Valid phases	Vapor-Liquid-Dirty Water
Aspen model used	Flash
Property method	Peng-Robinson

2.1.5 Catalytic Hydrocracking Reaction System (HCC)

After separation, the organic liquid is then isomerized/cracked to get smaller chains of iso-paraffines (HCC block, PFD). A conventional hydrocracking unit operation may vary between 300 °C to 450°C, with hydrogen pressure from 7.0 to 20 MPa, depending on the severity of the process. Conventional hydrocracking conversions are kept between 30-70% per pass to achieve good selectivity to naphta and middle distillates. Nevertheless, mild conditions are assumed, i.e. 350°C and 9.0 MPa (so called Mild Hydrocracking) for the reason that properties of the feed are those of a very light oil compared to a conventional vacuum gas oil (VGO), as shown in Table 2.8 [26] [27].

Table 2.8: Property of feed oil to hydrocracking unit. comparison between conventional VGO and study case oil.

Feed property	**Stream HC-MIX**	**VGO**
°API gravity	63	22.3
SG specific gravity	0.72	0.92
TBP °C	270-340	450-570
Watson factor Kw	13	10

Table 2.9: Hydrogen requirement for hydrocracking reactions

HCC variable	**Value**	**Unit**
Hydrogen / Oil	500	scf/bbl
Hydrogen / Oil	84.44	Nm^3 /m^3
Oil feed rate	63	m^3 /hr
H_2 density (STD)	0.0887	kg/m^3
STD Volume H_2	5320	m^3 /hr
Mass H_2	471.9	kg/hr

The operation of the hydrocracking unit is very flexible depending on the hydrogen to feed ratio, which is determined by the feedstock and the desired product distribution. In particular, an approximation of hydrogen requirement for the reaction can be estimated by the feed characterization factor Kw, API gravity and desired naphta fraction in the reactor product. From the properties given in Table 2.8 of oil (stream HC-mix, see PFD) it was estimated that a 500 scf/bbl (84.44 Nm^3H_2/m^3_{oil}) is required for the reaction with a minimum of 20-25 %vol production of Naphta [7]. In Table 2.9, the hydrogen required for hydrocracking reactions is summarized.

It is noteworthy that, hydrogen is typically fed in large excess to absorb the heat of reaction by direct quench at different stages of the reactor. Therefore, a higher amount of inert hydrogen is required in the reactor depending on the heat produced. The amount of hydrogen required for quench is estimated through an energy balance to keep the difference between inlet and outlet of reactor in the maximum range of 25°C of temperature. The modelling of the cracking reaction system is complex because of extremely high number of parallel and consecutive reactions. Hence, a Gibbs Reactor model is assumed for the hydrocracking unit. The products considered in the evaluation of Gibbs reactor are all kinds of hydrocarbon molecules from C1 to C18, including all isomers available in Aspen data base, for a total number of 358 components. This approach based on chemical equilibrium of components for material and energy balance was justified since the product distribution obtained was similar to empirical yields found in literature: 5 -9 %w LPG, 20-30 %vol of Naphta and 70-80 %vol of Kerosene in the liquid distillates [7, 11, 28, 29].

Process input parameters of HCC unit in Aspen Plus are given in Table 2.10. In

Table 2.10: Process input of hydrocracking unit HCC

Process input - HCC reactor	Value
Pressure MPa	9
Duty Q (adiabatic operation) kW	0
Hydrogen consumption kg/hr	472
Inert fraction of hydrogen	0.64
Products Included	All components from C1-C18 (including isomers)
Aspen model used	RGibbs
Property method	Peng-Robinson

particular, an adiabatic operation is specified. It has to be noted that the excess of hydrogen is modelled in Gibbs Reactor by means of the inert fraction of hydrogen. The inert fraction is calculated as hydrogen required for quench divided by total hydrogen in the inlet stream. This procedure will allow to consider into chemical equilibrium calculations only the amount of hydrogen used for the reaction, i.e. 472 kg/hr.

2.1.6 Recovery of Hydrogen and Recycle Pressure

Hydrogen is a valuable reagent and maximum recovery from the gaseous streams is required. Because it needs to be re-compressed up to 9.2 MPa, the influence of recovery pressure is crucial for overall process economics. In the process scheme, the make-up H_2 is compressed in the unit C-2 up to the pressure of the recycled stream. Then, the two hydrogen streams are mixed and compressed to the final pressure in the unit C-1. The hydrogen to be recycled comes from two streams (ACID GAS stream, V- HP stream, see PFD); the composition of the both determines the appropriate technology for the recovery. In the first one (intermediate HDO by-product separation), the gas mixture is characterized by large amount of CO_2 and CO, while the second mixture (from recovery of unconverted hydrogen from hydrocracking unit) comprises hydrogen and light hydrocarbons, as it can be seen in Stream Table of Appendix B. Processes to separate hydrogen from gas mixture of CO, CO_2, and light hydrocarbons, such as CH_4,C_2H_6, C_3H_8, are Pressure Swing Adsorption (PSA) and Membrane Technology. Both of them are characterized by high hydrogen purity and recovery. PSA is well developed and commercially applied, while Membranes is a novel technology and it is less advantageous in terms of economy of scale [30]. The adsorbents of PSA are normally made of molecular sieve/activated carbon/silica gel, depending on the specific application. Hydrogen is less adsorbed at high pressure than other components, as shown in Figure 2.2; so that, high pressure hydrogen is recovered. In this process, PSA is a conventional unit applied for the recovery of hydrogen.

Although PSA unit is not rigorously modelled (PSA-A and PSA-B SEP block, see PFD), its typical operating pressure is in a range of 1.0-4.0 MPa at room temperature

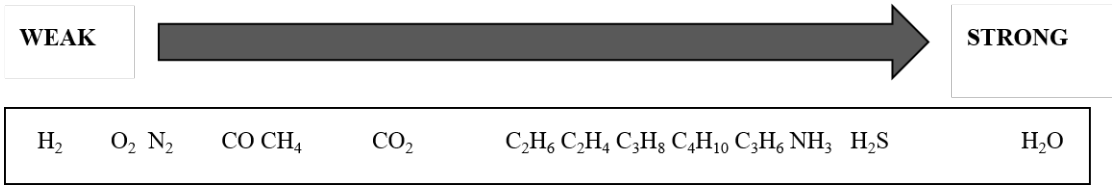

Figure 2.2: Degree of adsorption of components in PSA.

with 4 parallel beds for continuous operations [31]. Recently, higher pressure recovery is also applied, with 12-16 of pressure equalizations beds [23, 28]. The recovery at high pressure will be advantageous in terms of less compression load for the recycle of hydrogen. Nevertheless, large capital costs and efficient optimization of beds configuration are required. Therefore, we selected typical operation of 4 MPa of pressure as the base case.

It has to be noted that PSA-A and PSA-B are separated blocks in simulation (see PFD), in spite of that, they represent 1 unit of PSA for the recovery of hydrogen. As well, it has to be noted that to get to a pressure of 9.2 MPa multistage compression is required. The compression ratio takes into account the final temperature of each stage, which should not exceed approximately 225°C for H_2 that equals compression ratio of 4. An inter-stage cooling duty is estimated assuming a cooling water utility at available at 40°C.

Table 2.11 reports all inputs for PSA and multistage compressor in Aspen Plus. It is noted that a ratio of 3.4 is required for multistage compressor to get from 0.1 to 4.0 MPa.

Table 2.11: Process input of PSA and multistage compressor in Aspen Plus.

Process input PSA-A/B, C1 and C2	Value
Pressure PSA-A/B MPa	4
Outlet Pressure C1 MPa	9.2
Outlet Pressure C2 MPa	4
Number of stages C1	1
Number of stages C2	3 (Ratio=3.4)
Inter-stage Temperature C2 °C	40
Aspen model PSA used	SEP
Aspen model C1/C2 used	Multistage C
Property method	Peng-Robinson

2.1.7 Heat Integration and Design of the Heat Exchanger Network (HEN)

The integration of heat duties to minimize the thermal energy consumption is performed by means of pinch analysis. The inventory streams to be heated or cooled is reported in Table 2.12. For clarity, they are divided into two groups, hydrodeoxygenation and hydrocracking. However, the integration is performed over the whole process, including heat produced in the HDO reactor (which is exothermic). Hence, it is assumed an ideal isothermal operation of reactor. It is noted that the heat duty produced in the hydrodeoxygenation reactor is a net value that takes into account also the preheating of hydrogen from 157°C to 400°C (i.e. the reaction temperature). The heat produced from WGS reaction is instead negligible and it is not considered within the pinch analysis.

Table 2.12: Streams properties for the heat integration analysis.

Hydrodeoxygenation	Tin °C	Tout °C	Flow rate (ton/day)	M Cp (kJ /C hr)	Energy (kW)
Preheat H2	157	400	26	15815	1068
Preheat WCO	25	400	1000	105332	10972
Heat produced HDO	157(H_2) / 400(WCO)	400	1026	-	-5235
HDO preheat of H2	400	400	1026		-4168
Heat production WGS	-	-	1026	-	137
Cooling HDO	400	40	1026	128929	-12893
Hydrocracking	Tin °C	Tout °C	Flow rate(ton/day)	MCp(kJ/Chr)	Energy (kW)
Preheat HCC	59	350	911	114964	9293
Cooling HCC	350	40	931	124702	-10738

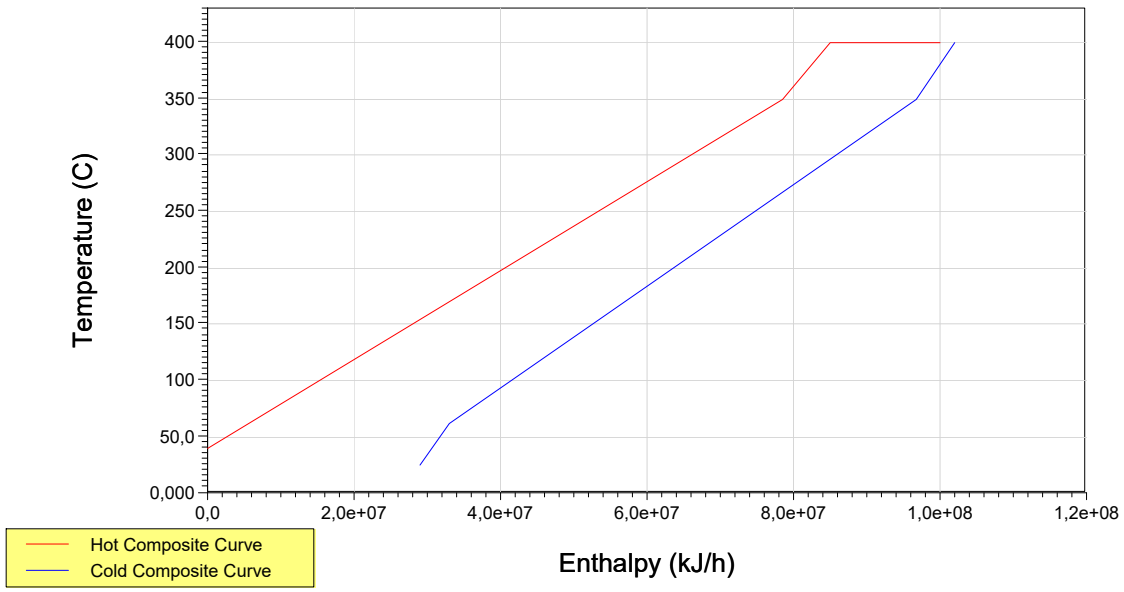

Figure 2.3: Composite curves of hot and cold streams.

The composite curve resulting from the pinch analysis is shown in Figure 2.3 considering a minimum temperature difference ΔTmin equal to 20°C. In particular, the straight

part of the line represents the heat produced in HDO reactor at constant temperature.

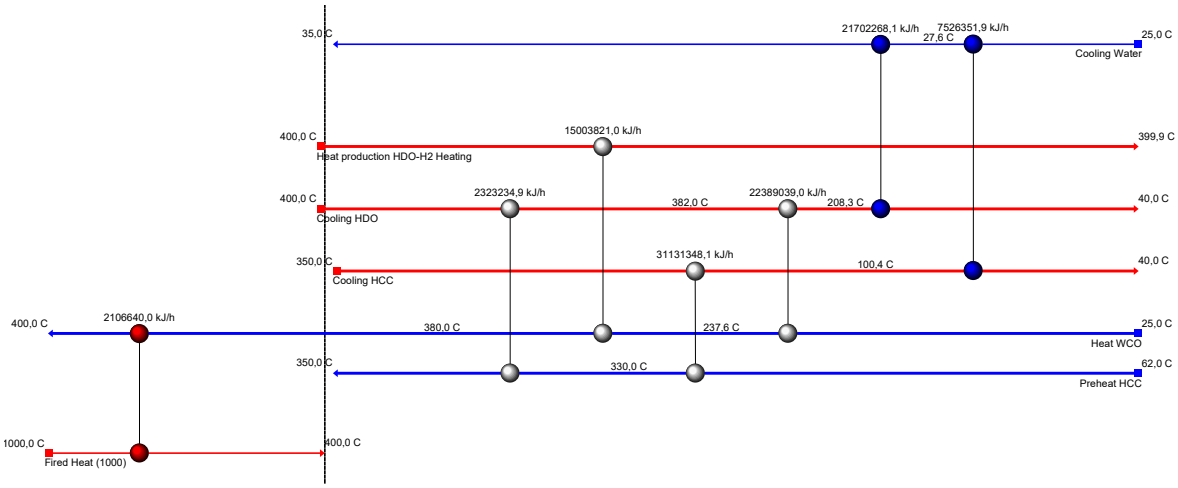

Figure 2.4: Heat Integration Network (HEN).

The integrated network design, which is shown in Figure 2.4, achieves 100% of heating target and 100% of cooling target. External process utilities needed by the process are Fired-Heater to reach 400°C and Cooling Water for cooling at 40°C (CW).
The heat exchanger network design results in 7 units overall: 4 integrated heat exchangers (HEx1, HEx2, HEx3, HEx4) and 3 utilities (CW1, CW2, Fired-Heater). In the process flow diagram (PFD), energy streams can be viewed with dashed green lines that represent integration between heat exchangers. The results of duties and temperatures of HEN, can be seen in Table 2.13 for integrated heat exchangers and Table 2.14 for utilities.

Table 2.13: HEx-integrated heat exchangers. Temperature of cold and hot streams and total duty required

	HOT STREAM		**COLD STREAM**		
Integrated HEx	Tin (°C)	Tout (°C)	T in (°C)	T out (°C)	Duty (kW)
HEx1	363	240	25	219	5046.8
HEx2	400	400	219	380	5228.5
HEx3	400	359	300	350	1867.4
HEx4	372	196	59	300	7425.6

Table 2.14: Utilities duty and process stream properties

Utility	T in (°C)	T out (°C)	Duty (kW)
Cooling Water - HDO effluent	259	40	-6196.6
Cooling Water - HCC effluent	196	40	-5735.7
Fired Heater - HDO	380	400	704.4

It is seen in Table 2.14 and Figure 2.3 that only 700 kW are needed to sustain the process heating duties, i.e. 0.017 kWh/kg of WCO processed, whereas the external cooling needed amounts at 0.29 kWh/kg.

2.1.8 Separation of propane and distillate fuels

The products from the HCC unit are separated by means of two flashes at high and low pressures. High pressure flash (HP-SEP block, PFD) is needed to recover unreacted hydrogen which is further recycled to the recovery unit; low pressure flash (LP-SEP block, PFD) separates gaseous products (C1-C4) from distillate liquids, which will be sent to an atmospheric fractionation tower to produce Naphta and Kerosene products. The low pressure flash can operate at 0.1 MPa or higher pressure depending on the amount of propane to be recovered, as shown in Table 2.15. It is assumed that the latter product is further distilled in a propane tower and sold as a by-product. Therefore, 0.1 MPa of pressure is used which recovers 94% of propane compared to 4.0 MPa. Atmospheric fractionation tower and LPG tower are not simulated in the process. The

Table 2.15: Propane recovery at different pressure of flash.

Parameter	0.1 MPa	1 MPa	2 MPa	3 MPa	4 MPa
Light fuel kg/hr	5174	1817	972	583	370
Liquid distillates kg/hr	32114	35470	36315	36704	36918
Propane in light fuel kg/hr	1233	319	133	70	41
Propane in liquid distillates kg/hr	296	1209	1396	1458	1488
Loss of propane from 1 to 40%	94%	77%	53%	26%	

respective yield of product is estimated by a distillation analysis of stream To FRAC and from the flow rate and composition of stream LIGHT (see PFD). Accordingly, a simulated True Boiling Point curve is shown in Figure 2.5 and the yield of Naphta and Kerosene is estimated taking into account the boiling point ranges as defined in Table 1.1 in Chapter 1.

2.2 Catalytic Transfer Hydrogenation process

Experiments of Catalytic Transfer Hydrogenation (CTH) reaction of waste cooking oil (WCO) using iso-propanol (ISO-P) as hydrogen donor for jet fuels production were carried out in a fixed-bed tubular reactor filled with charcoal catalyst. All the experimental information reported in the following paragraphs were provided by Dr Kumarâs Biomass Research Laboratory at Old Dominion University (ODU), USA.

The liquid product was characterized considering average properties of the products mixture. Different approaches were used for modelling the reaction system: a first one, based on a proposed kinetic model derived from experimental data and, a second one,

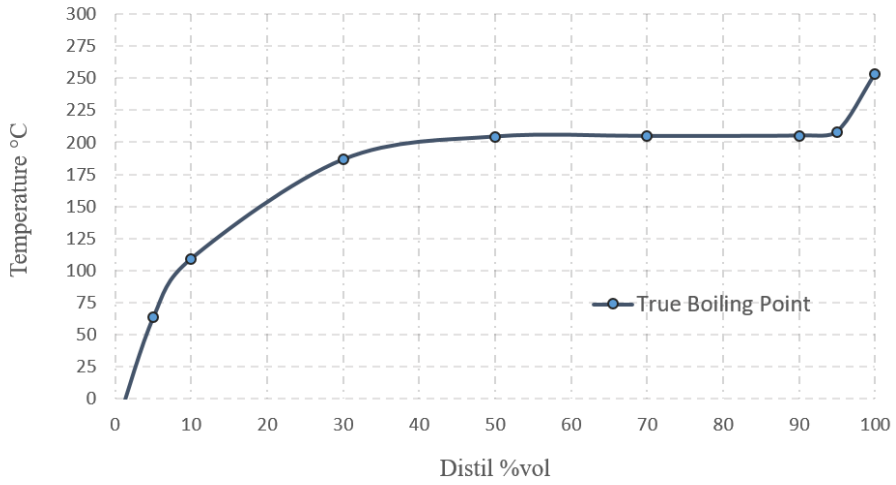

Figure 2.5: Simulated distillation analysis of liquid: calculation of True Boiling Points.

based on experimental yields. The CTH process is based on the following block diagram in Figure 2.6, which comprises the reaction system with preheated feed, cooling required for the separation of gaseous and liquid product and fractionation tower for the production of liquid distillates.

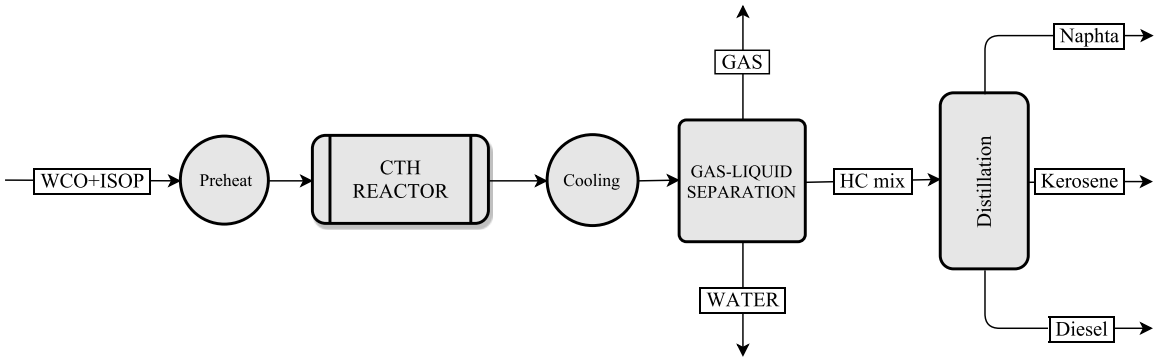

Figure 2.6: Block Flow Diagram of CTH process.

2.2.1 Experimental data of CTH and characterization of liquid products

Table 2.16-Table 2.25 summarize all the experimental information used in the following calculations and assumptions. In particular, Table 2.16 shows the flow-rates and the properties of reactants WCO and ISO-P. In Table 2.17 and Figure 2.7, the reactor dimensions and catalyst properties are reported. Table 2.18 shows the composition of WCO feedstock used in the laboratory in terms of fatty acids: since a number of compounds are present in small amounts (less than 1% the total of each), for the sake

of simplicity it was decided to consider only the most relevant components, which are highlighted in bold.

Table 2.16: Experimental feed of continuous fixed bed reactor

WCO	**Unit**	**Value**	**ISO-P**	**Unit**	Value
Mass	(g)	71.76	Mass	(g)	24.52
Density	(g/cm^3)	0.92	Density	(g/cm^3)	0.786
Average MW	(g/mol)	834	MW	(g/mol)	60.1
Volume flow	(mL/min)	0.5	Volume flow	(L/min)	0.2

Table 2.17: Reactor geometry and catalyst properties

Reactor	**Value**	**Catalyst**	**Value**
Diameter internal (cm)	1.4	Mass (g)	5.5
Length pipe (cm)	36	Volume (cm^3)	18.7
Bed length (cm)	14	Porosity (%)	0.51
Volume pipe (cm^3)	55.39	Density (g/cm^3)	0.98
Void fraction	0.132	Particle size (mm)	0.85-2.4
Bed volume (cm^3)	21.54		

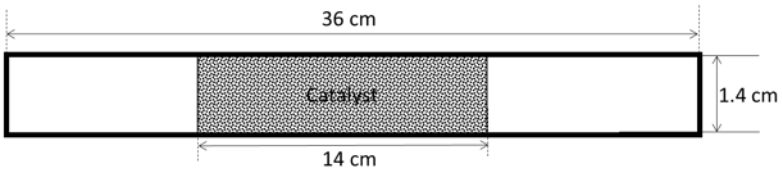

Figure 2.7: Block Flow Diagram of CTH process.

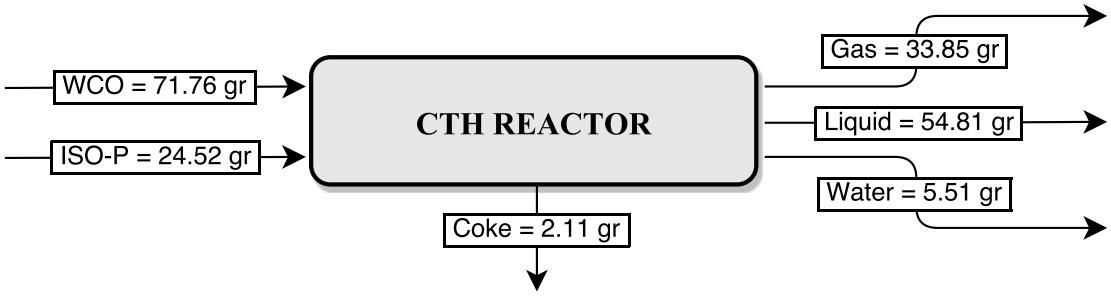

Figure 2.8: Experimental Mass Balance of CTH reactor at T = 380°C.

In Table 2.19, the experimental conversion of WCO at different temperatures is reported. Figure 2.8 shows the material balance of the experimental run carried out at T =380 °C.

An analysis of the liquid products identified at the reactor outlet was carried out. This was done based on the experimental results obtained at 380°C, which was found to be

Table 2.18: Fatty acid composition of WCO. Relevant components are highlighted in bold for the total of 96%w.

Name	Formula	wt%
9-Hexadecenoic acid-	$C_{16}H_{30}O_2$	1.36
Pentadecanoic acid	$C_{15}H_{30}O_2$	16.96
Heptadecanoic acid	$C_{17}H_{34}O_2$	0.25
8,11 Octadecadienoic acid	$C_{18}H_{32}O_2$	49.57
9-Octadecenoic acid	$C_{18}H_{34}O_2$	17.8
Stearic acid	$C_{18}H_{36}O_2$	10.68
9,11-Octadecadienoic acid	$C_{18}H_{32}O_2$	0.69
11-eicosenoate	$C_{20}H_{38}O_2$	0.92
Nonadecanoic acid	$C_{20}H_{40}O_2$	0.76
Heneicosanoic acid	$C_{21}H_{42}O_2$	0.1
Docosanoic acid	$C_{22}H_{44}O_2$	0.65
Tricosanoic acid	$C_{23}H_{46}O_2$	0.07
Tetracosanoic acid	$C_{24}H_{48}O_2$	0.19

Table 2.19: Experimental conversion at different temperatures.

Reactor Temperature [°C]	300	340	360	380	400
Experimental oil conversion X	0.866	0.972	0.971	0.989	0.997

the optimal temperature according to the highest Kerosene yield and WCO conversion achieved, among other reactor temperatures. The composition of product components that were identified by gas chromatography (GC) analysis after CTH at 380°C is presented Table 2.20-2.21-2.22. Here, the components were rearranged according to their increasing boiling point (Tb), and subdivided accordingly into Naphta, Kerosene and Diesel products, as defined in TABLE 1.1 in Chapter 1. It should be specified that, in order to simplify the analysis, it was decided to neglect oxygenate and cycloalkane compounds. In fact, the former components are mostly derived from fatty acids with more than 20 atoms of carbon, which were considered negligible in the WCO composition reported in Table 2.18, while the latter ones are formed in a very small amount. Therefore, only alkanes, alkenes and aromatics have been considered, which represent 88 mol% of the liquid product.

The total molar fraction of Naphta (38 mol%), Kerosene (41.2 mol%) and Diesel (8.7 mol%) were calculated as the sum of composition percentage of the respective components. It is specified that the percentage area (%) of a GC analysis was here assumed equal to the molar composition of component. The experimental gaseous products composition can be seen in Table 2.23. These are mainly by-products of carboxylation, carbonilation and cracking reactions.

Table 2.20: Total Naphta composition.

Component	MW	TB	Product	%area
C6H14	86.1772	68.73	Naphta	2.1
C6H6 AR	78.1136	80.09	Naphta	0.8
C7H14	98.1882	93.64	Naphta	4.3
C7H14-E4	98.1882	97.95	Naphta	0.4
C7H16	100.204	98.43	Naphta	3.2
C8H18	114.231	109.43	Naphta	3.6
C7H8	100.189	109.7	Naphta	3.2
C8H16	112.215	121.26	Naphta	4.3
C8H10 ethyl benzene	106.167	136.2	Naphta	1.7
C8H10 p-xylene	106.167	138.36	Naphta	2.9
C8H14	110.1	143	Naphta	0.9
C9H18	126.242	146.87	Naphta	2.1
C9H20	128.258	150.82	Naphta	2.8
C9H12	120.194	159.24	Naphta	3.7
C11H24	156.312	169.77	Naphta	2.2
TOTAL NAPHTA %				38

Table 2.21: Total Kerosene composition.

Component	MW	TB	Product	%area
C10H20 (Alkene)	140.269	170.6	Kerosene	1.9
C9H12 (AR)	118	177.97	Kerosene	0.8
C10H14 (AR)	134.221	183.3	Kerosene	2.2
C11H22 (Alkene)	154.296	192.67	Kerosene	6.2
C11H24 (Alkane)	156.312	195.93	Kerosene	1.6
C11H16 (AR)	148.248	205.46	Kerosene	2.8
C12H24 (Alkene)	168.323	213	Kerosene	3.2
C12H18 (AR)	162.2	215.9	Kerosene	1.1
C12H26 (Alkane)	170.338	216.32	Kerosene	3.9
C13H28 (Alkane)	184.365	235.47	Kerosene	2.4
C11H10 (AR)	142.1	244.68	Kerosene	1.5
C14H28 (Alkene)	196.376	251.1	Kerosene	2.7
C14H30 (Alkane)	198.3	253.57	Kerosene	1.8
C15H30 (Alkene)	210.403	268.46	Kerosene	3.5
C15H32 (Alkane)	212.419	270.68	Kerosene	5.6
TOTAL KEROSENE %				41.2

Table 2.22: Total Diesel composition.

Component	MW	TB	Product	%area
C16H34	226.446	286.86	Diesel	1.1
C17H34	238.457	292.39	Diesel	2.1
C17H34	238.457	300.33	Diesel	1.1
C17H36	240.473	302.15	Diesel	3.3
C23H46	322.618	384.66	Diesel	1.1
TOTAL DIESEL %				8.7

Table 2.23: Composition of gas phase.

Component	H_2	CO	CO_2	CH_4	C_2H_6	C_3H_8
Volume (%)	21	26	22	10	10	11

Table 2.24: Composition of liquid product: experimental and normalized molar percentage.

Composition	Experimental	Normalized	Unit
Kerosene	41.2	46.9	%mol
Naphta	38	43.2	%mol
Diesel	8.7	9.9	%mol

Table 2.25: Aromatics, Alkanes and Alkenes in Kerosene. Product characterization of liquid: average molecular weight MW and boiling point Tb.

Kerosene composition	**mol%**	**Product**	**MW Av.**	**Tb (°C) Av.**
Alkenes	42.5	Naphta	111.1	122.8
Alkanes	37.1	Kerosene	173	224.2
Aromatics	20.4	Diesel	248.3	308.1

Table 2.25 shows the amount of alkanes (37.1 mol%), alkenes (42.5 mol%) and aromatics (20.4 mol%) present in the Kerosene. In addition, the average boiling point Tb,av and molecular weight MWav of product liquid mixtures was estimated based on molar composition. The reported values show that Naphta, Kerosene, and Diesel have average properties similar to C_8H_{16}, $C_{12}H_{26}$ and $C_{17}H_{36}$, respectively. Hence, these specific components will be assumed in process simulation as representative for the conversion of WCO into Naphta, Kerosene and Diesel, respectively. Finally, the reaction is characterized by high formation of coke as it can be seen in mass balance chart of Figure 2.8. In particular, 2.1 g of coke are formed during the duration of the experiment and this number was increased to 5.5 g after 10 hr of operation when a prolonged analysis was performed. Accordingly, catalyst regeneration in continuous operation is required and will be addressed further in the design of CTH reactor (section (3.2.1)).

2.2.2 Kinetic model development

Based on the experimental data available, a simple kinetic model was developed to describe the conversion of WCO into products.

Stoichiometry

Simplified stoichiometric reactions were written considering the conversion of WCO into $C_{12}H_{26}$, C_8H_{16}, $C_{17}H_{36}$, which are representative components of Kerosene, Naphta and Diesel, as described in section (2.2.1), and gas components that were found experimentally (CO, CO_2, CH_4, C_2H_6, C_3H_8), as shown in Table 2.26. WCO is composed

by four predominant fatty acids ($C_{18}H_{34}O_2$, $C_{18}H_{32}O_2$, $C_{18}H_{36}O_2$ and $C_{15}H_{30}O_2$), as reported in Table 2.18. Isopropanol was assumed to be thermally degraded in the first section of the reactor, before reaching the catalyst, according to the reaction in Eq. (2.1) [32]. Thus, the stoichiometry of the catalytic reactions was written considering H2 as the reactant.

$$C_3H_7OH \rightarrow C_3H_6O + H_2 \tag{2.1}$$

Table 2.26: Stoichiometric reactions of conversion of WCO to $C_{12}H_{26}$, $C_8H_{16}$and $C_{17}H_{36}$.

	REACTIONS
1.a	$C_{18}H_{34}O_2+4H_2 \rightarrow C_{12}H_{26}+CO+H_2O +C_3H_8+C_2H_6$
1.b	$C_{18}H_{34}O_2+H_2 \rightarrow 2C_8H_{16}+CO_2+CH_4$
1.c	$C_{18}H_{34}O_2+2H_2 \rightarrow C_{17}H_{36}+CO+H_2O$
1.total	$C_{18}H_{34}O_2+(4a+b+2c)H_2 \rightarrow$ $aC_{12}H_{26}+2bC_8H_{16}+cC_{17}H_{36}+(a+c)CO+(a+c)H_2O+bCO_2+aC_3H_8+aC_2H_6+bCH_4$
2.a	$C_{18}H_{32}O+5H_2 \rightarrow C_{12}H_{26}+CO+H_2O +C_3H_8+C_2H_6$
2.b	$C_{18}H_{32}O+2H_2 \rightarrow 2C_8H_{16}+CO_2+CH_4$
2.c	$C_{18}H_{32}O+3H_2 \rightarrow C_{12}H_{26}+CO+H_2O$
2.total	$C_{18}H_{32}O+(5a+2b+3c)H_2 \rightarrow$ $aC_{12}H_{26}+2bC_8H_{16}+cC_{17}H_{36}+(a+c)CO+(a+c)H_2O +bCO_2+aC_3H_8+aC_2H_6+bCH_4$
3.a	$C_{18}H_{36}O+3H_2 \rightarrow C_{12}H_{26}+CO+H_2O +C_3H_8+C_2H_6$
3.b	$C_{18}H_{36}O \rightarrow 2C_8H_{16}+CO_2+CH_4$
3.c	$C_{18}H_{36}O+H_2 \rightarrow C_{12}H_{26}+CO+H_2O$
3.total	$C_{18}H_{36}O+(3a+0b+1c)H_2 \rightarrow$ $aC_{12}H_{26}+2bC_8H_{16}+cC_{17}H_{36}+(a+c)CO+(a+c)H_2O +bCO_2+aC_3H_8+aC_2H_6+bCH_4$
4.a'	$C_{15}H_{30}O+2H_2 \rightarrow C_{12}H_{26}+CO+H_2O +C_2H_6$
4.b'	$C_{15}H_{30}O+2H_2 \rightarrow C_8H_{16}+CO_2+C_3H_8+C_2H_6+CH_4$
4.total	$C_{15}H_{30}O+(2a'+2b')H_2 \rightarrow$ $a'C_{12}H_{26}+b'C_3H_8+a'CO+a'H_2O +(a'+b')C_2H_6+ b'CO_2+b'CH_4$
GLOBAL	**4 Oil+10.76 H_2 = 17.44 Products**

As reported in Table 2.26, for each C18 component (1 to 3), 3 reactions (a, b, and c) were written. Similarly, for $C_{15}H_{30}O_2$ only two reactions were assumed (respectively aâ and bâ coefficients), as can be converted into C_8H_{16} and $C_{12}H_{26}$ only. These reactions are then combined so that globally 1 mole of WCO (O), i.e. fatty acid compound, gives the experimental molar fraction of $C_{12}H_{26}$, C_8H_{16}, $C_{17}H_{36}$ by adjusting a, b, c, aâ and bâ coefficients, whose calculated values are reported in Table 2.27. In other words, the stoichiometric coefficient represents the selectivity of total reactions (1, 2, 3, and 4) towards the components in the product stream. These reactions consider arbitrarily decarbonilation, decarboxylation, hydrodeoxygenation reactions of fatty acids (see Chapter 1) and formation of CH_4, C_2H_6, C_3H_8 as cracking products. Therefore, the stoichiometry was balanced considering gaseous products and hydrogen. In particular, coefficients (a, b, c) were estimated considering that 2 moles of C_8H_{16} can be obtained from a C18 fatty acid.

Table 2.27: Calculated stoichiometric coefficients of conversion of WCO for reaction 1, 2, 3 and 4 in Table 2.26

Product coefficient	Value
a (Kerosene)	0.57
b (Naphta)	0.28
c (Diesel)	0.15
a' (Kerosene)	0.59
b' (Naphta)	0.41

Fitting of kinetic parameters

A fixed-bed Plug Flow Reactor (PFR) model Eq. (2.6) [33] was used to fit kinetic parameters using experimental data of WCO conversion, which is available at different reaction temperatures, as shown in Table 2.19. Fitting is performed by minimization of sum of square errors (SSE), as defined by Eq.(2.2):

$$SSE = \sum (X_{PFR} - X_{EXP})^2 \tag{2.2}$$

All the assumptions used to derive the final equation to fit kinetic parameters are listed below:

(a) The following lumped reaction stoichiometry was considered:

$$4Oil + 10.76H_2 = 17.44Products \tag{2.3}$$

This global reaction stoichiometry was calculated according to Table 2.26.

(b) The reaction rate was defined as a power law model of 2nd order, based on concentration of reactants, i.e. Oil (WCO) and H_2 (Eq. (2.7)).

(c) Pressure and temperature are constant along the reactor.

(d) The reaction occurs in the gas phase, with a change of total number of moles. Therefore, it was assumed that feed is vaporized before reaching the catalyst. The inlet concentration was estimated, for each temperature condition, by using the Ideal Gas Equation (Eq.(2.10)).

(e) Immediately after entering the reactor, all ISO-P decomposes thermally to give moles of hydrogen H_2, according to the reaction Eq. (2.1). Therefore, the moles of H_2 available at the inlet equal the inlet moles of ISO-P (stoichiometric ratio 1:1) [32]. This is a strong assumption based on literature. It should be mentioned that this assumption is not yet confirmed by experimental evidence, because no information were obtained for the ISO-P decomposition.

(f) The inlet WCO molar concentration was calculated assuming that ISO-P decomposes according to reaction Eq. (2.5), hence:

$$y_O^{in} = \frac{F_{oil}}{F_{CH_4} + F_{CO} + F_{H_2} + F_{C_2H_4}} \tag{2.4}$$

Assumption f) of isopropanol decomposition is based on the fact that isopropanol decomposes thermally into acetone and H_2, then all acetone is transformed into CH_4, CO, C_2H_4 [34]. Therefore, the overall stoichiometry of decomposition is:

$$C_3H_7OH \rightarrow C_3H_6O + H_2 \rightarrow CH_4 + CO + H_2 + 0.5C_2H_4 \tag{2.5}$$

According to these assumptions, and from Eq. (2.6-2.10), the material balance in Eq. (2.11) in terms of WCO conversion in the PFR fixed bed reactor can be written :

$$F_O^{in}\frac{dX}{dW} = R \tag{2.6}$$

$$R = kC_OC_{H_2} = Ae^{-Ea/RT}C_OC_{H_2} \tag{2.7}$$

$$C_O = \frac{F_O}{V_{mix}} = \frac{F_O^{in}(1-X)}{V_{in}(1+\xi X)} = \frac{(1-X)}{(1+\xi X)}C_O^{in} \tag{2.8}$$

$$C_{H_2} = \frac{F_{H_2}}{V_{mix}} = \frac{F_{H_2}^{in} - \frac{\upsilon_{H_2}}{\upsilon_O}XF_O^{in}}{V_{mix}} = F_O^{in}\frac{(R_{H_2}^{in} - \frac{\upsilon_{H_2}}{\upsilon_O}X)}{V_{mix}} =$$

$$= F_O^{in}\frac{(R_{H_2}^{in} - \frac{\upsilon_{H_2}}{\upsilon_O}X)}{V_O^{in}(1+\xi X)} = C_O^{in}\frac{(R_{H_2}^{in} - \frac{\upsilon_{H_2}}{\upsilon_O}X)}{(1+\xi X)} \tag{2.9}$$

$$C_O^{in} = y_O^{in}C_{total} \xrightarrow{IG} y_O^{in}\frac{P}{RT} \tag{2.10}$$

$$\frac{dX}{dW} = Ae^{-Ea/RT}S(1-\epsilon_{gas})\frac{\rho_{cat}}{F_O^{in}}C_O^{in2}\frac{(R_{H_2}^{in} - \frac{\upsilon_{H_2}}{\upsilon_O}X)}{(1+\xi X)^2} = \tag{2.11}$$

$$= [\frac{m_{gas}^6}{kg_{cat}molhr}][\frac{m_R^2m_{cat}^3}{m_R^3}][\frac{kg_{cat}}{m_{cat}^3}][\frac{hr}{mol}][\frac{mol^2}{m_{gas}^6}][-] = [1/m_R]$$

where F is the molar flow (mol/hr), C_O the concentration of oil (mol/m^3_{gas}), Ea is the activation energy (kJ/kmol), A the pre-exponential factor (m^6_{gas}/mol kg_{cat} hr), S the reactor section area (m^2_{react}), z is the length of reactor (m_{react}, the expansion coefficient (-), the void fraction (m^3_{gas}/m^3_{react}), ρ_{cat} the density of catalyst (kg_{cat}/m^3_{cat}), $R_{H_2}^{in}$ is

the hydrogen to oil inlet ratio (-), and v is the stoichiometric coefficient (-). Process inlet conditions at 380°C are given in Table 2.28.

Table 2.28: Estimation of inlet condition of reagents.

Inlet variable	**Value**
Molar fraction	0.0767
Concentration (@380°C) (mol/m^3)	2.826
Hydrogen flow rate F_{H_2} (mol/hr)	0.1569
Oil flow rate F_O (mol/hr)	0.0331
Ratio H_2/O	4.742
Pressure (MPa)	0.2
R gas constant (J/mol K)	8.314

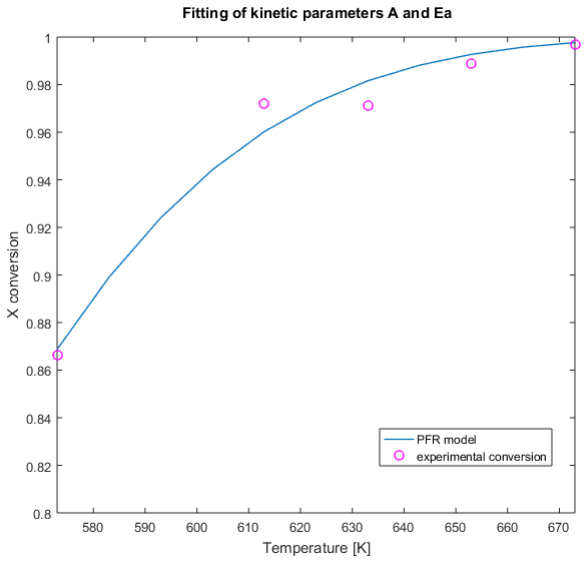

Figure 2.9: Results of fitting with PFR model and experimental conversion.

Finally, the results of the kinetic parameters fiting (pre-exponential factor A and activation energy Ea) are illustrated in Figure 2.9 and their values are reported in Table 2.29.

Table 2.29: Results of fitting: sum of error function SSE, pre-exponential factor A and activation energy Ea in SI units.

Results of fitting	**Unit**	**Value**
SSE	-	0.00274
A	m^6/kmol kg s	4315
Ea	kJ/kmol	53578

2.2.3 Kinetic model verification

All the assumptions used to derive kinetic parameters, i.e. the stoichiometry in Table 2.26 and results from kinetic fitting in Table 2.29, have to be verified before developing the simulation of the entire process. The verification is performed implementing the derived kinetics in a PFR model in Aspen Plus, according to the flowsheet shown in Figure 2.10. Data of experimental reactor geometry, process condition and fitted kinetic parameters, respectively from Table 2.17, Table 2.28, and Table 2.29, are the inputs in process calculations.
The process diagram used for verification includes the decomposition of ISO-P according to Eq. (2.1) in a RStoich block, the preheating of reactants at 380°C before reaching the catalyst bed (PREHEAT block), the fixed bed reactor (PFR block) and the separation of water, gas, and liquids (SEP blocks). It has to be specified that kinetic parameters in the PFR block have to be in SI units.

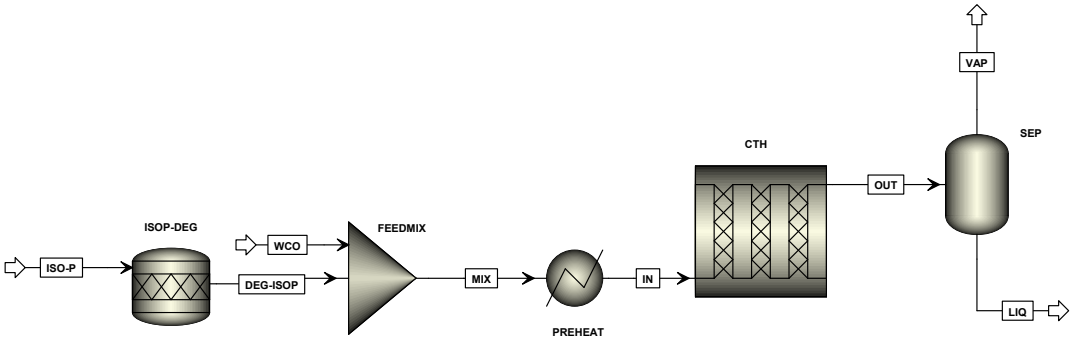

Figure 2.10: Process diagram used for verification of CTH results in PFR model from Aspen Plus.

Regarding the conversion of WCO in the PFR reactor it has been verified that the model well represents the experimental data, as shown in Table 2.30. In particular at higher temperatures (360°C, 380°C, 400°C) the conversion calculated from Aspen results very similar to the experimental one. Furthermore, the fractions of liquid products, as determined by stoichiometric coefficients, are well reproduced with respect to the experimental ones, as it can be seen in Table 2.31. Therefore, the liquid product composition and the conversion of oil predicted by stoichiometric reactions and kinetic model are verified in the process simulation.

Table 2.30: Conversion oil X: comparison between experimental and calculated with Aspen plus PFR model.

Temperature °C	300	340	360	380	400
X calculated %	82.8	93.4	96.4	98.2	99.2
X experimental %	86.6	97.2	97.1	98.9	99.7

Table 2.31: Composition of liquid product: comparison between experimental and calculated in Aspen PFR model.

	Experimental %	Calculated %
$C_{12}H_{26}$	47%	47%
C_8H_{16}	43%	43%
$C_{17}H_{36}$	10%	10%

Nevertheless, it was found that the calculated composition of gaseous products did not match the experimental results. In particular, it can be seen from Table 2.32 that the stoichiometry assumed for decomposition of ISO-P significantly affects the final composition of gas products, since the most abundant components are the ones from Eq. (2.1). This is determined by the molar feed ratio of ISO-P (MW=60.1g/mol) and WCO (MW=834g/mol), which is high, meaning that the assumptions of ISO-P decomposition will strongly affect the results of simulation. If a different decomposition of ISO-P is assumed, for example the one in Eq. (2.12) :

$$C_3H_7OH = 1H_2 + 0.5CO + 0.25CO_2 + 0.75C_3H_8, \tag{2.12}$$

closer values of gaseous composition can be found for H_2, $CO_2$and CO, but still with significant difference, as shown in Table 2.33. Therefore, these assumptions are not suitable for process simulation of the reaction system.

Table 2.32: Volumetric gas composition (% vol) comparison with experimental results.

	Experimental %vol	Calculated %vol
H_2	21%	11%
CO	26%	34%
CO_2	22%	2%
CH_4	10%	31%
C_2H_6	10%	4%
C_3H_8	11%	3%
C_2H_4	0%	15%
Total	100%	100%

The results of the kinetic model concerning the gaseous products are clearly sensitive to the assumptions of ISO-P decomposition. It is worth noting that the initial assumption of thermal decomposition of ISO-P into H_2 and acetone, before reaching the reactor, was not verified experimentally, but based on literature at different process condition. Therefore, if the kinetics is based on hydrogen, experimental data of decomposition of isopropanol at process condition would be necessary in order to estimate the actual amount of hydrogen available for the reaction. In conclusion, it is preferred to follow another approach for developing the process simulation, which is different from the one based on kinetic study.

Table 2.33: Gas composition with different ISO-P decomposition from Eq. (2.5).

	Experimental %	Calculated %
H_2	21%	15%
CO	26%	27%
CO_2	22%	13%
CH_4	10%	3%
C_2H_6	10%	6%
C_3H_8	11%	36%
C_2H_4	0%	0%
Total	100%	100%

2.2.4 CTH Reaction System

As explained in previous paragraph, the kinetic model with the proposed assumption of ISO-P decomposition does not reproduce the mass balance of the reaction system when it comes to the gas products. Therefore, a simple RYield reactor model was used to simulate the reaction system (see CTH block, PFD, Figure 2.16. This model overcomes issues related with ISO-P decomposition, since it is only based on mass yield of specified components. The yield of product Y_i is defined as the mass of component i in the outlet divided by the inlet mass of reagents, as given:

$$Y_i = \frac{m_i^{out}}{(m_{WCO}^{in} + m_{iso-p}^{in})} \tag{2.13}$$

In Table 2.34, the results of yield of each component are reported. The calculation is based on overall mass balance from Figure 2.8, gas composition reported in Table 2.23 and molar fraction of liquid products detailed in Table 2.24. It is noted that the yield of gas and liquid components is based on average MW of gases, Naphta, Kerosene, Diesel, calculated according to Eq. (2.14).

$$MW = \sum_{i=1}^{N} x_i MW_i \tag{2.14}$$

The calculated yields of all components reproduce perfectly the experimental mass balance of reactor, as shown in Table 2.35. In particular, specified yield values respect the atom balance of C, H, and O. Furthermore, carbon coke is formed in the reactor; thus, a SEP model is applied to remove solid phase from the outlet stream (see PFD Figure 2.16). In conclusion, the proposed approach of simulating the reaction system allows to reproduce exact results from the experiments. Nevertheless, the disadvantage of this approach consists of any possibility to perform sensitivity analysis. Anyway, an interesting analysis of the whole process could be carried out at the optimum operating conditions determined experimentally (T = 380°C) only.

Table 2.34: Yield of product components.

Product	Component	Yi
COKE	C	0.0219
WATER	H_2O	0.0572
LIQUID	C_8H_{16}	0.1779
	$C_{12}H_{26}$	0.3003
	$C_{17}H_{36}$	0.091
GAS	H_2	0.0055
	CO	0.0954
	CO_2	0.1268
	CH_4	0.021
	C_2H_6	0.0394
	C_3H_8	0.0635
	Total	1.0000

Table 2.35: Mass balance from RYield model.

Component	Unit	Calculated	Experimental
C	g	2.11	2.11
H_2	g	0.534	0.534
CO	g	9.181	9.182
CO_2	g	12.207	12.207
H_2O	g	5.51	5.51
CH_4	g	2.023	2.023
C_2H_6	g	3.791	3.791
C_3H_8	g	6.116	6.116
C_8H_{16}	g	17.128	17.128
$C_{12}H_{26}$	g	28.916	28.916
$C_{17}H_{36}$	g	8.764	8.764

2.2.5 Separation of products

The composition of the outlet stream from CTH reactor is reported in detail in Appendix B. In particular, it is characterized by a mixture of hydrocarbons (C_8H_{16}, $C_{12}H_{26}$, $C_{17}H_{36}$), water (H_2O) and gaseous products (CO_2, CO, C1 - C3) at 0.1 MPa of pressure. The separation of hydrocarbon mixture from gases and water can be achieved at low temperature, since the solubility of water is inversely dependent of temperature. Accordingly, a 3-phase flash model is used to simulate the required separation (see VLL-SEP block, PFD).

For a correct estimation of Vapor-Liquid-Liquid Equilibrium (VLLE) at low pressure, an appropriate thermodynamic model has to be chosen; here, NRTL thermodynamic model was selected. For the correct determination of mixture properties with NRTL model, all binary parameters should be available for each couple of components. The solubility of incondensable components in the gas phase (CO_2, CO, H_2) was determined

by Henry constants, available in Aspen database.

For the Liquid-Liquid Equilibrium, particular attention is directed towards H_2O -

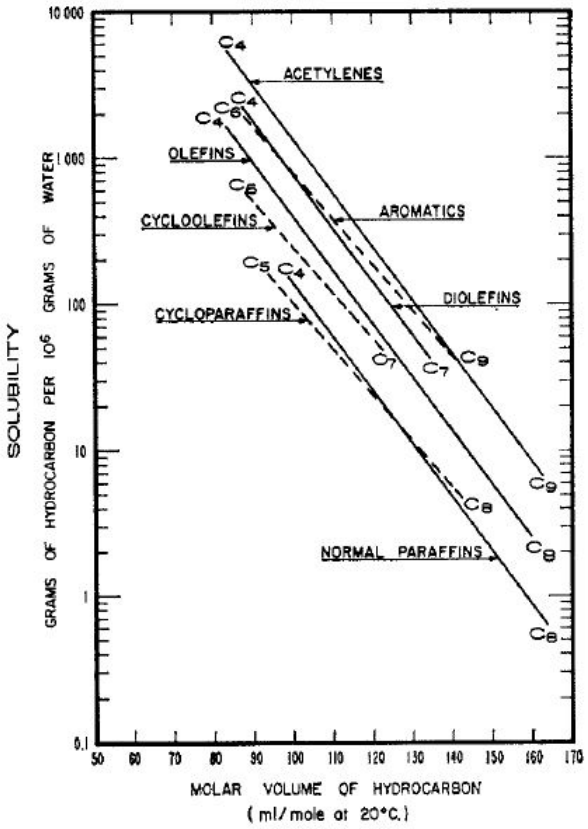

Figure 2.11: Solubility of hydrocarbon in water, as a function of group and molecular weight [28].

$C_{12}H_{26}$, H_2O - C_8H_{16} and H_2O - $C_{17}H_{36}$ binary mixtures. Binary interaction parameters are not available in Aspen database for H_2O - C_8H_{16} and H_2O - $C_{17}H_{36}$ binary systems, however binary parameters of H_2O - $C_{12}H_{26}$ mixture are present. Therefore, a user input of parameters was necessary.

Table 2.36: Binary Parameters of NRTL model.

Binary Parameter	**$C_{17}H_{36}$-H_2O**	**$C_{12}H_{26}$-H_2O**	**C_8H_{16}-H_2O**
Aij	28.2178	23.4291	0
Aji	-5.44545	-6.08871	0
Bij	-3920.97	-2638.14	2844.22
Bji	3588.23	3794.11	1431.52
C	0.2	0.2	0.2

In the literature, only a few number of experimental points exist for H_2O -C_8H_{16}, while no data could be found for $C_{17}H_{36}$-H_2O mixtures. Accordingly, the regression of NRTL binary parameters based on few data is not recommended and was avoided due to

consistency issues. Hence, it was decided to use existing binary parameters, available in Aspen database, of binary systems similar to the ones of the case. The similarity takes into account the type of hydrocarbons, i.e. an alkene should be selected for C_8H_{16} and a paraffine for $C_{17}H_{36}$, since the solubility depends on the type of hydrocarbons, as it shown in Figure 2.11. Furthermore, it is clear from the figure, that the solubility of hydrocarbons in water decreases with increasing molecular weight [35].
Considering all aspects above, binary interaction parameters of C_6H_{12} - H_2O and $C_{16}H_{34}$ - H_2O were used for C_8H_{16} - H_2O and $C_{17}H_{36}$ - H_2O respectively, i.e. considering a lower molecular weight component of the same type of hydrocarbons. The binary parameters used in the simulations are summarized in Table 2.36. Even though binary parameters were available in database, it was first verified that calculated values with NRTL model represent satisfactorily experimental data, as shown in Table 2.37.

Table 2.37: Verification of NRTL model: calculated and experimental values (%w/w), where W=water (H_2O) and HC=hydrocarbon.

	EXP	EXP	EXP	NRTL	NRTL	Relative Error	Relative Error	
	P (Pa)	T (°C)	HC in W	W in HC	HC in W	W in HC	HC in W	W in HC
$C_{16}H_{34}$	101000	298.1	-	6.80E-04	-	6.80E-04	-	0
	101000	313.1	-	1.30E-03	-	1.30E-03	-	0
	101000	298.2	3.00E-09	7.40E-04	4.90E-08	6.80E-04	0.94	0.09
$C_{12}H_{26}$	101000	298.1	-	6.10E-04	-	6.10E-04	-	0.01
	101000	313.1	-	1.20E-03	-	1.20E-03	-	0
	101325	293.2	-	5.00E-04	-	4.80E-04	-	0.03
	101325	303.2	-	6.00E-04	-	7.70E-04	-	0.22
C_6H_{12}	101325	293.1	1.00E-05	-	9.71E-06	-	0.03	
	101000	298	1.10E-05	-	1.14E-05	-	0.06	

Table 2.38: Amount of C_8H_{16} in VLL equilibrium.

C_8H_{16}	40 °C	25 °C	15 °C	Unit
Gases	25.7	10.9	5.8	ton/day
Water	0	0	0	ton/day
Liquid	213	227.8	232.9	ton/day
Total	238.7	238.7	238.7	ton/day

As in Conventional Jet Fuel process simulation (section 2.2.5), the simulation of the atmospheric fractionation tower for the separation of Naphta, Kerosene and Diesel is not considered in the analysis of the process. The respective yield of product is estimated by the simulated distillation analysis (ASTM D86) of HC stream (see PFD, Figure 2.16). Accordingly, the simulated True Boiling Point curve is shown in Figure 2.12, and the yield of product is estimated taking into account the boiling point ranges of respective products, as defined in Table 1.1 of Chapter 1.
Finally, it is noted that the small amount of GPL can be purged in the condenser of fractionation column and further, compressed at storage pressure; therefore, it is not

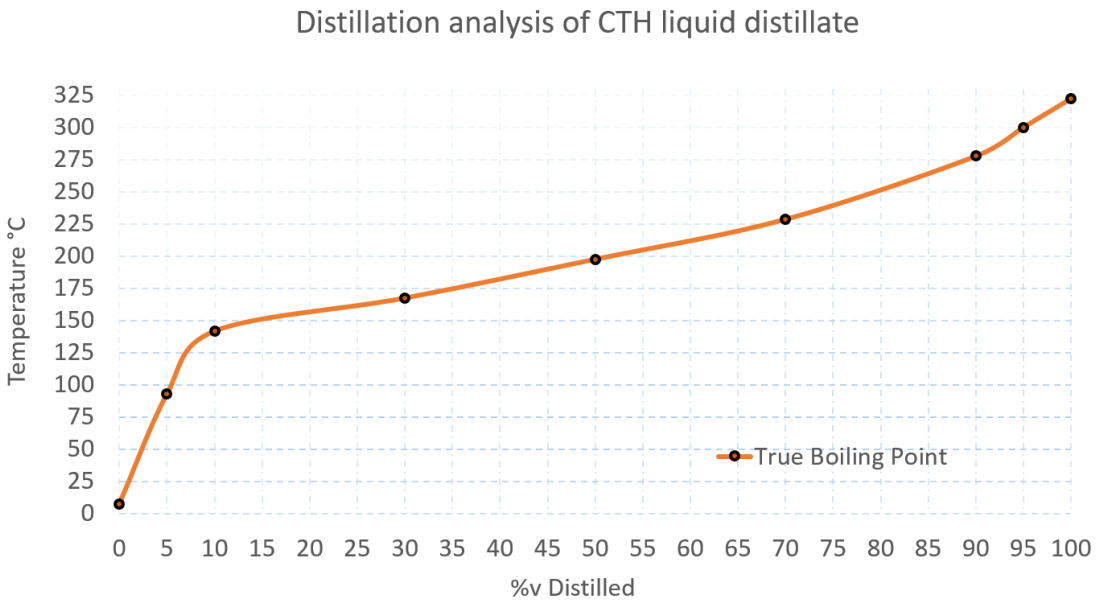

Figure 2.12: Distillation analysis (ASTM D86) of CTH liquid distillate.

required an additional tower for the separation.

2.2.6 Heat Integration

The integration of heat duties is necessary to minimize the thermal energy consumption. The inventory of the streams to be heated or cooled is reported in Table 2.39. In particular, the integration is carried out between the cold feed (which needs preheating) and the hot outlet (which needs cooling) streams of CTH reactor (see streams s4 and s8 in PFD). The temperature-enthalpy diagram of cold (blue line) and hot (red line) streams is shown in Figure 2.13, where similar slopes, representing heat capacities, are noticeable.

Table 2.39: Inventory streams for heat integration.

Stream	**Tin**	**Tout**	**Duty**	**Duty**	**Flow rate**	**Flow rate**
	°C	°C	MW	kJ/hr	kg/hr	ton/day
Hot	380	25	17	6.10E+07	54683	1312.4
Cold	25	380	19.4	6.99E+07	55908	1341.8

The heat balance for integration is worked out by decision of the outlet temperature for the preheated stream, which was set to be 300°C. This decision is justified taking into account the large amount of latent heat that has to be supplied to the mixed feed stream, i.e. 5 MW from 300°C to 380°C, which represents 25% of the overall required duty.

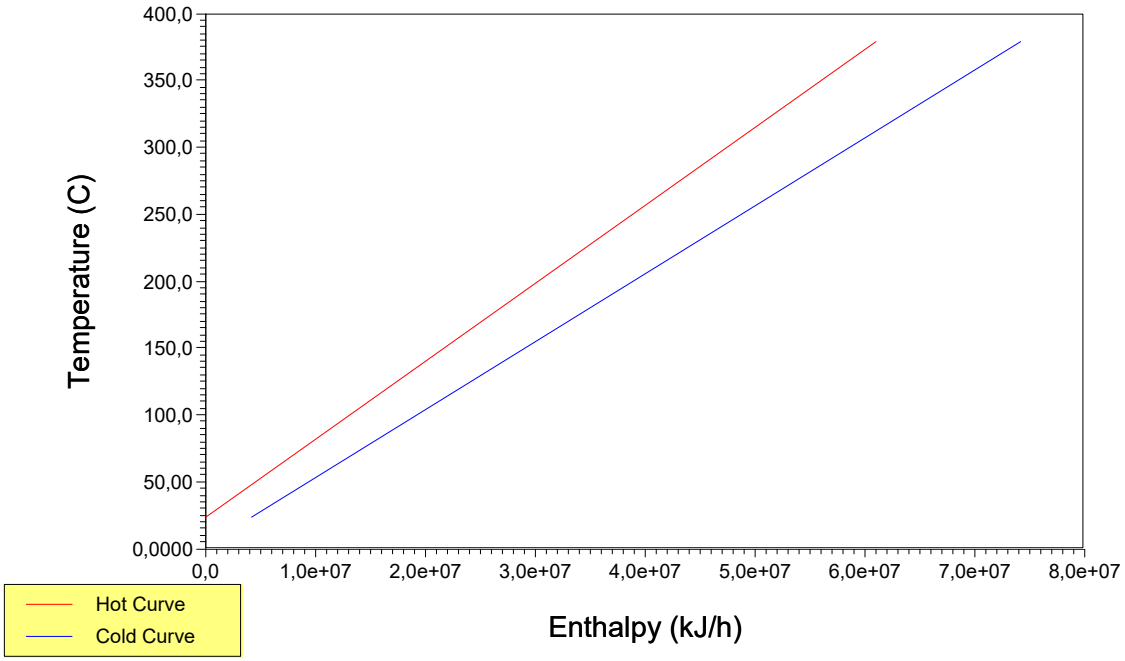

Figure 2.13: Temperature-Enthalpy diagram of two stream for heat integration.

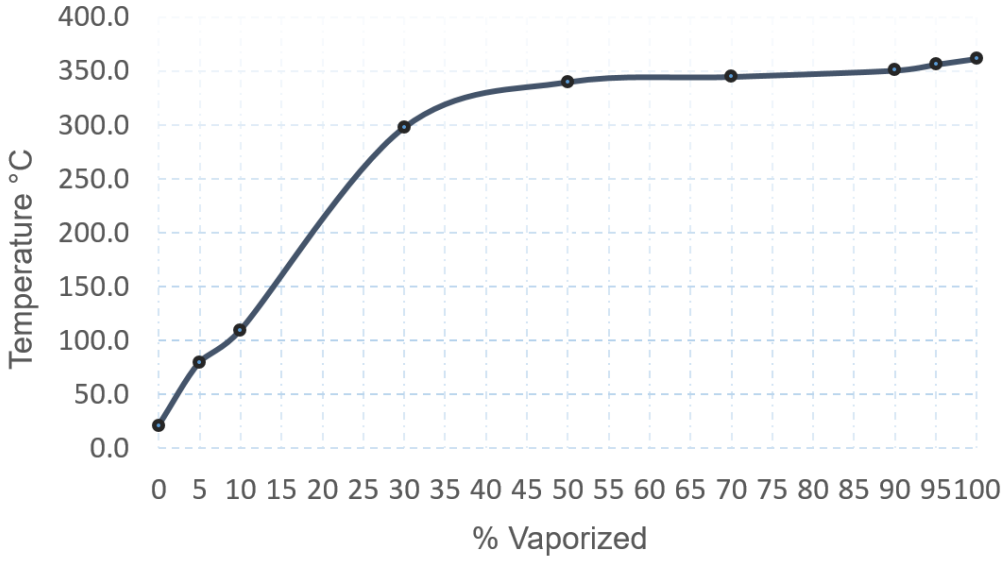

Figure 2.14: The evaporization range of feed WCO+ISO-P stream.

Therefore, it is decided that this heat will be supplied from an auxiliary duty, i.e. a Fired Heater unit. This decision implies better controllability and smaller surface area

for the integrated heat exchanger. In fact, Figure 2.14 shows that 70% of the mixed feed vaporizes in the range of 300-350°C, as determined by WCO boiling point. On the other hand, 30% of the feed vaporization, determined by ISO-P boiling point, will be located within the tubes of heat exchanger.
Furthermore, the temperature difference of 80°C and 25°C determined on two sides of heat exchanger is appropriate, since the two streams are 2-phase mixtures, characterized by a lower heat transfer coefficient. The auxiliary utilities to reach the 380°C of reaction temperature and the 25°C of the subsequent separation unit are the fired heater and the refrigerated cooling water which is available at 5°C and returned at 15°C.

2.3 Results of Simulation

2.3.1 Conventional Jet fuel process

The final results of the process simulation, base case with heat integration, are presented in Table 2.40.

Table 2.40: Reagent and utility specific consumption in conventional Jet fuel process.

Reagent Consumption	**Unit**	**Value**
Hydrogen H_2	ton/day	35.2
Waste cooking oil (WCO)	ton/day	1000
Hydrogen H_2	kg/hr	1465
Waste cooking oil (WCO)	kg/hr	41667
Overall Hydrogen/WCO ratio		3.5
Utility Specific Consumption	**Unit**	**Value**
Compression Work	kWh/kg (H_2)	3
Compression Work	kWh/kg (oil)	0.105
Cooling Water	kJ/kg (oil)	1031
Cooling Water (compressor cooling)	kJ/kg (oil)	267.7
Fired Heater Duty	kJ/kg (oil)	60.9
WCO Feed Pump (eff=0.95)	kWh/kg (oil)	0.003
HDO cooling (without integration)	kJ/kg (oil)	451.7
Total Thermal Energy (with HDO integration)	kJ/kg (oil)	1359.5
Total Thermal Energy (without HDO integration)	kJ/kg (oil)	2263
Total Electric	kWh/kg(oil)	0.108

All specific energy consumption of utilities are scaled to the mass of Waste Cooking

Oil feed. The overall hydrogen to WCO ratio equals to 3.5 %w/w, similar to the ones calculated by Pei Lin Chin et al. (2.6-3%w/w), Pearlson et al. (4%w/w) and Han et al. (2-3%w/w) [11, 36, 28],. Nevertheless, Pei Lin Chin et al. do not take into account the amount of hydrogen used for hydrocracking reactions assuming it as a factor of the degree of cracking, while Pearson et al. proposes that 4%w/w overall process ratio is the scenario for the maximum Jet fuel production based on literature data.
Approximately, 1-2%w/w of hydrogen is required for hydrocracking reactions, respectively 11 ton/day (500 scf/bbl in HCC) and 22 ton/day (1000 scf/bbl in HCC). Therefore, total hydrogen ratio is in the range between 3-4%w/w, depending on the degree of unsaturation of oil and process conditions in the hydrocracking unit.

All factors that determine hydrogen consumption are summarized in Table 2.41. The

Table 2.41: Overall hydrogen consumption in the process.

Hydrogen Consumption	**Unit**	**Value**
HDO reactions + Hydrogenation	ton/day	15.42
Triglyceride degradation	ton/day	7.332
WGS	ton/day	0.182
Hydrocracking	ton/day	11.304
Loss	ton/day	0.9312
Total	ton/day	35.2

total amount of hydrogen consumed in hydrodeoxygenation reactor is 22.93 ton/day, including. HDO + Hydrogenation + Triglyceride degradation + WGS. Therefore, the hydrogen to feed ratio in HDO reactor, which is 2.6%w (26 ton/day), leads to 88.2% of hydrogen conversion. In fact, a design optimization might be performed to achieve a minimum hydrogen partial pressure at reactor outlet. Hence, less amount of hydrogen would be necessary to be recovered. It should be noted that the loss of hydrogen is given only related to stream LIGHT (see PFD), i.e. in the gas phase of low-pressure flash (LP-SEP block). No loss of hydrogen is assumed in the recovery of recycle stream, even though in practice it may vary between 15-25% for PSA unit. Hence, an amount of hydrogen would be consumed slightly larger than that the one indicated.

The yield of products and by-products are based on the WCO feed, and can be seen in Table 2.42. In particular 77% of the feed is converted into liquid and 9% into light gases (mostly propane). Similar results are reported by Pearlson et al (79.7%w and 10.2%w), Pei Lin Chin et al (80.2-81.4%w and 6.9-8.8%w) and Han et al (74% and 7-7.8%w). Fuel gas by-product is characterized by large amounts of CO and CO2, determining a lower LHV. This fuel might be upgraded by a CO_2 treatment if a higher LHV is desired.
The yield of Kerosene and Naphta from liquid product is evaluated using simulated distillation analysis in Aspen Plus (section 2.1.8). The True Boiling Point curve is pre-

Table 2.42: Product and by-product rate. Overall yield based on WCO feed

Product Yield	**Unit**	**Value**
Total mass of liquid fuels	ton/day	770.7
Total volume of liquid fuels	m^3/day	1119
Total mass yield	%w/w(oil)	77
Naphta yield	%v/v	20
Kerosene yield	%v/v	80
By-Products Yield	**Unit**	**Value**
Light gases mass (without CO_2)	ton/day	90
Light gases yield (without CO_2)	%w/w (oil)	9
Propane Yield	%w/w	3.7
Fuel Gas (LHV=22.8 MJ/kg)	ton/day	148.6

sented in Figure 2.5, and calculated volumetric yields (%v) are summarized in Table 2.42 , based on typical product boiling point ranges, see Table 1.1 in Chapter 1.

Table 2.43: CO_2 and sour water wastes to treatment. Total formation of CO_2 from the WCO feed.

Waste to treatment	**Unit**	**Value**
CO_2	ton/day	103.3
CO_2/WCO	%w/w	10
Sour water	ton/day	37.8
Sour water/WCO	%w/w	3.8

The overall CO_2 formation and sour water products are given in Table 2.43. These by-products indicate performance from environmental point of view and represent additional operational and capital costs for the waste treatment and consequent storage. It has to be noted that 11%w of CO_2 is formed with respect to inlet WCO. Hence, the costs for waste treatment might have significant impact on total cost analysis. Nevertheless, waste treatment costs have not been considered in the first analysis of our study.

2.3.2 Catalytic Transfer Hydrogenation (CTH)

The final results of CTH process simulation are presented in Table 2.44. In particular, consumption of utilities are specific to the Waste Cooking Oil feed rate. The mass ratio of reactants, i.e. WCO to ISO-P, equals to 2.93. Fired heater and reactor cooling represent main thermal duties of the process, whereas the electricity consumption is negligible, determined by the load of the feed pumps only. In particular, the cooling of CTH reactor is the dominant duty in the process. The overall thermal energy consumption in fired heater is 485.1 kJ/kg, whereas for cooling is 1094 kJ/kg.

The products and by-products of CTH are presented in Table 2.45. The total liquid mass rate is 763.2 ton/day. The total yield of liquid product with respect to the WCO inlet is 76%w/w.

Table 2.44: Results of CTH process. Consumption of reagents and utilities.

Reagent consumption	**Unit**	**Value**
WCO	ton/day	1000
ISO-P	ton/day	341.8
RATIO WCO/ISO-P	-	2.93
Utility specific consumption	**Unit**	**Value**
Fired Heater	kJ/kg (oil)	485.1
Cooling Water	kJ/kg (oil)	272.4
Cooling Reactor	kJ/kg (oil)	821.5
Feed Pumps (eff=0.95)	kWh/kg (oil)	7.40E-05
Total Electric Energy	kWh/kg (oil)	7.40E-05

The gas by-product is a fuel gas characterized by 21.2 MJ/kg of Low Heating Value (LHV). High amount of CO_2 is present in the gaseous stream, as can be seen in Appendix B. Therefore, LHV value can be further upgraded for a higher LHV (38 MJ/m^3).

Table 2.45: Product and by-product of CTH process.

Product and By-product yield	**Unit**	**Value**
Total HC Liquid	ton/day	763.2
HC Volume Flow	m^3/day	1011.9
Total Gases	ton/day	478.1
LHV Gases	kJ/kg	21167
Yield HC liquid	%w/w (oil)	76%

The liquid product is analysed by simulated distillation method (ASTM D86) in Aspen Plus. The percent distilled volume (%v) at different temperatures is the one presented in Figure 2.12. Accordingly, the amount of distilled Naphta, Kerosene, Diesel and traces of GPL are given in Table 2.46.

Table 2.46: Amount of liquid products of CTH reactor

HC liquid products	**Unit**	**Value**
Naphta	%v/v	30%
Kerosene	%v/v	60%
Diesel	%v/v	10%

Waste streams to be sent to treatment are summarized in Table 2.47. The overall CO_2 formation and waste water is calculated. These undesired by-products indicate the performance of CTH process from environmental point of view and the loss of carbon. It has to be noted that 17%w/w of CO_2 is formed with respect to the WCO inlet, i.e.

169 ton/day. Moreover, part of CO_2 formation is determined as well from isopropanol decomposition, hence the overall CO_2 loss based on total inlet is precisely 12.6%.

Table 2.47: Waste to treatment streams: CO_2 and dirty water.

Waste to treatment streams	**Unit**	**Value**
CO_2	ton/day	169.4
Waste Water	ton/day	71.2
Loss CO_2	% w/w (oil)	16.90%
Loss CO_2	% w/w (feed)	12.60%
Loss Water	% w/w (oil)	7%

2.3.3 Performance comparison

The key results of process simulation are summarized in Table 2.48 to compare Conventional and CTH Jet Fuel process performances. In particular, the amount of liquid fuels, energy consumption and CO_2 emissions are listed, as they represent main factors to evaluate the performance in this process. The fraction of liquids produced from both processes are similar, i.e. 77 %w/w for Conventional and 76 %w/w for CTH. Nevetheless, the liquid mixture obtained by the Conventional process is characterized by a higher amount of Kerosene, which have 20% more than for CTH. On the other hand, the amount of Naphta and Diesel is higher in CTH process. The thermal energy consumptions are very similar for the base case, i.e. when a complete integration of heat produced in HDO reactor is achieved. Concerning the electric energy, the Conventional process has a very high consumption determined by high operating pressures and the handling of gaseous H_2 (compressors). On the contrary, the CTH process has negligible power consumption due to low operating pressure and the transport of liquid streams. The similar and different perfomances, respectively for thermal and electric energy, are highlightened by comparison of process conditions. In fact, it can be seen that maximum temperatures and pressures represent an indication of the energy demand. In the case when the HDO reactor thermal duty is not integrated in the heat balance, thermal consumption of the Conventional process is estimated to be for 43% larger than that of CTH. Another factor of comparison is given by the environmental parameters concerning the formation of CO_2, which largely exceeds in CTH process than in Conventional Jet Fuel process, i.e. 16.9 %w/w and 10 %w/w respectively with respect to the inlet WCO, and the waste water, which also in this case is larger in CTH than in Conventional process.

Eventually, the two process PFD's can be compared. It can be seen that the number of pieces of equipment necessary for the Conventional process is much larger, comprising 2 reaction systems (HDO and HCC), whereas in CTH only 1 reaction system is used. Moreover, CTH does not require the large recycle of gaseous streams, which is an advantage in terms of the sizing and operating of reaction system. An important

Table 2.48: Performance comparison of Conventional and CTH processes.

Performance parameter	**Conventional**	**CTH**	**Unit**
Waste cooking oil basis rate	1000	1000	ton/day
Liquid fuels products			
Naphta	20	30	%v/v
Kerosene	80	60	%v/v
Diesel	0	10	%v/v
Liquid Yield	77	76	%w/w
Waste to treatment			
% CO2	10	16.9	%w/w
% Water	3.8	7	%w/w
Energy consumption			
Heating Energy	60.9 (HDO - integrated) 513 (HDO - not integrated)	485	kJ/kg
Cooling Energy	1299 (HDO - integrated) 1750(HDO - not integrated)	1093	kJ/kg
Electric Energy	0.105	7.40E-05	kWh/kg
Maximum Pressure	9.2	0.2	MPa
Maximum Temperature	400	380	°C

comparison concerns the quality of liquid products. In CTH they are characterized by a high amount of aromatics and alkenes, whereas the Conventional process does not have any of these. For the Jet Fuel requirements maximum allowance for aromatics is 25% and a ppm order of magnitude for alkenes. Therefore, the product quality of CTH concerning the amount of alkenes is not satisfactorily at this stage of research (%, as shown in Table 2.49). However, it is expected that future experiments will be addressed towards catalyst optimization, which will include also noble metals able to offer selective hydrogenation which will improve the hydrogenation performances and reduce the amount of olefins in the liquid.

Table 2.49: Aromatics, Alkanes and Alkenes in Kerosene. Product characterization of liquid: average molecular weight MW and boiling point Tb.

Kerosene composition	**mol%**
Alkenes	42.5
Alkanes	37.1
Aromatics	20.4

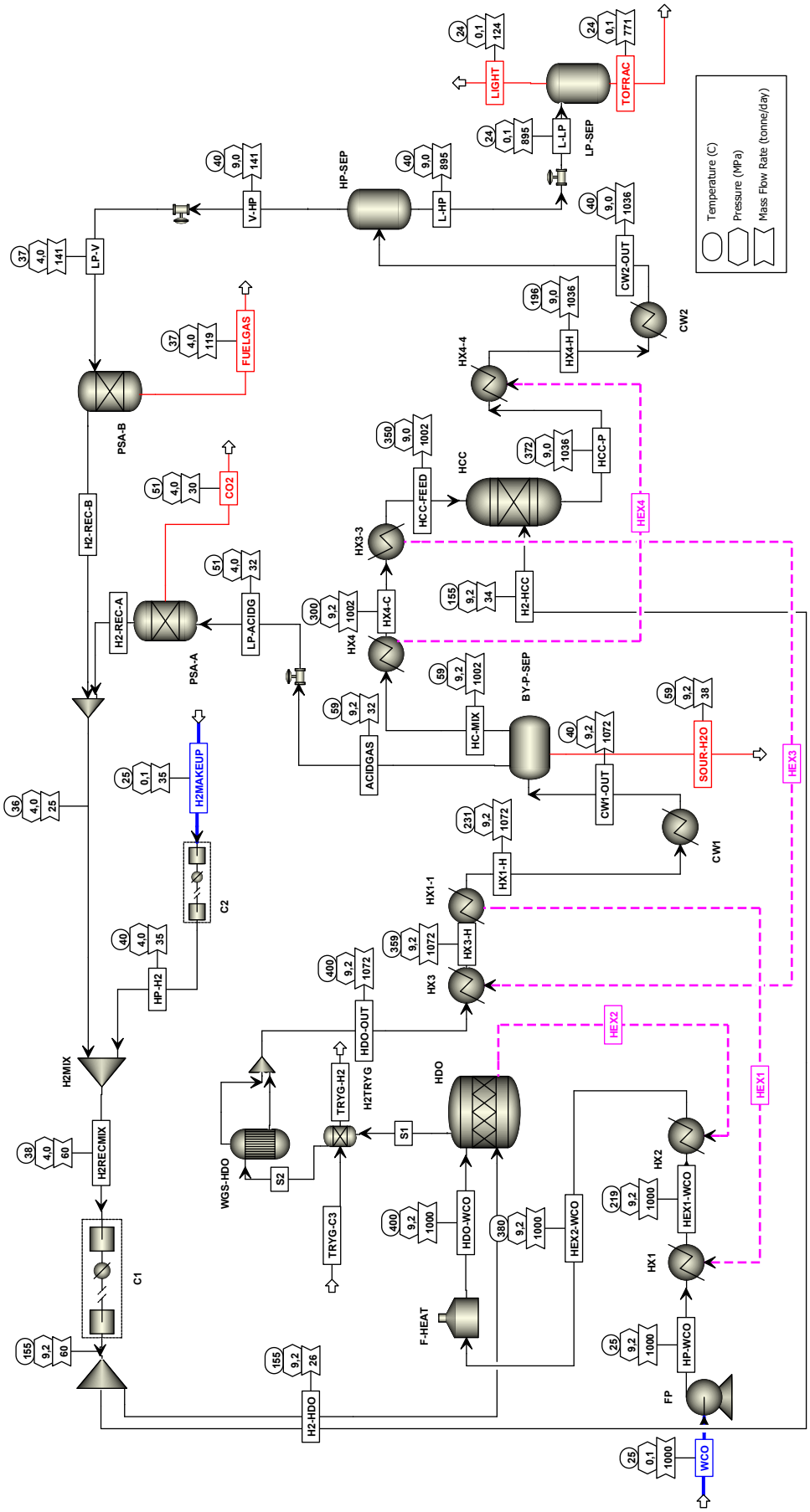

Figure 2.15: Conventional Process flow diagram (PFD) in Aspen Plus.

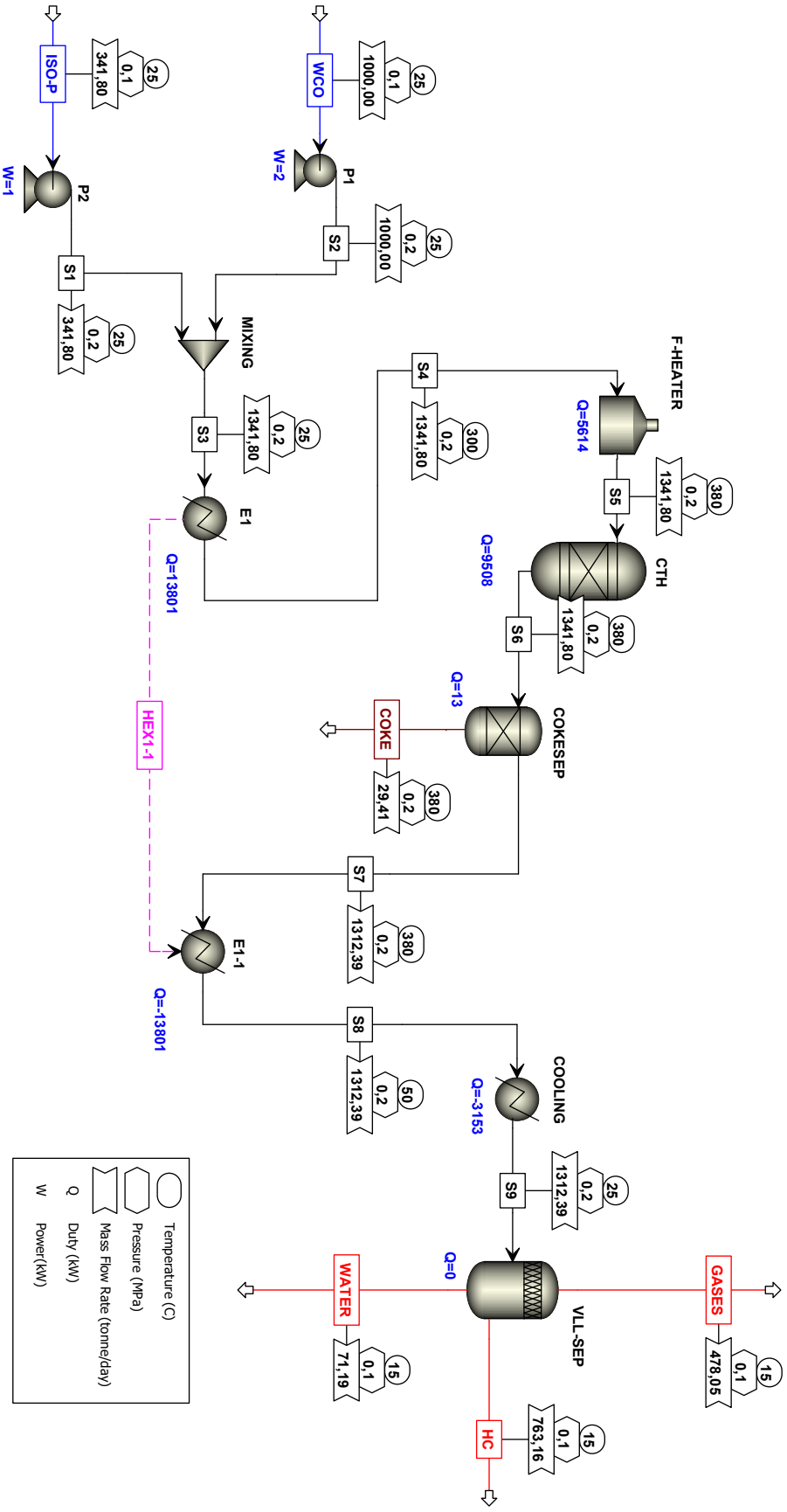

Figure 2.16: Catalytic Transfer Hydrogenation (CTH) process flow diagram in Aspen Plus.

Chapter 3

Selection and Sizing of equipment

The scope of this chapter is the selection and sizing of process equipment for Conventional and CTH Jet Fuel processes. Design information are necessary to evaluate the cost of the plant cost, which will be worked up from the cost of individual process equipment. The detailed sizing was carried out only for a part of process equipment, i.e. reactors, process vessels, heat exchangers, whereas, others as compressors, pumps, fire-heaters and PSA, the sizing of these is not addressed in this chapter and the cost will be based on their capacity factor, as indicated in Chapter 4.

3.1 Conventional Jet Fuel process

3.1.1 Hydrodeoxygenation-HDO reactor

Hydrodeoxygenation reactions are relatively slow in terms of mass transfer of reactants at process conditions (high pressure and temperature), due to numerous multistep reactions occuring. Accordingly, large catalyst hold-up is necessary to increase the rate of production. Moreover, HDO is characterized by a multiphase feed, i.e. the oil (WCO) in the liquid phase and hydrogen in the gas phase.
The selection of commercial hydrotreating reactors is directed towards Trickle Beds Reactor (TBR), which are characterized by long residence time for the liquid phase and large catalyst hold up. Moreover, among other multiphase reactors, Trickle Beds have many advantages, as summarized in Table 3.1 [37].
For exothermal reactions, such as hydrodeoxygenation ones, adiabatic multistage beds with inter-stage cooling are applied. Theoretically, tubes filled with catalyst with internal cooling might also be used for efficient thermal control, however it is less commercially used due to the problems related to catalyst wetting which should be homogenous in all the tubes.
On a reactor scale, gas and liquid phases are introduced from the top, and flow through the voids of catalyst bed. Several different flow regimes, namely trickle flow, pulsing

Table 3.1: Aspects of multiphase reactors. TBR performance [37].

Aspect	Slurry Stirred	Slurry Bubble Column	Three-phase Fluidized	Packed Bubble Column	Trickle Bed
Operation	*	***	****	*****	*****
Solid Loading	**	******	****	*****	*****
Particle Size	**	**	***	*****	*****
Catalyst separation	*	*	***	*****	*****
Lower Catalyst Attrition	*	***	***	****	*****
Heat transfer	*****	*****	****	**	*
Mass transfer	*****	*****	****	***	***
Plug flow/lower back mixing	*	**	*****	***	*****
Viscous/foaming liquid	****	******	****	****	**
Reactor Volume	***	***	***	****	*****
Pressure	**	***	***	*****	*****

flow, and spray flow regimes, may exist in trickle bed reactors depending on the levels of interphase interactions, as shown in Figure 3.1.

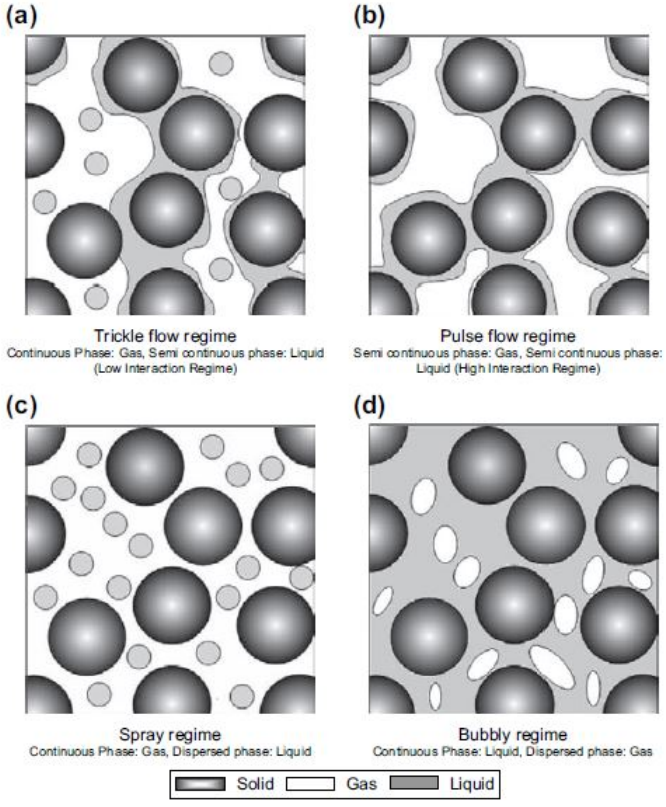

Figure 3.1: Scheme of interphase contacting of different TBR regimes: a) trickle, b) pulse, c) spray and d) bubbly Figure taken from Trickle Reactor Engineering [37].

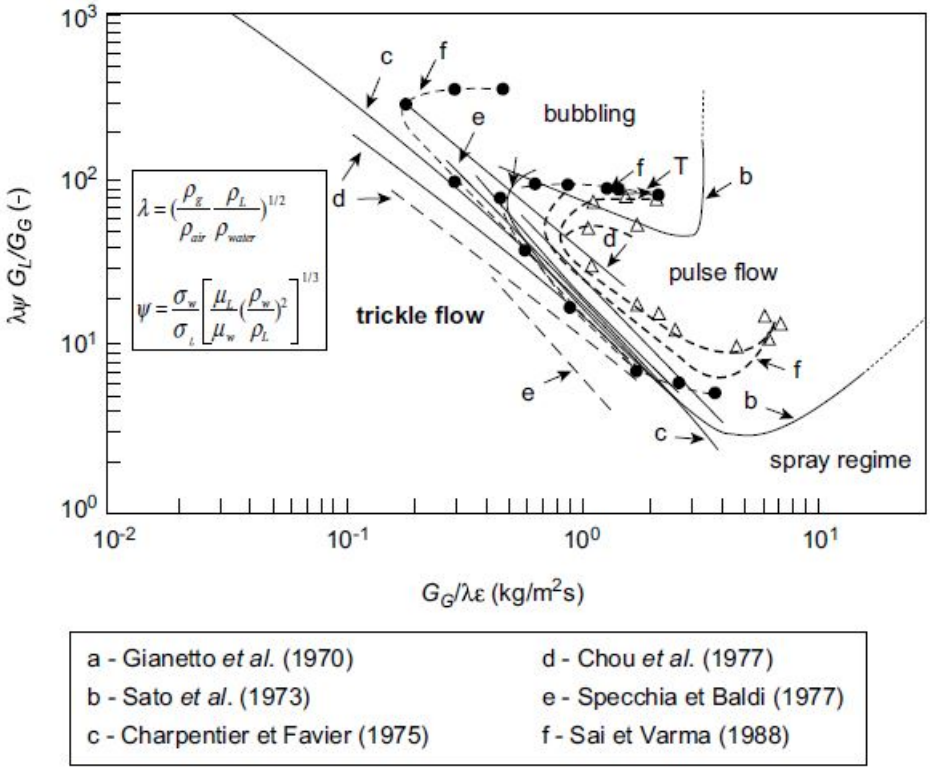

Figure 3.2: Flow regimes in Trickle Bed Reactor: pulse, trickle, bubbling and spray, source [37].

The most important design factor in the Trickle Bed scale up is the flow regime. A trickle flow regime is a typical operating regime for commercial TBR thanks to its wide range of operation and it because it enhances satisfactorily mixing and all interphases contact (liquid-gas-solid). Pulse regime has better catalyst wetting, nevertheless it is characterized by very narrow range of the liquid and gas flow rates.
Accordingly, for the sizing of TBR in trickle flow regime, a diagram showing transition curves is applied, which is illustrated in Figure 3.2. Many authors proposed experimental correlations for the transition curves based on air-water system, as the mostly studied system. The diagram uses dimensionless numbers, λ and ψ, that normalize physical properties by those of water and air, as defined in Figure 3.2.
The flowrates of gas (hydrogen) and liquid (WCO) in HDO reactor and their physical properties, estimated from Aspen, are reported in Table 3.2 and Table 3.3. Catalyst hold up of 60% is assumed as a typical value. The calculated diameter for trickle regime is reported in Table 3.2. In particular, the values of λ, ψ are estimated considering physical properties from Table 3.2. Therefore, the diameter is estimated: the value of $\lambda\psi G_L/G_G$ is calculated from the flow rates of gas (G_G) and liquid (G_L), then $G_G/\lambda\epsilon$ is assumed equal to approximately 0.1 from the Figure 3.1. The diameter calculated for trickle regime is 2.5 m, thus a standard dimension of vessel diameter of 3.048 m (10ft) is assumed.

Table 3.2: TBR diameter calculation: inlet flow rates of and estimation of λ, ψ.

Parameter	Unit	Value
Gas flow rate G	m^3/s	0.06
Liquid flow rate L	m^3/s	0.02
λ	-	1.52
ψ	-	5.77
Bed porosity ϵ	-	0.4
$\lambda\psi G_L/G_G$	-	338
$G_G/\lambda\epsilon$	kg/m^2s	0.1
Diameter calculated	m	2.5
STD Diameter (10ft)	m	3.08

Table 3.3: Physical properties of liquid, gas water and air (Aspen estimation).

Physical property	Unit	Value
surface tension of water-air	mN m^{-1}	73
surface tension of gas-liquid	mN m^{-1}	10
density of air	kg/m^3	1.225
density of water	kg/m^3	1000
density of gas	kg/m^3	5.017
density of liquid	kg/m^3	566.3
viscosity of liquid	mPa s	0.181
viscosity of water	mPa s	1.137

The overall size of TBR is based on kinetic similarity of the liquid phase, i.e. residence time of experimental reaction. Thus, the total volume of catalyst is calculated based on the liquid flow rate and time of reaction. The result of total reactor volume is 245 m^3. Commercial Trickle Bed have aspect ratio L/D between 1 and 10, depending on the properties of the reaction system. In general, higher aspect ratio will have better performance in terms of conversion. Very high aspect ratios however suffer bad distribution of liquid and gas due to higher porosity in the proximity of the walls, while this is less significant for the lower ones. In Figure 3.3, the relation between the number of stages and aspect ratio is presented for the estimated diameter (3.08m), for L/D values ranging between 1.5 and 7. Therefore, if a low aspect ratio is preferred for the reaction, a higher number of stages will be necessary and vice versa. Since the diameter of the column is large, with the consequence of large radial temperature dispersion, a higher number of stages and a low aspect ratio should be preferred, according to the scheme represented in the right side of the Figure 3.4. Therefore, 4-5 stages with L/D between to 2 and 3 appears as the better choice for temperature control of the reactor. As a base case, here 4 stages with aspect ratio 2.5 are selected.

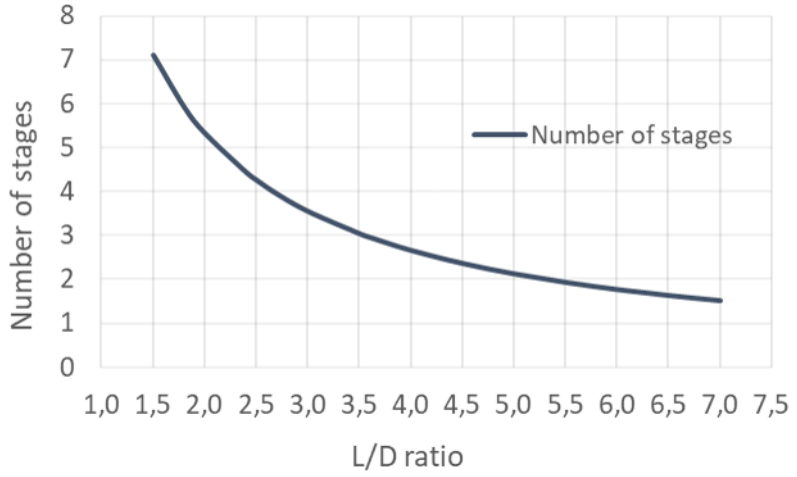

Figure 3.3: Trickle Bed Reactor: aspect ratio L/D and number of stages required for a given diameter (3.08m) of the column with a fixed volume of 245 m^3.

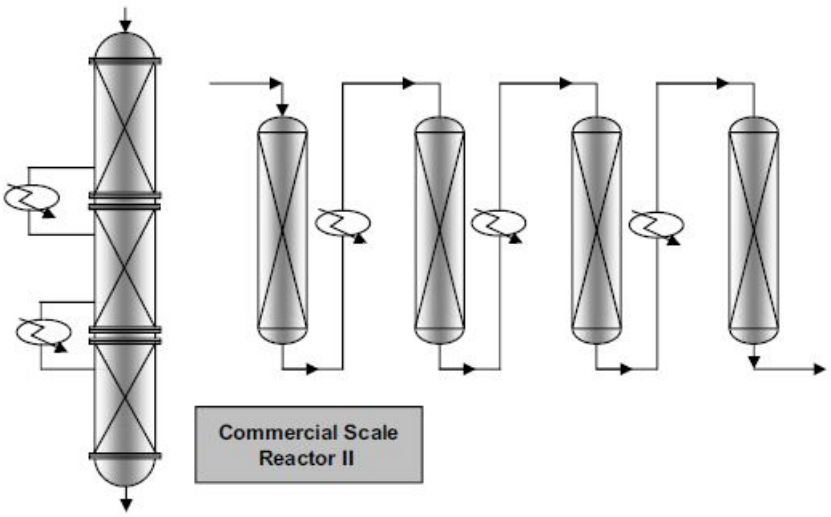

Figure 3.4: Commercial multi-stage beds TBR.

For a more detailed design, which is not addressed since it is out of the scope of this study, more accurate performance can be estimated based on the calculation of liquid and gas hold ups in the column.
Concerning the overall process performance, only pressure drop estimation of TBR is considered as it might have significant effect on the performance of the reactor and the compression load of the feed gas. Accordingly, Wammers correlation in Eq. (3.1) [38]

$$\frac{\Delta P}{0.5\rho_g U_g^2}\frac{d_p}{L} = 155[\frac{\rho_g U_g \epsilon_{bed} d_p}{\mu_g(1-\epsilon_{bed})}]^{-0.37}\frac{1-\epsilon_{bed}}{\epsilon_{bed}(1-\beta_{tot})} \tag{3.1}$$

is used for estimation of gaseous phase pressure drop [30]. In particular, Table 3.4 presents the values used in pressure drops estimation: the liquid hold up fraction

β_{tot} with respect to the total reactor volume can be assumed approximately 0.2, as a typical value for trickle regime, the interstitial velocity is calculated based on the volume occupied by gas, i.e. 20% of the total volume of reactor, and the total length of the reactor bed.

Table 3.4: Pressure drop estimation data in TBR.

Parameter	Unit	Value
Interstitial velocity Ug	m/s	0.04
Liquid hold up β_{tot}	-	0.2
Bed porosity ϵ_{bed}	-	0.4
Lenght of bed L	m	20.2

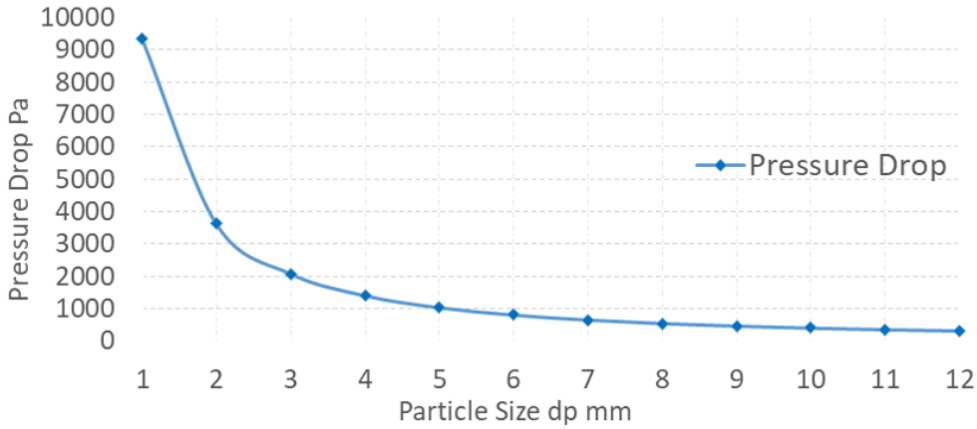

Figure 3.5: Pressure drop estimation in HDO reactor.

Figure 3.5 illustrates pressure drop estimation based on different particle size (dp). It is noted that, particle diameter highly affects the pressure drops. Accordingly, the size and the shape of catalyst represent the key decision parameters for the design of reactor. The typical size of particles are between 1 and 12 mm. It can be seen that very small particle size will determine very high pressure drops; for example, a $dp = 1$ mm has 0.1 MPa of pressure drop, whereas $dp = 5$ mm 0.01 MPa. Therefore, particles larger than 5 mm would represents better performance and less compression load. On the other hand, for larger particles, reaction rates may be limited by intra-particle and interphase mass and heat transfer. For a more detailed analysis of reactor performance based on particle size, mass transfer coefficients and kinetic parameters should be known, as this is suggested for a more detailed study.

Moreover, larger particle size might determine radial and axial dispersion of liquid and gas phases, which is prevented, by rule of thumbs, if L_{bed}/dp and D_{bed}/dp are respectively higher than 50 and 25.

It is worth noting that, if a particle diameter greater than 5 mm is chosen, the pressure

drop will not affect significantly the performance of the reactor and the compression load of the gas phase, hence this values was chosen in this work.

3.1.2 Hydrocracking Reactor - HCC

Commercial hydrocracking units are multistage packed bed reactors with the cooling provided by direct quench with hydrogen at the inlet of each stage, as schematized in Figure 3.6. The total reactor volume is calculated by determining the residence time required for the reaction, i.e. the sizing depends on the reaction rate similarity assuming that the scale up will not be limited by cooling inefficiency.

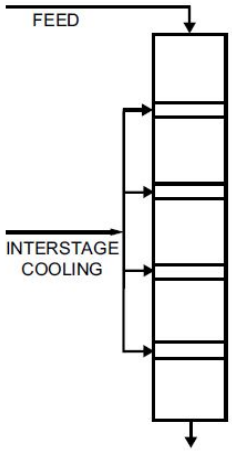

Figure 3.6: HCC reactor with interstage cooling.

The typical range of residence time is 0.5 to 2 hours, depending on the process conditions. Here, a residence time of 1 h is chosen for the gas, and the total volume of reactor calculated accordingly. It is specified that, this is a rough estimation of the total volume assumed by the residence time. Nevertheless, at the initial stage of design for the capital cost evaluation, it is sufficient to determine the overall volume and the diameter.
The calculated total volume is equal to 392.4 m^3 (Table 3.5), and it could be divided

Table 3.5: HCC reactor process conditions.

Reactor operating parameter	Value	Unit
Oil feed	41535	kg/hr
Hydrogen feed	1415	kg/hr
Pressure	90	bar
Temperature	350	°C
Residence Time	1	hr
Gas Total flow rate	392.4	m^3/hr
Volume of Reactor	392.4	m^3

into 4, 5 or 6 stages. Thus, if standard diameters of process vessel is equal to 3.048 or 3.810 meters are considered, i.e. 10 ft and 12.5 ft respectively, the height of each stage can be determined.

The aspect ratio H/D and the number of stages are important parameters for the determination of the temperature at the end of each bed and radial distribution of the temperature profile within the bed. However, if a detailed analysis of the temperature profile with different bed configurations and the heights is to be carried out, more detailed information should be available. Therefore, the energy balance for the estimation of temperature profile is not addressed in this of study.

The decision of the number of stages, can be made with a general consideration that when increasing number of stages for a given diameter, the aspect ratio H/D decreases. Therefore, the two limiting cases in this analysis are: the higher number of stages (n = 6) with a larger diameter (3.810m), that will decrease the aspect ratio (H/D=1.5), or the lower number of stages (n = 4) with a smaller diameter (3.048m) to increase the aspect ratio (H/D = 4.4), as indicated in Table 3.6.

A larger aspect ratio will determine higher adiabatic temperature at the inlet of each stage, while lower values will give a larger radial dispersion of temperature within the bed. Here, a 5 stages and the diameter of 3.81 m is chosen, determining an aspect ratio of 1.8. This preliminary sizing will have better profile along the length of reactor and the capital costs will be intermediate between those with 4 and 6 stages.

Table 3.6: HCC unit: number of stages and aspect ratio H/D.

	4 stages	5stages	6 stages	Unit
Volume x stage	98.1	78.5	65.4	m^3
D (12.5ft)	3.81	3.81	3.81	m
Height (12.5ft)	8.6	6.9	5.7	m
H/D (12.5ft)	2.3	1.8	1.5	-
D (10ft)	3.048	3.048	3.048	m
Height (10ft)	13.4	10.8	9	m
H/D (10ft)	4.4	3.5	2.9	m/m
Total height	34.4	34.4	34.4	-

As in the HDO reactor, an estimation of pressure drop over the height of the HCC beds is important to analyze if the size of particle diameter affects significantly the performances and the compression load.

Accordingly, Ergun equation [39] in Eq. (3.2) is used for the estimation of pressure drops in a packed bed, where U is the interstitial velocity (m/s), Ep is a void fraction (i.e. 40% of the reactor volume) and x the equivalent particle diameter (m). All the values used for calculating the pressure drops are given in Table 3.7. Assuming a cylindrical catalyst shape, the equivalent sphere diameter can be calculated in Eq. (3.3).

$$\frac{-\Delta P}{H} = 150\frac{\mu_g U(1-\epsilon)^2}{x^2\epsilon^3} + 1.75\frac{\rho_g U^2(1-\epsilon)}{x\epsilon^3} \tag{3.2}$$

$$D_{volume} = (\frac{6}{\pi}V_{particle})^{\frac{1}{3}} \tag{3.3}$$

Table 3.7: Pressure drops calculation in HCC unit.

Variables	Value	Unit
Ugas	0.024	m/s
Density gas mixture	364	kg/m^3
Viscosity mixture	36.6	Pas (10-6)
dp spheres (3-7mm)	0.006	m
d cylinder	0.006	m
length cylinder	0.018	m
d cylinder equivalent	0.01	m

Table 3.8: Results of pressure drops for cylindrical and spherical catalyst in HCC unit.

Catalyst	Value	Unit
Sphere ΔP/H	589.2	MPa (10^{-6}) / m
Sphere ΔP	0.202	MPa
Cylinder ΔP/H	352	MPa (10^{-6}) / m
Cylinder ΔP	0.12	MPa

The results of pressure drop calculations are reported in Table 3.8 . For a spherical catalyst, the pressure drop equals 0.2 MPa, whereas for the cylindrical particles of the same diameter it is approximately 2 times lower, i.e. 0.12 MPa. Therefore, cylindrical shape should be preferred.
It is worth noting that, pressure drops lower than 0.12 MPa not affect significantly the performance of the reactor and the compression load of the gas phase.

3.1.3 Gas-liquid separator

The selection of the gas-liquid vessel for the separation of the products of HDO and HCC reactors takes into account the possibility of using vertical or horizontal configurations. A vertical one configuration is more suitable for systems with large throughput of the gas phase, whereas a horizontal is applied for systems with large liquid hold-up. The final selection of both configurations will be decided by the cost of equipment, i.e by. the diameter and the volume of the vessel.
The sizing of a vertical vessel is based on the settling velocity ut, calculated according to Eq. (3.4). In particular, ut is multiplied by 0.15 if no demister is used in the vessel,

as in this case.

$$u_t = 0.15 * 0.07(\frac{\rho_l - \rho_g}{\rho_g})^{0.5} \tag{3.4}$$

Therefore, from the value of settling velocity the minimum diameter can be calculated, as it shown in Eq. (3.5). The diameter is usually rounded up to the nearest standard vessel size so that standard vessel closures can be used.

$$D = (\frac{4}{\pi}\frac{V_g}{u_t})^{0.5} \tag{3.5}$$

The height of the vessel outlet above with respect to the gas inlet should be sufficient to allow for disengagement of the liquid drops. A height equal to the diameter of the vessel should be used for this section, as shown in Figure 3.7. Moreover, the height of the liquid level depends on the hold-up time necessary for smooth operation and control. Hence, 10 minutes of liquid hold-up is typically assumed, as suggested by Towler. et al [40].

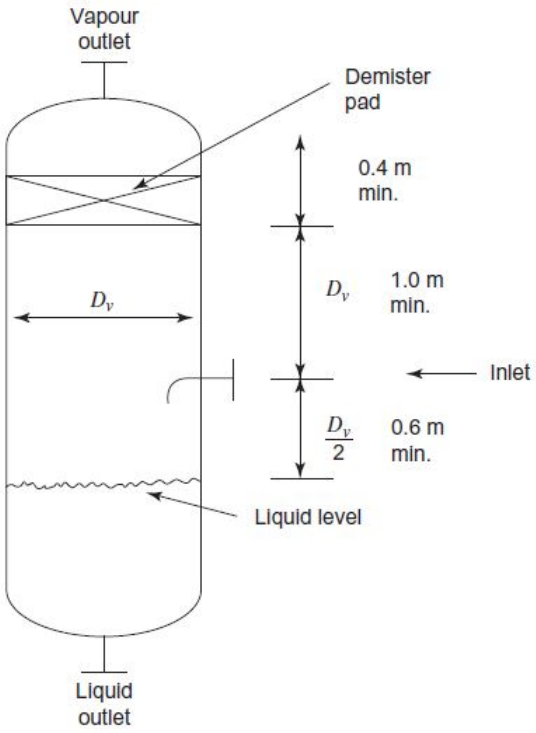

Figure 3.7: Vertical separator layout.

The layout of typical horizontal separator is instead shown in Figure 3.8. In this configuration, the vessel diameter cannot be determined independently of its length. The minimum diameter is estimated assuming that the liquid hold-up occupies 50% of the total vessel volume, i.e. the liquid height is set at half of the vessel diameter.

The economic length to diameter ratio depends on the operating pressure, i.e. for high pressure this ratio is typically 5 and for lower it is 3, as shown in Table 3.9.

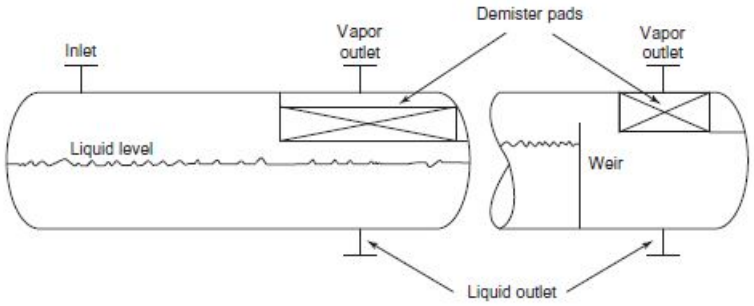

Figure 3.8: Layout of horizontal separator.

Table 3.9: Horizontal aspect ratio Lv/Dv [40]

Operating Pressure MPa	Lv/Dv
0-2	3
2.0-3.5	4
>3.5	5

Accordingly, the results of sizing and selection of the configuration are reported in Table 3.10 and Table 3.11 respectively for ByP-SEP, HP-SEP and LP-SEP blocks (see Conventional process - PFD - Fig.2.15) The result show that the horizontal configuration would be less expensive for the LP-SEP, determined giving a lower volume, whereas, the vertical configuration is more economic for the ByP-SEP block.

Table 3.10: Calculation of settling velocity of ByP-Sep, HP-Sep and LP-Sep gas-liquid separators.

Variable	ByP-SEP	HP-SEP	LP-SEP	Unit
settling velocity	0.04	0.046	0.221	m/s
liquid density	687.7	634.9	688.7	kg/m^3
vapor density	45.11	31.15	1.55	kg/m^3
Gas flow rate	0.005	0.052	0.927	m^3/s
Liquid flow rate	1.1	0.979	0.898	m^3/min
Liquid hold up (10min)	10.63	9.788	8.982	m^3

Table 3.11: Sizing of ByP-Sep, HP-Sep and LP-Sep gas-liquid vessels: vertical and horizontal configuration.

	ByP-SEP		HP-SEP	LP-SEP		Unit
	Vertical	Horizontal	Vertical	Vertical	Horizontal	
Min Diameter	0.399	1.756	1.2	2.31	1.88	m
Diameter	0.609 (2)	1.820 (6)	1.22 (4)	2.36 (7.75)	1.98 (6.5)	m (ft)
Height	37.39	9.1	10.21	5.59	5.94	m
Volume	10.9	23.67	11.92	24.47	18.29	m3

It can be noted that, the most economic configuration depends on the settling velocity, which is smaller for the system at high pressures, i.e. ByP-SEP and HP-SEP, determining vertical configuration as the most economic, on the other hand for the low pressure vessel, such as LP-SEP, a horizontal tank will be more advantageous due to the high settling velocity. Accordingly, for HP-SEP only vertical vessel is sized, since the horizontal will be more expensive due to the low settling velocity.

3.1.4 Heat Exchangers

Preliminary sizing of the heat exchangers in Conventional hydrogenation process route includes 4 shell&tube type heat exchangers, used for thermal integration, (HEx1-HEx2-HEx3-HEx4) and 2 auxiliaries (CW1-CW2), as shown in Figure 2.15. The sizing is based on the overall heat transfer coefficient U (W/m^{2}s) of two fluids. These values can be found in Towler et al. for different types of fluids [40]. In particular, the oil-oil and oil-water systems have U between 250-500 W/m2°C and 400-900 W/m2°C respectively. Thus, midpoint values are selected for the two ranges (400 W/m^2°C and 700 W/m^2°C).
The heat transfer area A (m^2) are estimated by Eq. (3.6), where Q is the heat transfer duty and ΔTml is mean log temperature difference as defined in Eq. (3.7), where *T1* is hot fluid inlet temperature, *T2* is hot fluid outlet temperature, *t1* is cold fluid inlet temperature and *t2* is cold outlet fluid temperature. The values of the temperature of hot and cold fluid are described in Chapter 2. The resulting areas are reported in Table 3.12.

$$A = \frac{Q}{U\Delta T_{ml}} \tag{3.6}$$

$$\Delta T_{ml} = \frac{(T1 - t2) - (T2 - t1)}{ln\frac{(T1 - t2)}{(T2 - t1)}} \tag{3.7}$$

Table 3.12: Heat Exchanger sizing of Conventional process.

Heat exchanger	Q (kW)	U (W/m^2°C)	ΔTml (°C)	Area (m^2)
HeX1	5046.77	400	170.9	73.8
HeX2	5228.45	400	73.1	178.8
HeX3	1867.4	400	54.4	85.9
HeX4	7425.61	400	101	183.7
Auxilary	Q (kW)	U (W/m^2°C)	ΔTml °C	Area(m^2)
CW1	6196.58	700	61.4	144.3
CW2	5735.74	700	53.1	154.2

The selection of the type of heat exchanger takes into account the fouling properties of the fluids. In particular, the 4 heat exchangers HEx of the process are characterized by hydrocarbon fluid on both sides, i.e. the shell and tube is the most appropriate configuration. Accordingly, a floating head type is preferred for these systems, as the one that can be cleaned on both sides (shell and tubes). An exception is made for HEx3, for which a Kettle type is selected due to the complete vaporization of the feed (stream HE4-C) and is therefore, more efficient. For the same reasons, floating head heat exchangers are selected for CW1 and CW2, which will allow eventually to select a dirty water produced in the stream Sour Water for cooling requirements.

3.2 Catalytic Transfer hydrogenation (CTH) process

3.2.1 CTH reactor

A packed bed reactor is selected for CTH according to the experimental set-up; therefore, the scale up of CTH reactor is based on the experimental value of weight hourly space velocity ($WHSV$), defined as:

$$WHSV = \frac{(MassFlowrateOil + MassFlowrateISOP)}{MassCatalyst} \tag{3.8}$$

The scaled-up feed flow rate and the experimental WHSV are reported in Table 3.13. Accordingly, the mass of catalyst, and the volume of the reactor, considering of 60% of catalyst hold up, are evaluated. The latter results equal to 27.4 m, hence much lower compared to that of the Conventional process route.

Table 3.13: Scale up CTH. Estimation of the reactor volume.

SCALE-UP FEED	Unit	Value
WCO	ton/day	1000
ISO-P	ton/day	341.8
Experimental WHSV	hr^{-1}	6.8
Weight of Catalyst	kg	8222
Catalyst density	kg/m^3	980
Catalyst porosity	-	0.51
Volume of catalyst	m^3	16
Catalyst hold up	-	0.6
Reactor Volume	m^3	27.4

It is worth noting that, the reaction system is characterized by high coke formation (section (2.2.1)). Since an interruption in process operation is not acceptable to remove coke, a cyclic regeneration o swing-bed regeneration can be used. In cyclic designs, the

plant has several reactors in parallel and it is designed so that one reactor can be taken off stream for regeneration without affecting the operation of the others. Cyclic regeneration can occur as often as several times in an hour, but longer cycles are preferred to reduce fatigue damage. Accordingly, since coke formation is determined to occur in a few hours, a minimum of 2 parallel beds of CTH reactors are necessary for the operation.
The regeneration of the catalyst might be performed by high pressure steam at very high temperatures or by high temperature flue gases from a fired heater. The specific method used for catalyst regeneration is not an objective of this study. Therefore, it can be assumed that the heat of flue gases is used for the regeneration, without affecting the operation costs of the process.

3.2.2 Gas-Liquid separator

Similarly as the Conventional process, gas-liquid separator might have horizontal and vertical configuration, and the sizing is based on settling velocity. In order not to be redundant, the sizing procedure is already presented in section (3.1.3).
The calculation of settling velocity and the liquid hold-up of VLL SEP unit (see CTH-PFD, 2.16) are reported in Table 3.14. The estimation of minimum diameter of both configuration are compared in Table 3.15.

Table 3.14: VLL-Sep sizing. Calculation of settling velocity and liquid hold-up.

Parameter	Value	Unit
ut settling velocity	0.2	m/s
liquid density	762	kg/m^3
vapor density	2.11	kg/m^3
Gas flow rate	2.45	m^3/s
Liquid flow rate	0.79	m^3/min
Volume for 10min hold up	7.9	m^3

Table 3.15: Calculation of the volume of VLL Sep.

Size	Vertical	Horizontal	Unit
Min Diameter	3.95	1.59	m
Diameter	3.96(13ft)	1.82(6ft)	m
Height/lenght	6.6	9.1	m
Volume	81.1	23.7	m^3

Since the pressure of separation is 0.1MPa, the densities of gas and liquid determine a large settling velocity u_t. Thus, the horizontal vessel will have lower volume, i.e. the horizontal vessel will be more economic. The ratio L_v/D is assumed equal to 3, as suggested in Table 3.9 of section (3.1.3).

3.2.3 Heat Exchangers

The preliminary sizing of heat exchangers (shell&tube type) in CTH process includes E1-1 and Cooling units (see CTH-PFD, Figure 2.16). As in previous case, a floating head heat exchanger type is selected because of the possibility of cleaning on both sides (shell and tubes), due to the fouling characteristics of hydrocarbon mixtures. Therefore, this decision allows to select a waste water stream characterized by ppm of hydrocarbons in the process for cooling requirements, i.e. stream Water of VLL Sep. The sizing is based on global heat transfer coefficient U, which is assumed taking into account the type of the fluid in the system. In particular, U for oils-water systems (Cooling block) is in the range of 400-900 W/m^2°C while for oil-oil (E1) is between 250-500 W/m^2°C. Thus, midpoint values of 700 and 400 W/m^2°C are selected respectively. Accordingly, the surface areas of E1 and Cooling units, calculated according to Eq. (3.6) are reported in Table 3.16. The temperatures of hot and cold fluid are reported in Chapter 2 and Figure 2.16.

Table 3.16: Heat exchanger sizing based on global heat transfer coefficient U.

Heat Exchanger	Duty (kW)	U (Wm^2 °C)	ΔTml (°C)	A (m^2)
E1	13801	400	47.29	730
Cooling Water	3152.5	700	26.8	168

Chapter 4

Economic Analysis

This chapter is focused on the economic analysis of both Conventional and CTH jet fuel production processes. According to the procedure by Towler et al.[40], first, the fixed capital investment (FCI) is estimated based on the two process flow diagrams and sizing of equipment, presented in Chapter 2 and Chapter 3 respectively; second, the cost of manufacturing (COM) is estimated, including direct cost of manufacturing (DCM), fixed cost of manufacturing (FCM) and general expenses (GE). Thirdl the revenues are determined considering a sale price of products at the refinery "gate", i.e. without taking into account taxes, market and distribution costs.. Lastly, the profitability analysis is carried out based on assumptions from the literature. The hours of operation per year are 8000, i.e. a stream factor of 0.913 is considered.

4.1 Capital and Operating Expenses

4.1.1 Fixed Capital Investment (FCI)

The fixed capital investment is the total cost of designing, constructing, and installing a plant and the associated modifications needed to prepare the plant site. The fixed capital investment is made up of [40]:

- The inside battery limits (ISBL) investment, i.e. the cost of the plant;
- The modifications and improvements that must be made to the site infrastructure,known as offsite or OSBL investment;
- Engineering and construction costs;
- Contingency charges.

$$FCI = ISBL + OSBL + ENG + CONT \tag{4.1}$$

At the early stage of design, it is important to define the ISBL carefully as, according to the simplified procedure adopted, other project costs are estimated based on ISBL cost. In fact, the overall project economics can be miscalculated if the ISBL estimate is poorly defined.

For the estimation of ISBL, a module cost technique based upon Guthrie method [41] is applied. Therefore, the cost for each equipment module (Cbm) is determined. Hence, the ISBL will be defined as the total bare module cost of the plant or as the sum of all bare module costs Cbm.

The Offsite costs (OSBL) are typically evaluated as a percentage of ISBL costs and 50% is usually applied as an initial estimate of the total plant cost at the base conditions if no details of the site are known. For an established site with well-developed infrastructure, offsite costs will generally be lower. It is worth noting that the total bare module at base conditions does not depend on materials and pressure factor of the plant.

Engineering costs are best evaluated individually based on project scope, as they are not directly proportional to the project size. A rule of thumb for engineering costs is assuming 30% of ISBL+ OSBL cost for smaller projects, and 10% of ISBL+OSBL cost for larger projects. However, it should be specified that the Guthrie method applied for estimating bare module cost of equipment takes already into account the engineering work. Therefore, the total bare module cost of the plant is the sum of ISBL and Engineering cost.

Contingency charges are extra costs added to the project budget to allow for variations

Table 4.1: The equipment list of CTH and Conventional processes.

Conventional	**CTH**
Reactors	
HDO reactor	CTH reactor (x 2)
HCC reactor	(1CTH for regeneration)
SMR - Hydrogen production plant	
Compressors and Pumps	
Centrifugal compressor C1	P1 Centrifugal Pump WCO
Centrifugal compressor C2	P2 Centrifugal Pump ISO-P
Centrifugal Feed Pump	
Separation	
HP Vessel for by-products	LP Vessel for product
HP Vessel for product	
LP Vessel for product	
PSA towers for hydrogen	
Heat Exchangers	
Fired Heater	Fired Heater
E1/E2/E3/E4	E1
CW1/CW2	CW

from the cost estimate. A minimum contingency charge of 10% of ISBL+OSBL is suggested. In this case, a value of 15% of the total bare module cost is applied.
The equipment related to the process flow diagrams used for the estimation of the FCI are summarized in Table 4.1.
The location factor of the plant is set equal to 1, i.e. the study assumes that the plant will be based in the U.S. It is worth noting that all correlations used for equipment purchase are already based on the data from U.S. Gulf Coast (UGSC). Shipping and transporting costs of equipment will be negligible. Moreover, the currency exchange rate is not present, which for some locations might have significant impact.
For the calculation of the Cbm of equipment, first the purchase costs (Cp) of single units are obtained from the cost-curves method which can be found in Turton et al. updated till 2001 [41]. This cost-curves of equipment are expressed as a function of the type and the size of the corresponding unit.
Additionally, the cost of purchase is affected by inflation along with time; hence, the Chemical Engineering Plant Cost Index (CEPCI) is applied, according to Eq. (4.2). The values of CEPCI in the years of reference of some equipment are reported in Table 4.2 [42].

$$Cp(2017) = Cp(time\ of\ reference)\frac{Cepci(2017)}{Cepci(time\ of\ reference)} \tag{4.2}$$

Table 4.2: Cepci values [42].

Year	Cepci
1999	390.6
2001	397
2006	478.6
2017	558

It is worth noting that the Guthrie method takes into account the design factor of material and pressure, as shown in Appendix A. In fact, the Conventional hydrogenation process is characterized by high pressure 9.2 MPa, so that it is important to take it into account in the purchase cost of equipment. In particular, the cost of the vessels is significantly sensitive to the operating pressure.
Furthermore, the material chosen for HDO and HCC reactors are stainless steel (SS), because of hydrogen gas in compatibility with respect to the normal carbon steel (CS). In fact, the tensile ductility of CS is degraded by hydrogen, hence, materials with more resistant properties are necessary for a long life operation, as reported in Technical Reference for hydrogen compatibility of materials [43].
In order to get more reliable costs of main equipment, such as process reactors (HDO,

HCC and CTH), the evaluation is carried out by considering the costs associated with reactor vessel and those related to the type of catalyst used separately. The cost of catalyst for HDO reactor is estimated from the loading of NiMO-γAl_2O_3 catalyst, given in Table 2.3, while for the HCC a price of hydrocracking catalyst per cubic meter of oil is applied from a typical hydrocracking unit [7]. The cost of CTH charcoal catalyst is estimated from the price of activated carbon.

The hydrogen production plant cost (Steam Methane Reforming (SMR) plant), required for the conventional process route, is obtained according to correlations of SMR plant cost from Hydrocarbon Processing that can be found in Towler et al. [40]. Specifically, the investment cost is based on the capacity S of hydrogen production, expressed as MMscft/day, as it shown in Eq. (4.3). The amount of hydrogen required for the Conventional process is 0.39 Mm^3/day, i.e. 13.804 MMscf/day. The values of a (1.759) and n (0.79) are on 2006 year basis; thus, the inflation rate is corrected by CEPCI reference, as indicated in Eq. 4.2.

$$C_{SMR} = aS^n \tag{4.3}$$

The cost of the PSA unit employed in the Conventional process is based on at similar process unit for hydrogen recovery from flue gases, built in Canada in 1999. This reference unit has a different capacity [30]. Therefore, the purchase cost is estimated using a capacity factor with a cost exponent, according to Eq. (4.4). The reference unit considered is the amount of gas to be treated, in m^3/s. As a rough estimation, the exponent factor is assumed as 1, for the reason that the main part of the cost in the equipment will be based on the packing of adsorbent, the amount of which will be linearly proportional to the feed rate. It is specified that this method will slightly overestimate the cost, since generally the exponent factor is lower than 1.

$$Cp = (\frac{Capacity}{Capacity_{ref}})^n Cp_{ref} \tag{4.4}$$

Results of equipment bare module costs Cbm are summirized in Table 4.3 for Conventional and CTH processes, divided in groups by their function. Thus, the total bare module costs of these processes can be calculated. It must be noted that the total cost of CTH plant is 2.5% that of Conventional hydrogenation process, which is mainly due to the high operating pressure of the latter. In fact, the total bare module cost at base condition (i.e. ambient pressure and CS as construction material) is only 13.5M$, while the one at process conditions is 10 times greater. It is worth specifying that the CTH process conditions are the same as the base conditions, i.e. no special material is required and the process operating pressure is atmospheric (see material and pressure factor in Appendix A).

In addition, Figure 4.1 shows the pie chart of the capital costs of Conventional process,

Table 4.3: Total bare module cost of Conventional and CTH process.

Conventional			**CTH**	
Reaction system	Cbm @base	Cbm	**Reaction system**	Cbm
HDO (4xBed)	$ 1.650.989	$ 40.814.775	HCC	$ 132.396
HCC (5xBed)	$ 2.972.309	$ 76.618.490	2ndHCC Regen.	$ 132.396
SMR plant cost	$ 3.441.561	$ 16.313.000		
Fired Heater	$ 1.450.520	$ 1.675.585	Fired Heater	$ 3.010.655
Compression			**Pumps**	
Compressor 1	$ 448.539	$ 1.704.448	Feed pump WCO	$ 12.046
Compressor 2 (3stages)	$ 1.234.069	$ 4.689.461	Feed pump ISOP	$ 11.158
Feed Pump WCO	$ 73.966	$ 174.098		
Separation			**Separation**	
By-P HP separation	$ 74.603	$ 663.506	LP Sep	$ 74.603
Product HP-Separation	$ 53.829	$ 581.563		
Product LP-Separation	$ 63.636	$ 63.636		
PSA-hydrogen recovery	$ 890.909	$ 2.940.000		
Heat Exchangers			**Heat Exchangers**	
E1	$ 104.310	$ 123.010	E1	$ 469.833
E2	$ 157.024	$ 185.175		
E3	$ 387.390	$ 456.232		
E4	$ 159.540	$ 187.891		
CW1	$ 139.372	$ 164.358		
CW2	$ 144.417	$ 169.854		
Total (2017)	**$ 13.446.983**	**$147.525.082**	**Total (2017)**	**$ 3.843.086**

displaying the weight of each unit on the overall capital cost. Thus, it can be seen that the cost of HCC unit accounts for 52% and the HDO reactor for 28% on the overall plant cost. Together, the two reaction system sum up to 80% of the plant investment. This large contribution is determined by slow reactions that unavoidably increase the volume of reactors and critical operating conditions. The third large part of the cost is represented by SMR plant for hydrogen production, i.e. 11% of the total.

The pie chart of cost of equipment for CTH process is given in Figure 4.2. It can be noted that in this case the major contribution to the capital cost is related to the fired heater (78%). Therefore, it is noticeable that the reaction system is less expensive with respect to the other units.

Finally, the fixed capital investment FCI of the two processes is reported in Table 4.4. In particular, the FCI of CTH process is 3.5% only of the Conventional one, demonstrating that, the capital investment for CTH is negligible respect to other one.

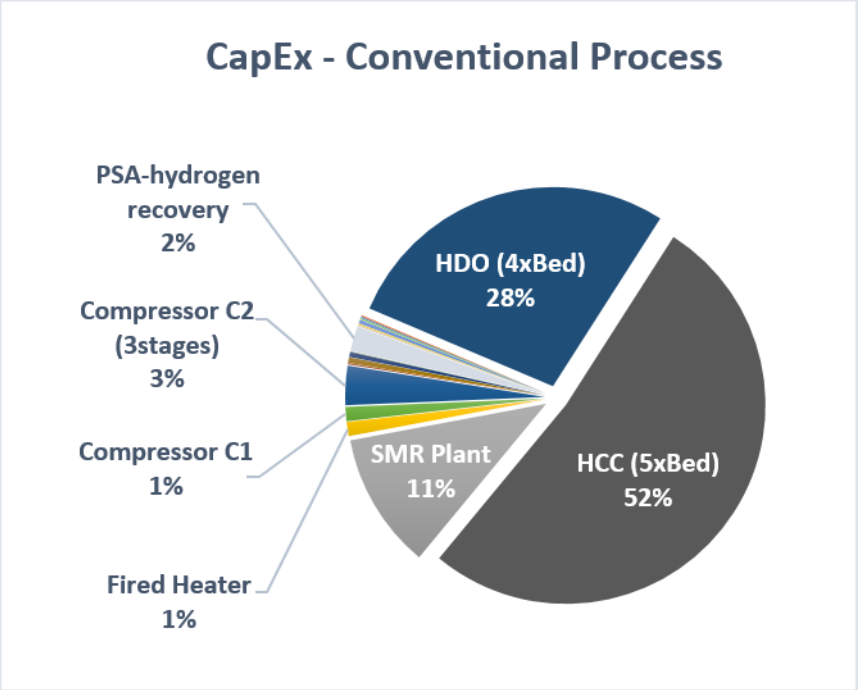

Figure 4.1: Pie chart of the equipment cost in Conventional process for the total of 147.5M$.

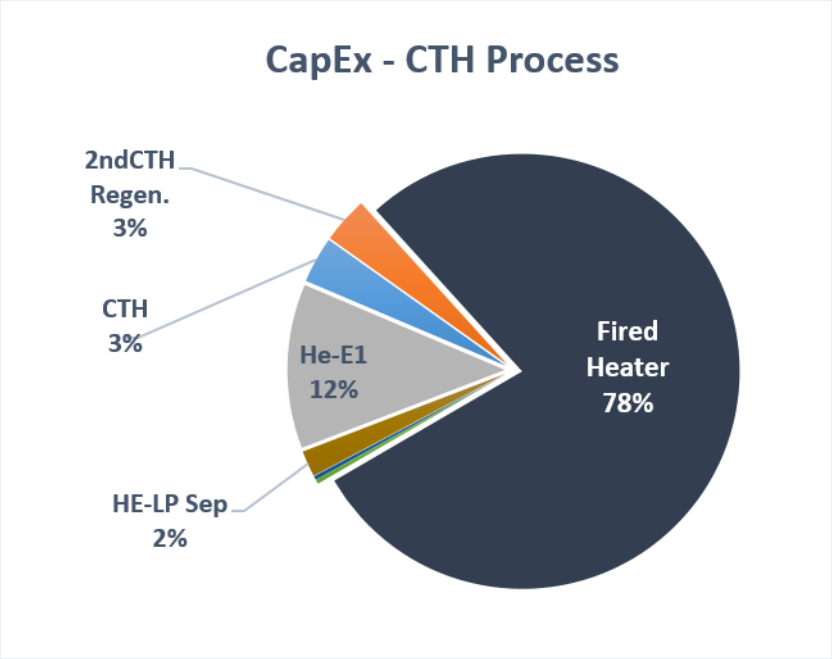

Figure 4.2: Pie chart of the equipment cos of CTH process for the total of 3.8M$.

Table 4.4: Fixed Capital Investment for CTH and Conventional process.

Fixed Capital Investment	**Conventional**	**CTH**
ISBL+Engineering	$ 147.525.082	$ 3.843.086
OSBL (50% Total Cbm base)	$ 6.723.492	$ 1.921.543
Contingency (15% Total Cbm)	$ 26.554.515	$ 576.463
Total	**$ 180.106.853**	**$ 6.341.092**

4.1.2 Cost of Manufacturing (COM)

The Costs of Mmanufacturing (COM) of Conventional and CTH process are estimated by dividing costs into Direct Manufacturing (DMC), Fixed Manufacturing Cost (FMC) and General Expenses (GE) as follows:

$$COM = DMC + FMC + GE \tag{4.5}$$

Direct manufacturing costs represent operating expenses and vary with the throughput. Therefore, these expenses comprise the costs of raw materials (RM), utilities (UT), staff and operating labor, maintenance, miscellaneous supplies and patent with royalties. The fixed manufacturing cost are independent of changes in production rate, they are charged at constant rates even when the plant is not in operation. Therefore, they include property taxes, insurance and depreciation.
The general expenses cost represent administration and development costs required to carry out all the business functions. In particular, the product distribution and selling costs are also included in general expenses if it is assumed that the product is delivered to the final user. In this case, product gate prices are assumed as explained in section (4.2.1). The cost of utilities and raw material for Conventional and CTH are presented in Table 4.5. The price of waste cooking oil is approximately 150 $/ton. Isopropanol

Table 4.5: Direct operating expenses: cost of raw material and utilities.

Variable Expense	Unit	Value
Raw Material		
Waste cooking Oil	$/ton	150
Hydrogen	$/kg	1.6
Isopropanol	$/kg	1.3
Utility		
Electric power	$/kWh	0.087
Natural gas (LHV=38.42MJ/m^3)	$/m^3	0.13
Cooling Tower Water @30°C	$/GJ	0.354
Refrigerated water @5°Cand returned at 15°C	$/GJ	4.43
Hot Oil in CTH	$/kW	0.074

price in CTH process is assumed to be 1.3 $/kg , as reported by ICIS for the year 2008 [44]. Hydrogen is considered as self - produced material in situ. The cost of production is between 120-200 euro/1000 Nm^{3}of hydrogen. Hence, since hydrogen density is 0.0899 kg/m3 at normal condition, the cost varies between 1.33-2.22 euro/kg. This reference is an updated estimation provided from a company with hydrogen producing facility in Europe. Thus, the hydrogen production cost in US, taking into account the euro-dollar exchange value of 1.23 (average of 2017), will be more or less 1.6 - 2.7 $/kg. It is worth noting that the cost of hydrogen production is significantly sensitive by 60-80% to the natural gas price, which is the main source for hydrogen production through

Steam Methane Reforming (SMR). In the literature, F.Mueller et al. [45] reports that hydrogen production price in Europe will be approximately 1.5 euro/kg for a large size SMR conversion in 2020. Pearlson et al. in their economic analysis assumed an average price of 1.45 $/kg for 2005-2010 when the natural gas had higher trend of price.
Accordingly, the cost of hydrogen production is assumed to be 1.6 $/kg in this study, as a lower limit, considering that in the US the price of natural gas is much lower than in Europe. The real producing price probably is even less than 1.6 $/kg. Since the overall economics will be sensitive to the hydrogen production cost, a sensitivity study might be important.

Table 4.6: Average US price of Natural gas: LNG and pipeline.

Price	$/1000ft^3	$/m^3
Natural Gas (LNG)	4.58	0.13
Natural Gas (pipeline)	2.49	0.071

The cost of electricity is 0.087 $/kWh, according to the national average price in U.S. for industries in 2017. The price of natural gas is based on the type of transportation used, i.e. pipeline or LNG (see Table 4.6. In our case, a liquefied natural gas (LNG) is assumed.. Utility consumption prices of natural gas and electric power are taken from U.S. Energy Information Administration reports for 2017 [1]. The reference of the cost of refrigeration water and tower water, respectively at 15°Cand 30°C, can be found in Turton et al [41].
For the estimation of natural gas utility in the Fired Heater unit, an efficiency of 80% of the thermal system was assumed, i.e. the cost is based on natural gas LHV equal to 30.74 MJ/m3 (80%) instead of 38.42 MJ/m^3.
The utility required for cooling the CTH reactor is based on the amount of heat produced in the reactor. The utility used is hot oil or molten salts due to the high operating temperature, i.e. 380°C. The price of this utility was estimated based on the reference for Hot Oil/Molten Salts for reactor cooling [46]. More specifically, the cost is based on the price of natural gas that would be required to heat the hot oil/molten salts, and the CEPCI value.

Table 4.7 and Table 4.8 summirezes the results of the calculation of direct and fixed manufacturing and of general expenses for Conventional and CTH processes, respectively. Total manufacturing costs are estimated by the sum of single factors for FMC, DMC and GE, based on heuristic values for petroleum industry because of similarity with petroleum refining [7]. In particular, the maintenance, local taxes and insurance are assumed to be 5.5% and 1.5% of fixed capital investment respectively. The distribution and selling costs are assumed equal to zero, since the product price will be defined at the "gate" of the plant, i.e. not a user selling price.

Table 4.7: Direct (without RM+UT+WT), Fixed and General costs of Manufacturing for Conventional process.

Direct (without RM+UT+WT)		**$/year**
Total Staff and operators	29	1.740.000
Maintenance and repairs	5,5% FCI	9.944.170
Miscellanous supply	0,15% FCI	271.205
Patent and royalties	0,94 $/m3 of feed	355.151
Fixed (without depreciation)		
Local taxes and insurance	1,5% FCI	2.712.046
Plant overhead	60% (Staff+Maintenance)	7.010.502
depreciation	-	-
General Expenses		
Administration costs	15% (Staff+Maintenance)	1.752.625
Distribution and selling costs	Product based on "Gate" prices	-
Research and development	5% COM	5.048.501
Total		**28.834.201**

Table 4.8: Direct (without RM+UT+WT), Fixed and General costs of Manufacturing for CTH process.

Direct (without RM+UT+WT)		**$/year**
Total Staff and operators	25	1.500.000
Maintenance and repairs	5.5% FCI	348.76
Miscellaneous supply	0.15% FCI	9.512
Patent and royalties	0.94 $/m3 of feed	355.151
Fixed (without depreciation)		
Local taxes and insurance	1.5%FCI	95.116
Plant overhead	60% (Staff+Maintenance)	1.109.256
depreciation	-	-
General Expenses		
Administration costs	15% (Staff+Maintenance)	277.314
Distribution and selling costs	Product based on "Gate" prices	-
Research and development	5% COM	10.771.825
Total		**14.466.935**

The number of operators per shift was determined by the Eq. (4.6) , and multiplied by 4.5 to cover all shifts in the year. Neq is the total number of equipment from Table 4.9. The number of all staff (clerical, engineers, technicians etcâ) is estimated assuming a modern plant staff for refinery, as detailed in Table 4.9. The average labor wage for staff and operators in a chemical plant is 60000$/year, as reported in the Bureau of Labor Statistics for 2016 [47].
Accordingly, the total manufacturing cost of Conventional and CTH processes are calculated and summarized in Tables 4.10 and 4.11. Operating costs of raw materials and utilities are added to the direct cost of manufacturing. It is specified that in this study the waste treatment costs (WT) were not analyzed.

$$N_{op} = (6.29 + 0.23N_{eq})^{0.5} \tag{4.6}$$

Table 4.9: Staff and operators in a Conventional and CTH processes. The number of staff is taken from a modern refinery.

Staff	N per shift	Conventional	CTH
Refinery manager		1	1
Operations manager		1	1
Maintenance manager		1	1
Engineers		3	3
Operators	4.5 shift per roll	15	12
Lab personnel		2	2
Technicians		2	2
Clerical personnel		4	4
Total		29	26

Table 4.10: Total Cost of Manufacturing (COM) for Conventional process.

Raw material RM	**Value**	**Unit**	**Cost $/year**
WCO	1000	ton/day	50.000.000
Hydrogen	35.2	ton/day	18.773.333
Utilities UT			
Compressor 1	1196	kW	836.586
Compressor 2 (make up)	3191	kW	2.230.902
Feed WCO Pump	125	kW	87.54
Cooling Water 1	6197	kW	63.175
Cooling Water 2	5736	kW	58.477
Fired Heater (LHV= 38.42MJ/m3)	704	kW	85.807
Waste treatment WT	-	-	-
Direct+Fixed+GE from Table 4.7			**28.834.201**
Total COM (without depreciation)			**100.970.022**

A graphical representation, of Conventional and CTH processes operating expenses (OpEx) is given in Figures 4.3-4.4. It is worth noting that the OpEx of Conventional

Table 4.11: Total Cost of Manufacturing (COM) for CTH process.

Raw material	**Value**	**Unit**	**Cost $/year**
WCO	1000	ton/day	50.000.000
Isopropanol	341.8	ton/day	148.113.333
Utilities			
Hot oil CTH	9508	kW	2.138.041
FEED WCO Pump	2.1	kW	1.458
FEED ISOP Pump	1	kW	696
Cooling Water 1	3153	kW	32.14
Fired Heater (LHV= 38,42MJ/m3)	5614	kW	683.904
Waste treatment	-	-	-
Direct+Fixed+GE from Table 4.8			**14.466.935**
Total COM (without depreciation)			**215.436.508**

process are 72.1 M$/year, while the those of CTH are 206 M$/year, hence 3 times larger. This huge difference is determined by the cost of isopropanol (148 M$/year), which accounts for almost 74% of the total operating costs of the process.
It has to be specified that the COM in Table 4.10 and 4.11 does not include the capital depreciation value which will be based on MACRS method and added in the Economic Model in section (4.3).

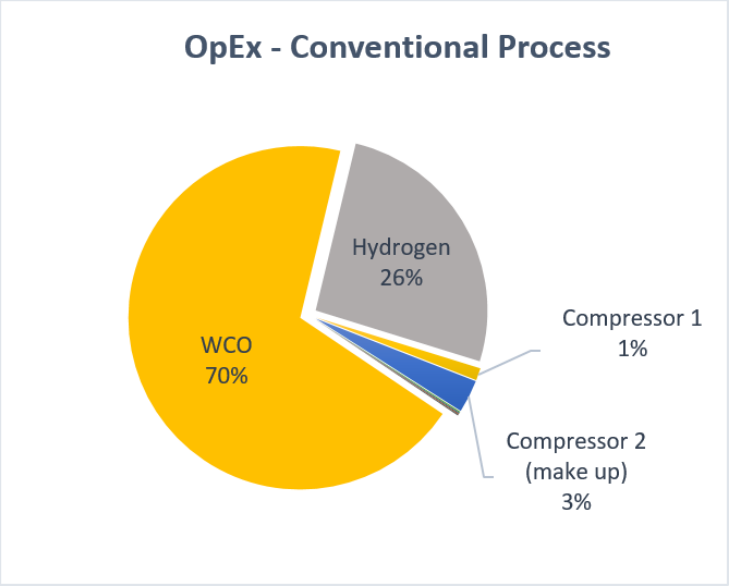

Figure 4.3: OpEx Conventional Process for the total of 72.1M$/year.

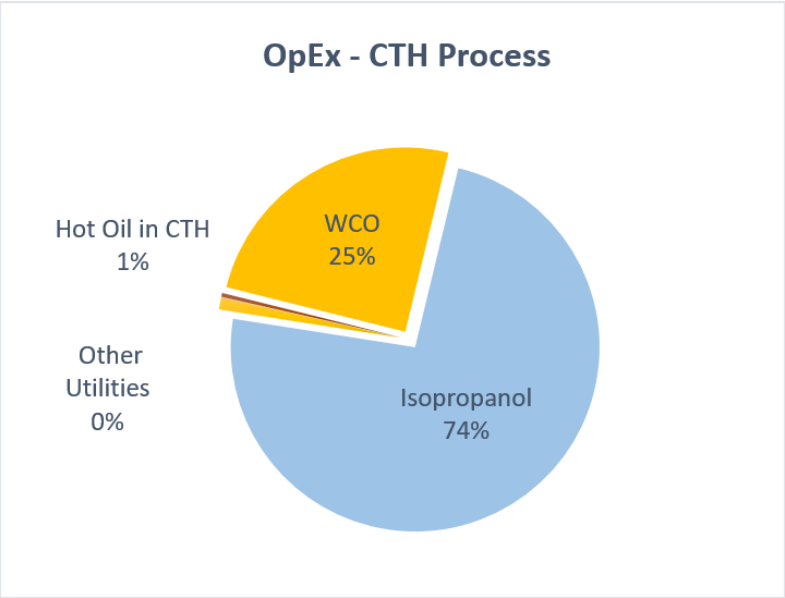

Figure 4.4: OpEx - CTH process for the total of 201M$/year.

4.2 Products profile and gross profit

4.2.1 Products profile and Revenues

The gross income from refinery products sales was calculated considering prices at the refinery gate, which include the cost of production and refiner profit. They do not account for the costs for distribution, transportation, retail mark-up and taxes. Figure 4.5, shows how these factors contribute to the total retail price. The gate prices for gasoline and diesel were calculated subtracting the average percentage of taxes (TAX%) and distribution and market (D&M) price from the corresponding average retail price of 2017. (see Appendix C). In this way, only gate price is accounted for the revenues of gasoline and diesel. The kerosene and propane prices are instead already defined at refinery gate, since U.S Energy Information and Administration provide prices of distillates in the refinery [1]. The detailed calculation of the average prices of 2017 can be found in Appendix C.

Note that in the production of jet fuel from oil, naphtha range co-products are produced. Naphtha can be upgraded to high-octane gasoline by branching or by creating rings. Nevertheless, the capital investment for the reformer unit for the upgrade would be large respect to the low amount of naphta produced (CITATION PEARSLON). Therefore, it will not be economically advantageous. Naphta might also be blended without the need of high-octane number upgrading, as an additive for gasoline. Accordingly to Pearlson et al., since the production of naphta is low, this co-product from can be blended at 5-10% volumes without degrading the octane number of the gasoline [4]. Therefore, it is assumed that naphta could be sold without upgrading. It is worth

noting that the prices of Naphta and LPG are taken as a surrogate of gasoline and propane respectively.

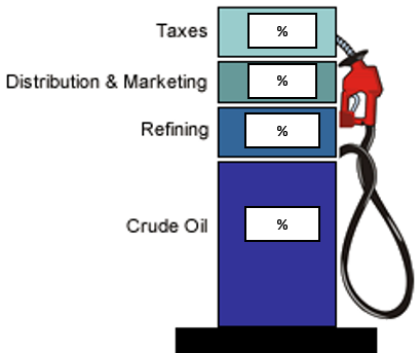

Figure 4.5: Example of percentage of Taxes, Distribution and Marketing, Refining and Crude oil in the final retail price (EIA).

Table 4.12: Gate prices of products: naphta, kerosene, diesel and propane. Naphta and LPG are taken as a surrogate of gasoline and propane respectively.

Product gate price	Average (2017)
Kerosene - JET-F	0.443 $/L
Naphta (Gasoline)	0.426 $/L
Propane	0.186 $/L
Diesel	0.440 $/L

The volumetric yield of each product (n=naphta, k=kerosene, d=diesel) is estimated deriving the mass balance Eq. (4.7-4.10) at standard conditions, where m is the mass, ρ is the density, SG is the specific gravity, V is volumetric rate, yv is the volumetric fraction of the product and Vt is total volumetric rate of the products.

$$m_{mix} = m_n + m_k + m_d \tag{4.7}$$

$$\rho_{mix} V_{mix} = \rho_n V_n + \rho_k V_k + \rho_d V_d \tag{4.8}$$

$$SG_{mix} V_{mix} = SG_n V_n + SG_k V_k + SG_d V_d \tag{4.9}$$

$$SG_{mix} V_{mix} = SG_n y_n^v V_t + SG_k y_k^v V_t + SG_d y_d^v V_t \tag{4.10}$$

Since all variables values in Eq. 4.10 are known, the total volume production Vt can be calculated; therefore, the volumetric rate of each product is estimated with the %vol

reported in Table 2.42 and 2.46 for Conventional and CTH processes, respectively. It is specified that the mixture (mix) is represented by the streams TO FRAC and HC, in the two respective PFDs, that have to be sent to the fractionation tower, and whose properties can be found in Results of Simulation section (2.3). The LPG production by the Conventional process is based on the amount of hydrocarbons in the stream LIGHT and a liquid density of 495 kg/m^3(25°C).
It is noted that the specific gravity SG of naphta, kerosene and diesel can be calculated from the definition of °API (Eq. (4.11)). The average values of °API gravity of naphta, kerosene, diesel based on respective temperature ranges are shown in Table 4.13.

Table 4.13: Specific gravity of products.

	°API	SG
Naphta (80-170 °C)	62	0.731
Kerosene (170-270°C)	42	0.815
Diesel (270-380°C)	38	0.835

$$^{\circ}API = \frac{141.5}{SG} - 131.5 \tag{4.11}$$

Table 4.14: Product incomes of Conventional process.

Products	Produced L/hr	Income $/year
Naphta	8041	27.405.246
Kerosene	32166	113.969.798
Diesel	0	-
LPG	6339	9.433.018
Total		150.808.063

Table 4.15: Product incomes of CTH process.

Products	**Price**	**Unit**	**Produced**	**Unit**	**Income $/year**
Fuel gas (LHV=32.89 MJ/m^3)	0.13	$/m^3	12978	Nm^3/hr	13.497.224
Naphta	0.426	$/L	12042	L/hr	41.038.506
Kerosene	0.443	$/L	24084	L/hr	85.333.119
Diesel	0.436	$/L	4014	L/hr	13.997.406
Total					**153.866.254**

In particular, a large amount of fuel gas is produced in the CTH process, characterized by high composition of C1-C3 fractions (Stream Table of Appendix B). This by-product can be either used to produce electric energy or sold as a fuel gas.
The amount of power energy that can be produced depends on the efficiency of the power plant. In general, a power plant efficiency is around 33-44% depending on the quality of the fuel. If an average values of 35% is assumed, the production of energy

can be estimated, and consequently the income based on the electric energy price. Alternatively, since the LHV of the fuel gas (32.89 MJ/m3) is very similar to that of natural gas LHV (32-40 MJ/m3), it can be assumed the selling of fuel gas is sold at the natural gas price.
The comparison of revenues from fuel gas according to the two scenario described are given in Table 4.16. It should be specified that the scenario of selling electric energy would require also to take into account the power plant facility, therefore, the operating and capital costs will be larger. At this stage, since the operating and capital costs of the power plant are unknown and would require more detailed analysis, it is assumed that fuel gas is sold at the price of natural gas.

Table 4.16: Fuel gas income from electric energy and natural gas.

Description	Flow Nm^3/hr	Price	MW Generation	Income $/year
@Electric Energy	12978	0.0874 kWh	41.5	30.184.201
@Natural Gas	12978	0.13$/$m^3$	0	13.497.224

4.2.2 Gross profit (GP)

The GP is defined as the difference between revenues from the products and the cost of manufacturing without depreciation (COMd) Eq. (4.12). The estimation of the gross profit GP without depreciation for Conventional and CTH are reported in Table 4.17.

$$Gross\ Profit\ (GP) = Revenue(R) - COM_d \tag{4.12}$$

Table 4.17: Gross profit of Conventional and CTH processes.

	Conventional $/year	**CTH $/year**
Revenues R	150.808.063	153.866254
Cost of Manufacturing COMd	100.970.022	215.436.508
Gross Profit	49.838.041	-61.570.254

As it can be seen, the manufacturing cost of CTH largely exceed the revenues, i.e. the gross profit is enormously negative. The reason for this is the large amount of isopropanol required, whose cost alone equals all the revenues from the products. As a rule of thumb, the revenues in a profitable process should be approximately 1.5-2 times larger than the cost of raw materials. Accordingly, the cost of isopropanol should not exceed more or less 30 M$/year. Since the fixed capital investment of CTH is significantly lower with respect to that of the Conventional hydrogenation process, a cost of isopropanol higher than 30M$/year might be profitable too.
It can be concluded that CTH process based on the experimental conditions is not economically profitable. The operating costs of CTH is 201 M$/year and it has to be

reduced by 61.6 M$/year in order to get a positive gross profit, i.e. the cost of raw material should be reduced by 3 times since the cost of utilities is only 1%.
As a conclusion, the profitability analysis of CTH process has the aim of understanding the conditions that lead to a positive profit. In particular, we will consider the calculation of the maximum amount of ISOP to WCO feed ratio that would allow a profitable process (assuming that the product yields and corresponding revenues are unchanged) or of the maximum price of isopropanol in order to have a profitable and competitive process respect to the Conventional. Moreover, a scenario of government tax credit for each liter of fuel ($/L) might be supposed, for the reason that isopropanol is considered as a renewable and green source compared to the production of hydrogen, characterized by high CO_2 emissions. Therefore, the government incentives for the production of bio-derived fuels with Isopropanol might be also a factor of profitability.
Accordingly, a rigorous profitability analysis is performed for the Conventional process in order to evaluate the discounted profitability indexes, such as Net Present Value (NPV), Internal Rate of Return (IRR) and Pay Back Period (PBP). Subsequently, these criteria will represent an objective function for the CTH process to estimate the aforementioned cases.

4.3 Economic Model and Profitability analysis

4.3.1 Economic model

For the profitability analysis an economic model should be well defined. The assumptions used are summarized in the Table 4.18. In this study, similar values are adopted as those of other authors from the U.S. that have recently worked on the profitability of similar processes [48, 36].

Table 4.18: Economic Model assumptions.

Economic Assumption	
Interest/discount rate	8%
Plant Life	25 years
Income Tax rate	35%
Working capital	15% of ISBL+OSBL
Depreciation Method	MACRS
Depreciation period	7 years
Construction + Start-Up period	2 years
Construction plan 1st/2nd year	70% / 30%
Plant salvage value	No value
Land Cost	not included
Operating hours per year (91.3%)	8000 hours

Specifically, the life plant is 25 years of production; the discount rate is taken as a

simple interest rate of 8%, therefore, not based on a debt ratio and loan interests; the tax rate is assumed as 35% of the gross profit GP, similarly as to the one for processes with very high revenues. The completion of start-up and construction time is fixed at the end of the 2nd year, i.e. the production starts at the beginning of the 3rd year.
The method for estimation of depreciation is the Modified Accelerated Cost Recovery System (MACRS) since it is the one used in the U.S. The MACRS approach assumes that all property is aquired midyear and hence assigns half of the full year depreciation to the first and last years of the recovery period. The depreciation period is 7 years, starting at the beginning of the 3rd and ending at the end of the 10th year.
No salvage value of the plant is assumed. Thus, the total capital to be depreciated equals the fixed capital investment FCI. Working capital cost is 15% of ISBL+OSBL, as the typical value for a refinery.
Moreover, no inflation rate is taken: assuming as many authors that although the prices may suffer inflation, margins and hence the cash flows will be insensitive to inflation. Therefore, inflation is generally neglected for the purpose of comparing the economic performance of different projects. The cost of the land for both process is not considered relevant at this stage of analysis.
The cash flow (CF) is defined as the amount of money transferred at given time. Therefore, it depends on the fixed capital investment (FCI) distributed over the time of construction, the working capital WC, the net profit and the depreciation allowance d. Accordingly, the CF after the plant was started-up is determined by the net profit in Eq. (4.13) plus the depreciation allowance as reported in Eq. (4.14):

$$After - Tax\ Profit\ or\ Net\ profit = (GP - d_k)(1 - t) \tag{4.13}$$

$$CF = Net\ profit\ +\ depreciation\ allowance = (GP - d_k)(1 - t) + d_k \tag{4.14}$$

where dk is the value of depreciation at year k, GP the gross profit calculated with Eq. (4.12) and t is the tax rate.
The MACRS method for the depreciation uses following equations Eq. (4.15):

$$MACRS\ d_k = \begin{cases} d_k^{DDB} = \dfrac{2}{n}(FCI - \sum_1^{k-1} d_j), \\ d_k^{SL} = \dfrac{(FCI - \sum_1^{k-1} d_j)}{n}, \qquad \text{when } d_k^{DDB} < d_k^{SL} \end{cases} \tag{4.15}$$

where n is the depreciation period. In particular, in MACRS method the depreciation starts with the double declining balance dDDB, calculated over 7 years of depreciation, hence, changed to the straight line dSL for the remaining period, when the latter value is bigger than d^{DDB}.

The Annualized Cash Flow (ACF) of each year is discounted back to the year 0 as given in Eq. (4.16), with an interest rate equal to 8%;

$$ACF_k = \frac{CF_k}{(1+i)^k} \tag{4.16}$$

The three discounted profitability criteria are time, cash and interest rate, i.e. Discounted Pay Back Period (DPBP), the Net Present Value (NPV), the Internal Rate of Return (IRR) and Present Value Ratio (PVR), evaluated by equations 4.17-4.18-4.19-4.20:

$$NPV = \sum_{1}^{plantlife} \frac{CF_k}{(1+i)^k} \tag{4.17}$$

$$\sum_{1}^{plantlife} \frac{CF_k}{(1+IRR)^k} = 0 \tag{4.18}$$

$$\sum_{1}^{2} \frac{FCI_k}{(1+i)^k} = \sum_{3}^{DPBP-3} \frac{CF_k}{(1+i)^k} \tag{4.19}$$

$$PVR = \frac{present\ value\ of\ all\ positive\ CF}{present\ value\ of\ all\ negative\ CF} \tag{4.20}$$

The internal rate of return (IRR) is the value of interest rate in Eq. (4.18), when the net present value NPV is set to zero. The equation (4.19) assumes that the completion of construction lasts 2 years hence the DBPB starts from the 3rd year, as reported in Table 4.18. The DPBP can be also estimated from the working capital cost WC, i.e. it is the time when the cumulative cash flows equals the amount of WC. The Present Value Ratio (PVR) in Eq. (4.20) is ratio between all positive cash flows and all negative ones. When the difference of investments of two projects is very large, it might be useful to compare this term rather than NPV.

4.3.2 Results of Profitability analysis of Conventional Process

As aforementioned in section (4.2.2), the rigorous profitability analysis and calculation of the indexes is carried out for the Conventional process only. The results obtained are then used as a reference to analyze when CTH process might have competitive and profitable conditions.

A cumulative cash flow diagram helps to easily highlight the criteria for profitability. Therefore, with the assumptions from Table 4.18, the cumulative cash flow diagram of Conventional process is shown in 4.6. The numerical values of profitability analysis are reported in Appendix D, where it is noticeable that deprecation is constant after

the 7th year, i.e. follows the straight line method.

Figure 4.6 shows that the Net Present Value (NPV) in the last year of the project life is equal to 157.4 M$. In addition, it shows the time when the process starts to generate the profit from the total investment (WC included), i.e. the cumulative cash flow is positive from the year 9. The Discounted Pay Back Period (DPBP) is 5.9 years after the plant start-up (i.e. in the 3rd year), which means that at the year 7.9, the fixed capital investment FCI is completely paid off. The results of the IRR is 17.84 % and represent a factor of the risk of the investment. Since the production of Jet fuel is a mature technology with a low risk, 17.84% represent an attractive value for the investment. Results of profitability indexes are summarized in Table 4.19.

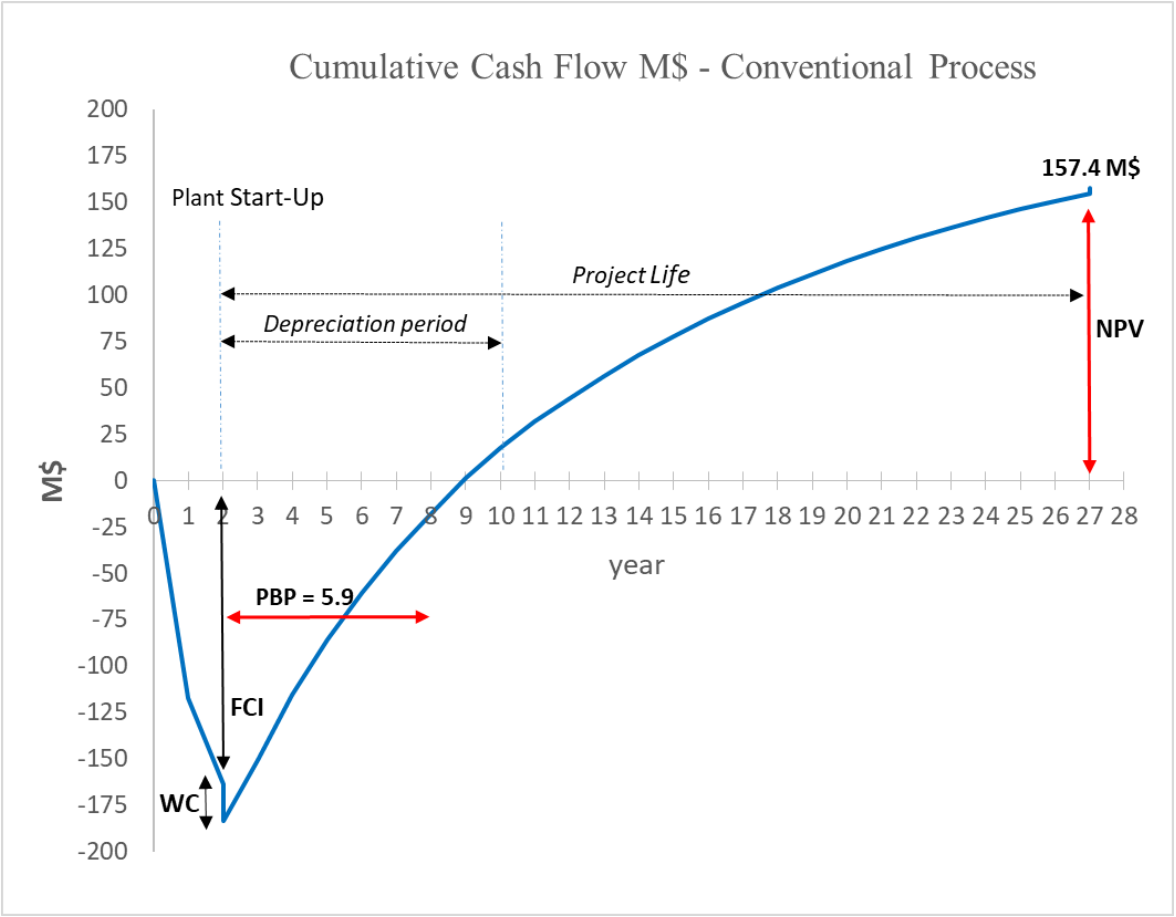

Figure 4.6: Cumulative Cash Flow of Conventional Process.

Table 4.19: Results of profitability criteria.

Profitability Criteria	**Value**
PVR	1.9
IRR	17.84%
PBP	5.9 years
NPV	$157.407.074

4.3.3 Results of profitability analysis of CTH process

The profitability analysis for CTH process was evaluated. As anticipated in section (4.2.2), different cases are considered. Specifically, the isopropanol price and its feed rate are analyzed in order to have, first, a profitable process at the end of the project life (NPV $>$ 0) and secondly, to compete with Conventional process. Accordingly, the values of PBP and PRV of Conventional process, given in Table 4.19, are used as objective functions.
Moreover, a possible government incentive tax credit ($/L) is discussed and calculated as a revenue from each liter of kerosene produced, according to Table 4.15.
It is worth specifying that, the isopropanol feed is kept constant at 341.8 ton/day, vice versa when the sensitivity to the flow rate is studied the isopropanol price is 1.3$/kg, according to the base case described in section (4.1.2). When discussing of government subsidies, the flow rates and the price of isopropanol are kept constant, i.e. 341.8 ton/day and 1.3 $/kg respectively. Therefore, the cases investigated (1-12) are as follows:

1. Price of isopropanol ($/kg) to have NPV = 0. Thus, it is a measure of the maximum price that project could pay for isopropanol and still break even by the end of the project.

2. Price of isopropanol ($/kg) to have NPV = Conventional NPV.

3. Price of isopropanol ($/kg), when the PBP is the same for Conventional PBP.

4. Price of isopropanol ($/kg), when the PVR is the same as Conventional PVR.

5. Amount of isopropanol (ton/day) to have NPV = 0; This, it is a measure of the maximum feed rate that to reach profitable condition at the end of the project life.

6. Amount of isopropanol (ton/day) to have the same NPV as in Conventional process.

7. Amount of isopropanol (ton/day) to have the same PBP as in Conventional process.

8. Amount of isopropanol (ton/day) to have the same PRV as in Conventional process.

9. Incentive Tax for Kerosene-Jet Fuel ($/L) to have NPV = 0. Thus, the minimum incentive to reach a profit at the end of the project.

10. Incentive Tax for Kerosene-Jet Fuel ($/L) to have NPV = NPV Conventional.

11. Incentive Tax for Kerosene-Jet Fuel ($/L) to have PBP = PBP Conventional.

12. Incentive Tax for Kerosene-Jet Fuel ($/L) to have PVR = PVR Conventional.

Table 4.20: Profitability analysis of CTH: isopropanol price, feed, and incentive tax credit analysis.

Cases	**Isopropanol Price**	**Price**	**Unit**
1	Profitable NPV>0	0.781	$/kg
2	CTH same NPV as Conventional	0.637	$/kg
3	CTH same PBP as Conventional	0.774	$/kg
4	CTH same PVR as Conventional	0.775	$/kg
	Isopropanol Feed	**Feed**	**Unit**
5	Profitable NPV>0	205.3	ton/day
6	CTH same NPV as Conventional	167.6	ton/day
7	CTH same PBP as Conventional	203.6	ton/day
8	CTH same PVR as Conventional	203.9	ton/day
	IncentiveTax Credit For Kerosene	**Tax Credit**	**Unit**
9	Profitable NPV>0	0.323	$/L
10	CTH same NPV as Conventional	0.427	$/L
11	CTH same PBP as Conventional	0.327	$/L
12	CTH same PVR as Conventional	0.326	$/L

The results of profitability analysis are summirized in Table 4.20 for all the cases listed above. It can be noted that the CTH process would be profitable if the isopropanol price is lower than 0.781$/kg or if the feed rate does not exceed 205.3 ton/day (i.e. the maximum ratio of ISOP/WCO is 20.5%), or if an incentive tax credit equals to at least 0.323 $ for each liter of kerosene produced is issued.

In addition, the results show that, in order to compete with Conventional process, i.e. to obtain the same values of PBP and PRV, the maximum price or amount of isopropanol are slightly lower compared to the case when NPV is set to 0. This demonstrates that if the CTH process have profitable conditions, it will be more competitive with respect to the Conventional.

It is worth noting that, while the price of isopropanol are determined by market criteria and cannot be arbitrarily optimized, the results of the analysis on isopropanol feed ratio are an important indication for the process (i.e. catalyst) optimization, since it indicates the maximum value of isopropanol and oil ratio to be used in the experiments for a profitable process. Therefore, the catalyst development should be focused not only on the hydrogenation of the unsaturated molecules which were found experimentally, but also on processing a lower amount of isopropanol to obtain similar products. In other words, the source of isopropanol for selective production of hydrogen should be optimized, lowering the need of the amount of isopropanol in the reactor feed.

The cases 2, 6 and 10, i.e. when the NPV values are equal, they are rather insignificant

in the analysis, since the fixed capital investment of the CTH is only 3.5% of the Conventional as shown in Table 4.4, hence, the comparison would not take it into account. Therefore, PVR ratio is more suitable for the comparison of both processes with such a large difference in the fixed capital investments.

Conclusions

The aim of this thesis was to simulate both the Conventional Hydroprocessed Renewable (HRJ) and the Catalytic Transfer Hydrogenation (CTH) processes for the production of Jet fuel from a renewable waste cooking oil (WCO) feedstock, and to analyse their performance. This evaluation is based on the raw material and utilities consumption, yield and quality of the products and on operating and capital expenses. Moreover, a profitability analysis was performed in order to evaluate the economic attractiveness of HRJ process and compare it with the one of Catalytic Transfer Hydrogenation.

In the Conventional HRJ process simulation, an accurate calculation of the hydrogen requirement was essential for the economic analysis since it represents the main cost, for both the production facility and operating costs. Hence, rigorous calculations were performed taking into account the degree of unsaturated compounds in the WCO, the degradation of triglycerides into fatty acids and the properties (aromatization, molecular weight) of the hydrocracking inlet stream. The results of HRJ process simulation, on a WCO feed rate basis, show that the total hydrogen consumption is 3.5% w/w, the total electric consumption is 0.1 kWh/kg, while the heating and cooling requirements are 60.9 kJ/kg and 1300 kJ/kg, respectively. These figures result in 72.1 M$/year of operating expenses for a capacity of 1000 ton/day of WCO treated, determined predominantly by the cost of raw materials (70% WCO and 26% hydrogen).

The process simulation of CTH was derived from laboratory experimental data of the reaction system. The experimental analysis of product stream contained numerous components; therefore, an averaging approach, based on the boiling points and molecular weight, was performed to estimate the yield of products. The results of CTH process simulation estimated 485 kJ/kg and 1094 kJ/kg for heating and cooling requirement respectively, while the power consumption is negligible. The isopropanol to WCO ratio is 34.2 %w/w, hence 10 times larger than hydrogen used in HRJ process. For the same WCO feed rate, the operating expenses are 201 M$/year, of which 74% and 25% are determined by isopropanol and WCO raw materials, respectively. The operating expenses of CTH is almost 3 times larger the ones of Conventional. This huge difference is determined by the cost of isopropanol (148 M$/year).

The yield of liquid fuel products of the two processes are quantitatively similar, i.e.

77%w/w and 76%w/w for HRJ and CTH respectively. Therefore, the total revenues are comparable (151 M$/year and 154 M$/year for HRJ and CTH respectively). In particular, the Jet fuel production in HRJ (80%v/v) is larger than in CTH (60%v/v), which is characterized by a higher amount of naphta (30%v/v). The product quality of CTH is not satisfactorily at this stage of research concerning the amount of alkenes with regard to Jet fuel specifications. However, the research for a new catalyst for selective hydrogenation is still under development and will improve performances and reduce the olefin in the liquid.

The results of the economic analysis showed that the CTH process based on the experimental conditions is not economically profitable. The operating expenses have to be reduced by 61.6 M$/year in order to get a positive profit, i.e. the cost of raw material should be reduced by 3 times, since the cost of utilities is only 1% of the total. On the other hand, the gross profit of the HRJ process was estimated as 50M$/year.

The estimated fixed capital investment of HRJ process is 180M$, determined significantly by the high operating pressure of 9.2MPa. On the other hand, the CTH fixed capital investment is only 3.5% that of the HRJ one, demonstrating that the capital investment for CTH at low pressure would be negligible respect to other one.

Finally, the results of profitability analysis of the HRJ process revealed its economic attractiveness: the internal rate of return (IRR) was found to be 18%, the Pay Back Period (PBP) 5.9 years and the Net Present Value of 154M$ at the end of the project life. The profitability analysis of CTH process showed that, to compete with HRJ process, the maximum isopropanol to WCO ratio should be 20.5%w/w. Therefore, the catalyst development should be focused not only on the hydrogenation of the unsaturated molecules which were found experimentally, but also on processing a lower amount of isopropanol to obtain similar products.

APPENDIX A

CAPITAL COST OF EQUIPMENT

Purchase cost of equipment Cp ($) are estimated from cust-curves correlations taken from Turton et al.
Bare modul cost of equipment Cbm ($) is based on Guthrie method with coefficients B_1, B_2, F_{bm}, F_p and F_m.

$$Log_{10}Cp^{\circ} = [K_1 + K_2 Log_{10}(A) + K_3\left(Log_{10}(A)\right)^2]$$

$$C_{BM} = Cp^{\circ}(B_1 + B_2 F_P F_M) \;\; or \;\; C_{BM} = Cp^{\circ} F_{BM} F_P$$

$$Log_{10}F_P = [C_1 + C_2 Log_{10}(A) + C_3\left(Log_{10}(A)\right)^2]$$

$$F_{P,vessel} = ((P \cdot D)/(2\,(850 - 0.6\,D)\,) + 0.00315)/0.0063$$

where *D – diameter of vessel [m];*
P – pressure [bar]
A – capacity factor [cum or kW or sqm];
Fp, Fm– pressure and material factor.

Equipment	K1	K2	K3
Compressor	2.2897	1.3604	-0.1027
HE Floating head	4.8306	-0.8509	0.3187
HE Fixed Tube	4.3247	-0.303	0.1634
HE Kettle	4.4646	-0.5277	0.3955
Vessel Horizontal	3.5565	0.3776	0.0905
Vessel Vertical	3.4974	0.4485	0.1074
Pump	3.3892	0.0536	0.1538
Fired-Heater	7.3488	-1.1666	0.2028

Equipment	B1	B2
Heat Exchanger	1.63	1.66
Process Vessel-Horizontal	1.49	1.52
Process Vessel-Vertical	2.25	1.82
Pump	1.89	1.35

Equipment	C1	C2	C3
Fired Heater	0.1347	-0.2368	0.1021
Pump	-0.3935	0.3957	-0.00226
HE (shell&tube)	0.03881	-0.11272	0.08183
Compressor	0	0	0

Conventinal equipment: material factor

Equipment	HDO	HCC	HEx 1/2/3/4	CW 1/2	Fired-Heater	Pump	By-P-Sep	High-P-Sep	Low-P-Sep
Material	SS	SS	CS	CS	CS	CS	CS	CS	CS
Fm	3.1	3.1	1	1	1	1.8	1	1	1

CTH equipment: material factor

Equipment	CTH	E1	CW1	Fired-Heater
Material	CS	CS	CS	CS
Fm	1	1	1	1

APPENDIX B

STREAM TABLE : CONVENTIONAL

FIRST PART

Stream Name	Units	ACIDGAS	CO2	CW1-OUT	CW2-OUT	FUELGAS	H2	H2-HCC	H2-HDO	H2MAKEUP	H2REC
Temperature	C	59	51	40	40	37	155	155	155	25	36
Pressure	MPa	9.2	4.0	9.2	9.0	4.0	9.2	9.2	9.2	0.1	4.0
Mass flow rate	ton/day	32.40	30.06	1072.13	1035.91	118.55	59.96	33.96	26.00	35.16	24.80
Average MW		17.15	41.20	95.29	41.45	28.19	2.02	2.02	2.02	2.02	2.02
Mass Fractions											
H2		0.072	0.000	0.003	0.023	0.000	1.000	1.000	1.000	1.000	1.000
C15H30O2		0.000	0.000	0.000	0.000	0.000	0.000	0.000	0.000	0.000	0.000
C19H38O2		0.000	0.000	0.000	0.000	0.000	0.000	0.000	0.000	0.000	0.000
C18H34O2		0.000	0.000	0.000	0.000	0.000	0.000	0.000	0.000	0.000	0.000
C18H32O2		0.000	0.000	0.000	0.000	0.000	0.000	0.000	0.000	0.000	0.000
CO		0.104	0.112	0.005	0.008	0.062	0.000	0.000	0.000	0.000	0.000
CO2		0.694	0.748	0.098	0.079	0.400	0.000	0.000	0.000	0.000	0.000
H2O		0.003	0.003	0.039	0.000	0.000	0.000	0.000	0.000	0.000	0.000
CH4		0.000	0.000	0.000	0.044	0.309	0.000	0.000	0.000	0.000	0.000
C2H6		0.000	0.000	0.000	0.010	0.042	0.000	0.000	0.000	0.000	0.000
C3H8		0.127	0.137	0.050	0.048	0.107	0.000	0.000	0.000	0.000	0.000
C14H30		0.000	0.000	0.097	0.002	0.000	0.000	0.000	0.000	0.000	0.000
C15H32		0.000	0.000	0.042	0.001	0.000	0.000	0.000	0.000	0.000	0.000
C16H34		0.000	0.000	0.000	0.001	0.000	0.000	0.000	0.000	0.000	0.000
C17H36		0.000	0.000	0.402	0.001	0.000	0.000	0.000	0.000	0.000	0.000
C18H38		0.000	0.000	0.237	0.000	0.000	0.000	0.000	0.000	0.000	0.000
C19H40		0.000	0.000	0.027	0.000	0.000	0.000	0.000	0.000	0.000	0.000
(C4-C18) RGibbs		0.000	0.000	0.000	0.783	0.080	0.000	0.000	0.000	0.000	0.000
Stream Name	**Units**	**H2-REC-A**	**H2-REC-B**	**H2RECMIX**	**HCC-FEED**	**HCC-P**	**HC-MIX**	**HDO-OUT**	**HDO-WCO**	**HEX1-WCO**	**HEX2-WCO**
Temperature	C	51	34	38	350	372	59	400	400	219	380
Pressure	MPa	4.0	4.0	4.0	9.0	9.0	9.2	9.2	9.2	9.2	9.2
Mass flow rate	ton/day	2.34	22.47	59.96	1001.95	1035.91	1001.95	1072.13	1000.00	1000.00	1000.00
Average MW		2.02	2.02	2.02	137.87	41.45	137.87	95.29	274.97	274.97	274.97
Mass Fractions											
H2		1.000	1.000	1.000	0.001	0.023	0.001	0.003	0.000	0.000	0.000
C15H30O2		0.000	0.000	0.000	0.000	0.000	0.000	0.000	0.179	0.179	0.179
C19H38O2		0.000	0.000	0.000	0.000	0.000	0.000	0.000	0.113	0.113	0.113
C18H34O2		0.000	0.000	0.000	0.000	0.000	0.000	0.000	0.186	0.186	0.186
C18H32O2		0.000	0.000	0.000	0.000	0.000	0.000	0.000	0.523	0.523	0.523
CO		0.000	0.000	0.000	0.002	0.008	0.002	0.005	0.000	0.000	0.000
CO2		0.000	0.000	0.000	0.082	0.079	0.082	0.098	0.000	0.000	0.000
H2O		0.000	0.000	0.000	0.004	0.000	0.004	0.039	0.000	0.000	0.000
CH4		0.000	0.000	0.000	0.000	0.044	0.000	0.000	0.000	0.000	0.000
C2H6		0.000	0.000	0.000	0.000	0.010	0.000	0.000	0.000	0.000	0.000
C3H8		0.000	0.000	0.000	0.049	0.048	0.049	0.050	0.000	0.000	0.000
C14H30		0.000	0.000	0.000	0.104	0.002	0.104	0.097	0.000	0.000	0.000
C15H32		0.000	0.000	0.000	0.045	0.001	0.045	0.042	0.000	0.000	0.000
C16H34		0.000	0.000	0.000	0.000	0.001	0.000	0.000	0.000	0.000	0.000
C17H36		0.000	0.000	0.000	0.430	0.001	0.430	0.402	0.000	0.000	0.000
C18H38		0.000	0.000	0.000	0.254	0.000	0.254	0.237	0.000	0.000	0.000
C19H40		0.000	0.000	0.000	0.029	0.000	0.029	0.027	0.000	0.000	0.000
(C4-C18) RGibbs		0.000	0.000	0.000	0.000	0.783	0.000	0.000	0.000	0.00	0.00

APPENDIX B

STREAM TABLE : CONVENTIONAL

SECOND PART

Stream Name	Units	HP-H2	HP-WCO	HX1-H	HX3-H	HX4-C	HX4-H	L-HP	LIGHT	L-LP	LP-ACIDG
Temperature	C	40	25	231	359	300	196	40	24	24	51
Pressure	MPa	4.0	9.2	9.2	9.2	9.2	9.0	9.0	0.1	0.1	4.0
Mass flow rate	ton/day	35.16	1000.00	1072.13	1072.13	1001.95	1035.91	894.90	124.17	894.90	32.40
Average MW		2.02	274.97	95.29	95.29	137.87	41.45	92.79	37.95	92.79	17.15
Mass Fractions											
H2		1.000	0.000	0.003	0.003	0.001	0.023	0.001	0.008	0.001	0.072
C15H30O2		0.000	0.179	0.000	0.000	0.000	0.000	0.000	0.000	0.000	0.000
C19H38O2		0.000	0.113	0.000	0.000	0.000	0.000	0.000	0.000	0.000	0.000
C18H34O2		0.000	0.186	0.000	0.000	0.000	0.000	0.000	0.000	0.000	0.000
C18H32O2		0.000	0.523	0.000	0.000	0.000	0.000	0.000	0.000	0.000	0.000
CO		0.000	0.000	0.005	0.005	0.002	0.008	0.001	0.006	0.001	0.104
CO2		0.000	0.000	0.098	0.098	0.082	0.079	0.039	0.269	0.039	0.694
H2O		0.000	0.000	0.039	0.039	0.004	0.000	0.000	0.000	0.000	0.003
CH4		0.000	0.000	0.000	0.000	0.000	0.044	0.010	0.072	0.010	0.000
C2H6		0.000	0.000	0.000	0.000	0.000	0.010	0.006	0.039	0.006	0.000
C3H8		0.000	0.000	0.050	0.050	0.049	0.048	0.041	0.238	0.041	0.127
C14H30		0.000	0.000	0.097	0.097	0.104	0.002	0.002	0.000	0.002	0.000
C15H32		0.000	0.000	0.042	0.042	0.045	0.001	0.001	0.000	0.001	0.000
C16H34		0.000	0.000	0.000	0.000	0.000	0.001	0.001	0.000	0.001	0.000
C17H36		0.000	0.000	0.402	0.402	0.430	0.001	0.001	0.000	0.001	0.000
C18H38		0.000	0.000	0.237	0.237	0.254	0.000	0.001	0.000	0.001	0.000
C19H40		0.000	0.000	0.027	0.027	0.029	0.000	0.000	0.000	0.000	0.000
(C4-C18) RGibbs		0.000	0.000	0.000	0.000	0.000	0.783	0.896	0.368	0.896	0.000

Stream Name	Units	LP-V	S1	S2	SOUR-H2O	TOFRAC	TRYG-C3	TRYG-H2	V-HP	WCO	WGS-L	WGS-V
Temperature	C	37	400	398	59	24	400	398	40	25	400	400
Pressure	MPa	4.0	9.2	9.2	9.2	0.1	9.2	9.2	9.0	0.1	9.2	9.2
Mass flow rate	ton/day	141.01	1026.00	1072.13	37.78	770.73	53.46	7.33	141.01	1000.00	618.47	453.65
Average MW		9.19	75.02	95.29	18.02	120.93	44.10	2.02	9.19	274.97	112.40	78.91
Mass Fractions												
H2		0.159	0.010	0.003	0.000	0.000	0.000	1.000	0.159	0.000	0.002	0.004
C15H30O2		0.000	0.000	0.000	0.000	0.000	0.000	0.000	0.000	0.179	0.000	0.000
C19H38O2		0.000	0.000	0.000	0.000	0.000	0.000	0.000	0.000	0.113	0.000	0.000
C18H34O2		0.000	0.000	0.000	0.000	0.000	0.000	0.000	0.000	0.186	0.000	0.000
C18H32O2		0.000	0.000	0.000	0.000	0.000	0.000	0.000	0.000	0.523	0.000	0.000
CO		0.052	0.003	0.003	0.000	0.000	0.000	0.000	0.052	0.000	0.004	0.007
CO2		0.337	0.106	0.102	0.001	0.002	0.000	0.000	0.337	0.000	0.072	0.133
H2O		0.000	0.039	0.037	0.999	0.000	0.000	0.000	0.000	0.000	0.031	0.049
CH4		0.259	0.000	0.000	0.000	0.000	0.000	0.000	0.259	0.000	0.000	0.000
C2H6		0.035	0.000	0.000	0.000	0.000	0.000	0.000	0.035	0.000	0.000	0.000
C3H8		0.090	0.000	0.050	0.000	0.009	1.000	0.000	0.090	0.000	0.039	0.065
C14H30		0.000	0.101	0.097	0.000	0.002	0.000	0.000	0.000	0.000	0.098	0.096
C15H32		0.000	0.044	0.042	0.000	0.002	0.000	0.000	0.000	0.000	0.044	0.041
C16H34		0.000	0.000	0.000	0.000	0.001	0.000	0.000	0.000	0.000	0.000	0.000
C17H36		0.000	0.420	0.402	0.000	0.001	0.000	0.000	0.000	0.000	0.426	0.368
C18H38		0.000	0.248	0.237	0.000	0.001	0.000	0.000	0.000	0.000	0.255	0.212
C19H40		0.000	0.029	0.027	0.000	0.000	0.000	0.000	0.000	0.000	0.030	0.024
(C4-C18) RGibbs		0.068	0.000	0.000	0.000	0.982	0.000	0.000	0.068	0.000	0.000	0.001

APPENDIX B

STREAM TABLE : CTH

Stream Name	Units	COKE	GASES	HC	ISO-P	S1	S2	S3	S4
Temperature	C	380	15	15	25	25	25	25	300
Pressure	MPa	0.20	0.10	0.10	0.10	0.20	0.20	0.20	0.20
Mass flow rate	ton/day	29.4	478	763.2	341.8	341.8	1000	1341.8	1341.8
Average MW		12.01	268.51	150.24	600.96	600.96	273.56	143.62	143.62
Mass Fractions									
C18H32O2		0.000	0.000	0.000	0.000	0.000	0.523	0.390	0.390
C18H34O2		0.000	0.000	0.000	0.000	0.000	0.186	0.139	0.139
C18H36O2		0.000	0.000	0.000	0.000	0.000	0.112	0.083	0.083
C15H30O2		0.000	0.000	0.000	0.000	0.000	0.179	0.133	0.133
H2		0.000	0.016	0.000	0.000	0.000	0.000	0.000	0.000
CO		0.000	0.268	0.000	0.000	0.000	0.000	0.000	0.000
CO2		0.000	0.354	0.001	0.000	0.000	0.000	0.000	0.000
H2O		0.000	0.012	0.000	0.000	0.000	0.000	0.000	0.000
CH4		0.000	0.059	0.000	0.000	0.000	0.000	0.000	0.000
C2H6		0.000	0.110	0.001	0.000	0.000	0.000	0.000	0.000
C3H8		0.000	0.170	0.005	0.000	0.000	0.000	0.000	0.000
C12H26		0.000	0.000	0.528	0.000	0.000	0.000	0.000	0.000
C8H16		0.000	0.012	0.305	0.000	0.000	0.000	0.000	0.000
C17H36		0.000	0.000	0.160	0.000	0.000	0.000	0.000	0.000
ISO-P		0.000	0.000	0.000	1.000	1.000	0.000	0.255	0.255
COKE		1.000	0.000	0.000	0.000	0.000	0.000	0.000	0.000

Stream Name	Units	S5	S6	S7	S8	S9	WATER	WCO
Temperature	C	380	380	380	50	25	15	25
Pressure	MPa	0.2	0.2	0.2	0.2	0.2	0.1	0.1
Mass flow rate	ton/day	1341.8	1341.8	1312.4	1312.4	1312.4	71.2	1000
Average MW		143.62	458.23	489.08	489.08	489.08	180.20	273.56
Mass Fractions								
C18H32O2		0.390	0.000	0.000	0.000	0.000	0.000	0.523
C18H34O2		0.139	0.000	0.000	0.000	0.000	0.000	0.186
C18H36O2		0.083	0.000	0.000	0.000	0.000	0.000	0.112
C15H30O2		0.133	0.000	0.000	0.000	0.000	0.000	0.179
H2		0.000	0.006	0.006	0.006	0.006	0.000	0.000
CO		0.000	0.095	0.098	0.098	0.098	0.000	0.000
CO2		0.000	0.127	0.130	0.130	0.130	0.000	0.000
H2O		0.000	0.057	0.059	0.059	0.059	1.000	0.000
CH4		0.000	0.021	0.021	0.021	0.021	0.000	0.000
C2H6		0.000	0.039	0.040	0.040	0.040	0.000	0.000
C3H8		0.000	0.064	0.065	0.065	0.065	0.000	0.000
C12H26		0.000	0.300	0.307	0.307	0.307	0.000	0.000
C8H16		0.000	0.178	0.182	0.182	0.182	0.000	0.000
C17H36		0.000	0.091	0.093	0.093	0.093	0.000	0.000
ISO-P		0.255	0.000	0.000	0.000	0.000	0.000	0.000
COKE		0.000	0.022	0.000	0.000	0.000	0.000	0.000

APPENDIX C

PRODUCT GATE PRICE

GASOLINE	RETAIL $/gallon	REFINING %	D&M%	TAX %	CRUDE OIL %
Jan-17	2.35	15.5	13.7	19.5	51.4
feb-17	2.3	14.7	12.7	19.8	52.7
mar-17	2.33	16.8	13.8	19.7	49.7
apr-17	2.42	19.2	13.2	18.9	48.7
May-17	2.39	15.8	16.8	19.1	48.3
Jun-17	2.35	16.5	18.2	19.5	45.8
Jul-17	2.3	19	12.3	20.2	48.5
Aug-17	2.38	22.1	10.2	19.5	48.2
Sep-17	2.65	20.8	16.4	17.5	45.2
Oct-17	2.51	17.4	14	18.5	50
nov-17	2.56	16.5	12.3	18.1	53.1
Average	2.41	17.66	13.96	19.12	49.24
Gate Price	**1.61**	**$/gallon**	**Gate Price**	**0.43**	**$/L**

DIESEL	RETAIL $/gallon	REFINING %	D&M %	TAX %	CRUDE OIL %
jan-17	2.58	14.8	18.1	20.3	46.8
feb-17	2.57	14.8	17.5	20.4	47.3
mar-17	2.55	14.4	19.9	20.5	45.3
apr-17	2.58	15.4	18.7	20.3	45.6
may-17	2.56	13.6	20.8	20.4	45.1
Jun-17	2.51	17	19.3	20.8	42.8
Jul-17	2.5	16.6	17.9	21.2	44.2
aug-17	2.6	18.9	16.5	20.4	44.2
sep-17	2.79	21.8	16.2	19	42.9
oct-17	2.79	20	16.1	19	44.9
nov-17	2.91	18.2	16.7	18.2	46.8
dec-17	2.91	16.2	17	18.2	48.6
Average	2.65	16.81	17.89	19.89	45.38
Gate Price	**1.65**	**$/gallon**	**Gate Price**	**0.44**	**$/L**

Gate Prices (2017)	Jan	Feb	Mar	Apr	May	Jun	Jul	Aug	Sep	Oct	Nov	Dec	Av. $/gal.	**Av. $/L**
KEROSENE	1.76	1.66	1.58	1.57	1.48	1.36	1.47	1.63	1.81	1.81	1.96	2.03	1.68	**0.4429**
PROPANE	0.79	0.79	0.67	0.64	0.63	0.59	0.63	0.74	0.86	0.94	1	0.99	0.71	**0.1863**

(from Energy Information Administration (EIA) U.S.)

APPENDIX D

PROFITABILITY ANALYSIS

Year	Investment	Investment not depreciated	Depreciation dk	Book value	Revenues R	COMd	After tax profit + depreciation	Cash flow	Annualised cash flow	Cumulative cash flow
0	$0	$0	$0	$0	$0	$0	$0	$0	$0	$0
1	-$126,562,162	$0	$0	$126,562,162	$0	$0	$0	-$126,562,162	-$117,187,187	-$117,187,187
2	-$54,240,926	$0	$0	$180,803,088	$0	$0	$0	-$54,240,926	-$46,502,852	-$163,690,039
2	$0	-$23,137,286	$0	$180,803,088	$0	$0	$0	-$23,137,286	-$19,836,493	-$183,526,532
3	$0	$0	$25,829,013	$154,974,075	$150,808,063	$100,970,022	$41,434,881	$41,434,881	$32,892,344	-$150,634,188
4	$0	$0	$44,278,307	$110,695,768	$150,808,063	$100,970,022	$47,892,134	$47,892,134	$35,202,148	-$115,432,039
5	$0	$0	$31,627,362	$79,068,406	$150,808,063	$100,970,022	$43,464,303	$43,464,303	$29,581,075	-$85,850,965
6	$0	$0	$22,590,973	$56,477,433	$150,808,063	$100,970,022	$40,301,567	$40,301,567	$25,396,824	-$60,454,141
7	$0	$0	$16,136,409	$40,341,023	$150,808,063	$100,970,022	$38,042,470	$38,042,470	$22,197,416	-$38,256,725
8	$0	$0	$16,136,409	$24,204,614	$150,808,063	$100,970,022	$38,042,470	$38,042,470	$20,553,163	-$17,703,562
9	$0	$0	$16,136,409	$8,068,205	$150,808,063	$100,970,022	$38,042,470	$38,042,470	$19,030,706	$1,327,144
10	$0	$0	$8,068,205	$0	$150,808,063	$100,970,022	$35,218,598	$35,218,598	$16,313,025	$17,640,169
11	$0	$0	$0	$0	$150,808,063	$100,970,022	$32,394,727	$32,394,727	$13,893,543	$31,533,712
12	$0	$0	$0	$0	$150,808,063	$100,970,022	$32,394,727	$32,394,727	$12,864,392	$44,398,104
13	$0	$0	$0	$0	$150,808,063	$100,970,022	$32,394,727	$32,394,727	$11,911,474	$56,309,578
14	$0	$0	$0	$0	$150,808,063	$100,970,022	$32,394,727	$32,394,727	$11,029,142	$67,338,720
15	$0	$0	$0	$0	$150,808,063	$100,970,022	$32,394,727	$32,394,727	$10,212,169	$77,550,889
16	$0	$0	$0	$0	$150,808,063	$100,970,022	$32,394,727	$32,394,727	$9,455,712	$87,006,601
17	$0	$0	$0	$0	$150,808,063	$100,970,022	$32,394,727	$32,394,727	$8,755,289	$95,761,890
18	$0	$0	$0	$0	$150,808,063	$100,970,022	$32,394,727	$32,394,727	$8,106,749	$103,868,639
19	$0	$0	$0	$0	$150,808,063	$100,970,022	$32,394,727	$32,394,727	$7,506,249	$111,374,888
20	$0	$0	$0	$0	$150,808,063	$100,970,022	$32,394,727	$32,394,727	$6,950,231	$118,325,118
21	$0	$0	$0	$0	$150,808,063	$100,970,022	$32,394,727	$32,394,727	$6,435,399	$124,760,517
22	$0	$0	$0	$0	$150,808,063	$100,970,022	$32,394,727	$32,394,727	$5,958,702	$130,719,219
23	$0	$0	$0	$0	$150,808,063	$100,970,022	$32,394,727	$32,394,727	$5,517,317	$136,236,536
24	$0	$0	$0	$0	$150,808,063	$100,970,022	$32,394,727	$32,394,727	$5,108,627	$141,345,163
25	$0	$0	$0	$0	$150,808,063	$100,970,022	$32,394,727	$32,394,727	$4,730,210	$146,075,373
26	$0	$0	$0	$0	$150,808,063	$100,970,022	$32,394,727	$32,394,727	$4,379,824	$150,455,198
27	$0	$0	$0	$0	$150,808,063	$100,970,022	$32,394,727	$32,394,727	$4,055,393	$154,510,590
27	$0	$23,137,286	$0	$0	$150,808,063	$100,970,022	$32,394,727	$23,137,286	$2,896,483	$157,407,074

Bibliography

[1] *U.S. Energy Information Administration (EIA)*. URL: https://www.eia.gov/ (visited on 03/06/2018).

[2] Tekalign Kasa and Fisseha Gebrewold. "Chemistry of Biodiesel and Its Environmental Impact A Review Article". In: 7.2 (2017), pp. 58–66.

[3] ATAG. "Aviation benefits beyond borders". In: *Atag* April (2014), p. 72.

[4] *Biodiesel — Energy Justice Network*. URL: http://www.energyjustice.net/biodiesel (visited on 03/04/2018).

[5] Jia Wang et al. "Successive desilication and dealumination of HZSM-5 in catalytic conversion of waste cooking oil to produce aromatics". In: *Energy Conversion and Management* 147 (2017), pp. 100–107. DOI: 10.1016/j.enconman.2017.05.050.

[6] David Pimentel et al. "Food versus biofuels: Environmental and economic costs". In: *Hum. Ecol.* 37.1 (2009), pp. 1–12. DOI: 10.1007/s10745-009-9215-8.

[7] Glenn E.Handwerk James H.Gary. *Petroleum refining : technology and economics*. Ed. by Inc Marcel Dekker. New York: Marcel Dekker, Inc, 2001, ix, 414 p. ISBN: 0824771508.

[8] Wei-Cheng Wang et al. "Review of Biojet Fuel Conversion Technologies". In: July (2016), p. 98.

[9] Stella Bezergianni. "Catalytic Hydroprocessing of Liquid Biomass for Biofuels Production". In: *Liq. Gaseous Solid Biofuels - Convers. Tech.* (2013), pp. 299–326. ISSN: 978-953-51-1050-7. DOI: 10.5772/52649. arXiv: 0803973233.

[10] Emil Raymond Riegel and James a. Kent. "Kent and Riegel's Handbook of Industrial Chemistry and Biotechnology". In: *Ebook* (2007), pp. 1–1833. DOI: 10.1007/978-0-387-27843-8.

[11] Pei Lin Chu et al. "Process modeling of hydrodeoxygenation to produce renewable jet fuel and other hydrocarbon fuels". In: *Fuel* 196 (2017), pp. 298–305. DOI: 10.1016/j.fuel.2017.01.097.

[12] Tom N. Kalnes, Michael M. McCall, and David R. Shonnard. "Renewable Diesel and Jet-Fuel Production from Fats and Oils". In: *Thermochem. Convers. Biomass to Liq. Fuels Chem.* 1 (2010), pp. 468–495. DOI: 10.1039/9781849732260-00468.

[13] Edward Furimsky. "Catalytic hydrodeoxygenation". In: *Appl. Catal. A Gen.* 199.2 (2000), pp. 147–190. DOI: 10.1016/S0926-860X(99)00555-4.

[14] Christos Kordulis et al. "Development of nickel based catalysts for the transformation of natural triglycerides and related compounds into green diesel: A critical review". In: (2016), pp. 156–196. DOI: 10.1016/j.apcatb.2015.07.042.

[15] Douglas C. Elliott. "Historical developments in hydroprocessing bio-oils". In: *Energy and Fuels* 21.3 (2007), pp. 1792–1815. DOI: 10.1021/ef070044u.

[16] Stella Bezergianni et al. "Hydrotreating of waste cooking oil for biodiesel production. Part I: Effect of temperature on product yields and heteroatom removal". In: *Bioresour. Technol.* 101.17 (2010), pp. 6651–6656. DOI: 10.1016/j.biortech.2010.03.081.

[17] Hernandez-Lloyo S.Boyas, Treho-Zarraga. "Hydroconversion of Triglycerides into Green liquid fuels". In: *INTECH* (2016). DOI: 10.577248710.

[18] Publisher Taylor, Sergiy Popov, and Sandeep Kumar. "Biofuels Renewable fuels via catalytic hydrodeoxygenation of lipid-based feedstocks Renewable fuels via catalytic hydrodeoxygenation of lipid-based feedstocks". In: 4.September 2015 (2014), pp. 219–239. DOI: 10.4155/bfs.12.89.

[19] Tom Kalnes, Terry Marker, and David R Shonnard. "INTERNATIONAL JOURNAL OF CHEMICAL Green Diesel : A Second Generation Biofuel Green Diesel : A Second Generation Biofuel". In: 5 (2007).

[20] Tom N Kalnes et al. "Green diesel production by hydrorefining renewable feedstocks". In: *Biofuels Technol.* 4 (2008), pp. 7–11.

[21] Gottfried Brieger and Terry J. Nestrick. "Catalytic transfer hydrogenation". In: *Chem. Rev.* 74.5 (1974), pp. 567–580. DOI: 10.1021/cr60291a003.

[22] Alexander Asiedu Kumar Sandeep. *Aquathermolysis of Waste Triglycerides in a Continuous Flow Reactor for Jet Fuels Production*. 2016.

[23] Honeywell UOP. *Honeywell Green Jet Fuel*. 2011. URL: https://www.uop.com/ (visited on 02/15/2018).

[24] Bambang Veriansyah et al. "Production of renewable diesel by hydroprocessing of soybean oil: Effect of catalysts". In: *Fuel* 94 (2012), pp. 578–585. DOI: 10.1016/j.fuel.2011.10.057.

[25] *InfoMine - Mining Intelligence and Technology*. URL: http://www.infomine.com/ (visited on 02/14/2018).

[26] Marcello Rigutto. *Cracking and Hydrocracking*. Vol. 2. 2010, pp. 547–584. DOI: 10.1002/9783527630295.ch18.

[27] G. Valavarasu, M. Bhaskar, and K. S. Balaraman. "Mild HydrocrackingâA Review of the Process, Catalysts, Reactions, Kinetics, and Advantages". In: *Petroleum Science and Technology* 21.7-8 (2003), pp. 1185–1205. DOI: 10.1081/LFT-120017883.

[28] Jeongwoo Han et al. "Life-cycle analysis of bio-based aviation fuels". In: *Bioresource Technology* 150 (2013), pp. 447–456. DOI: 10.1016/j.biortech.2013.07.153.

[29] Ling Tao et al. "Techno-economic and resource analysis of hydroprocessed renewable jet fuel". In: *Biotechnology for Biofuels* 10.1 (2017), pp. 1–16. DOI: 10.1186/s13068-017-0945-3.

[30] S.Peramanu. "Economics of hydrogen recovery processes for the purification of hydroprocessor purge and off-gases". In: 24.5 (1999), pp. 405–424.

[31] *Hydrogen recovery and purification — Linde Engineering*. URL: https://www.linde-engineering.com (visited on 02/14/2018).

[32] B. H. Bui, R. S. Zhu, and M. C. Lin. "Thermal decomposition of iso-propanol: First-principles prediction of total and product-branching rate constants". In: *Journal of Chemical Physics* 117.24 (2002), pp. 11188–11195. DOI: 10.1063/1.1522718.

[33] H Scott Fogler. "Elements of chemical reaction engineering". In: *Prentice Hall PTR international series in the physical and chemical engineering sciences* 4th (2006), p. 1080. DOI: 10.1016/0009-2509(87)80130-6.

[34] F. O. Rice and R. E. Vollrath. "The thermal decomposition of acetone in the gaseous state". In: *Pnas* 15.1 (1929), p. 702. ISSN: 0027-8424.

[35] Clayton McAuliffe. "Solubility in Water of Paraffin, Cycloparaffin, Olefin, Acetylene, Cycloolefin, and Aromatic Hydrocarbons". In: *The Journal of Physical Chemistry* 70.4 (1966), pp. 1267–1275. DOI: 10.1021/j100876a049.

[36] Matthew; Pearlson, Christoph Wollersheim, and James Hileman. "A techno-economic review of hydroprocessed renewable esters and fatty acids for jet fuel production." In: *Biofuels, Bioproducts and Biorefining* 6.3 (2012), pp. 246–256. DOI: 10.1002/bbb.

[37] Vivek V.Ranade, Raghunath V.Chaudhari, and Prashant R.Gunjal. *Trickel Bed Reactors : Reactor Engineering & Applications*. Ed. by Elsevier. Elsevier Ltd, 2001, p. 285. ISBN: 9780444527387.

[38] W. J.A. Wammes et al. “Hydrodynamics in a cocurrent gasâliquid trickle bed at elevated pressures”. In: *AIChE Journal* 37.12 (1991), pp. 1849–1862. DOI: 10.1002/aic.690371210.

[39] Gerhart Eigenberger, Chemische Verfahrenstechnik, and Universitiit Stuttgart. *Fixed-Bed Reactors*. Ed. by Ulmann’s Encyclopedia of Industrial Chemistry. Vol. B4. VCH, 1992, p. 199. ISBN: 0895735393.

[40] Gavin Towler and Ray Sinnott. *Chemical Engineering Design*. 2013, A1–I8. ISBN: 9780080966595.

[41] Richard Turton et al. *Analysis, Synthesis, and Design of Chemical Processes*. Vol. 53. 9. 2012. ISBN: 978-0-13-261812-0.

[42] *The Chemical Engineering Plant Cost Index - Chemical Engineering*. URL: http://www.chemengonline.com/ (visited on 03/06/2018).

[43] C San Marchi and B P Somerday. “Technical Reference On Hydrogen Compatibility Of Materials”. In: *Sand2008-1163* code 4001 (2012), p. 292.

[44] *Chemicals A-Z*. URL: https://www.icis.com (visited on 03/06/2018).

[45] F. Mueller-Langer et al. “Techno-economic assessment of hydrogen production processes for the hydrogen economy for the short and medium term”. In: *International Journal of Hydrogen Energy* 32.16 (2007), pp. 3797–3810. DOI: 10.1016/j.ijhydene.2007.05.027.

[46] Gael D. Ulrich and Palligarnai T. Vasudevan. “How to estimate utility costs”. In: *Chemical Engineering* 113.4 (2006), pp. 66–69.

[47] *U.S. Bureau of Labor Statistics*. URL: https://www.bls.gov/home.htm (visited on 03/15/2018).

[48] Eric CD Tan et al. “Conceptual process design and economics for the production of high-octane gasoline blendstock via indirect liquefaction of biomass through methanol/dimethyl ether intermediates”. In: *Biofuels, Bioproducts and Biorefining* (2015), pp. 246–256. DOI: 10.1002/bbb.